Dissertation

Control and Stability of AC/DC Microgrids

Eneko Unamuno Ruiz

Mondragon Goi Eskola Politeknikoa
Electronics and Computing Department

Arrasate-Mondragón, 4th December 2017

Control and Stability of AC/DC Microgrids

Eneko Unamuno Ruiz

Supervisor:

Dr. Jon Andoni Barrena
Electronics and Computing Department
Mondragon Unibertsitatea

Submitted in partial fulfilment of the requirements
for the Degree of Doctor of Philosophy under the program:
Mechanical and Electrical Energy Engineering

Thesis Committee:
President: Dr. Jon Are Suul (Norwegian University of Science and Technology and SINTEF Energy Research)
Vocal: Dr. Pablo Arboleya (Universidad de Oviedo)
Vocal: Dr. Juan José Valera (Ingeteam Power Technology)
Vocal: Dr. Salvador Ceballos (Tecnalia Corporación Tecnológica)
Secretary: Dr. Gonzalo Abad (Mondragon Unibertsitatea)

Arrasate-Mondragón, 4th December 2017

To my family

“Whether you think you can or you can’t, you’re right”
Henry Ford

Abstract

The current society is facing several challenges related to the field of energy, such as the high dependency on fossil fuels, the constant increment in the energy consumption and the environmental problems caused by these factors. The integration of distributed generation systems—mainly based on renewable energies—combined with energy storage systems is the most interesting solution to tackle these issues.

However, most of these systems are connected to the grid through electronic converters that actively control the power exchange. This fact causes various problems not suffered since the origins of electric grids in the transition from an electric model dominated by synchronous machines to a model where power electronics gain more importance—even being the dominating systems in some cases. The lack of inertial response and primary reserve, the instabilities caused by the interactions of power electronic systems or the premature situation of direct current grids, which are being employed more widely, stand out as some of the most important challenges that we want to address with this thesis.

In this context, the **main purpose** of the thesis is the **development of ac/dc microgrid control strategies** that improve the dynamic behaviour of the system.

In order to achieve this objective we contemplate four main lines that consist of the identification and analysis of different microgrid topologies and control techniques, the study of primary control operation modes of the systems that compose these microgrids and finally the the development and evaluation of various low-level control strategies for ac and dc microgrids. These techniques are based on the concept of operation of classical synchronous generators, enabling their autonomous operation as well as providing inertial response under grid perturbations.

Among the contributions of the thesis, we can highlight on the one hand, the analysis and comparative evaluation of synchronous machine emulation techniques for ac microgrids, where we evaluate their behaviour for different types of perturbations and we examine their stability applying the generalized Nyquist criterion. Regarding dc microgrids, on the other hand, we propose novel control techniques that are analogous to the ones analysed for ac grids. We call these techniques virtual-capacitors, as they emulate the behaviour of these passive elements connected to dc grids. In this case, we thoroughly study their transient as well as steady-state behaviour, and we demonstrate that they can be adapted by simply modifying control parameters. Moreover, we analyse the stability of these techniques through parametric analysis of their dominant eigenvalues.

Laburpena

Gaur egungo gizartea energiaren arloko hainbat erronkaren aurrean aurkitzen da, besteak beste, erregai fosilekiko dependentzia handia, kontsumo energetikoaren etengabeko igoera, eta faktore hauek eragiten dituzten ingurumen arazoak. Generazio bananduko sistemen integrazioa—bereziki iturri berriztagarrietan oinarritutakoa—metatze sistemekin bateratuta, arazo horiei aurre egiteko aukera interesgarriena bilakatu da.

Hala ere, sistema hauetako gehienak bihurgailu elektronikoen bitartez konektatzen dira sare elektrikotara, potentziaren hartu-emana modu aktiboan kontrolatzen dutelarik. Honek, makina sinkronoez menderatutako modelo elektriko batetik, potentzia elektronika garrantzia hartzen hasten den—edo kasu batzuetan mendean dagoen—modelo baterako trantsizioan hainbat arazo eragiten ditu, sare elektrikoak sortu zirenetik jasan ez direnak. Erantzun inertzial eta erreserba primario eza, bihurgailuen interakzioaren ondoriozko estabilitate arazoak edo korronte zuzeneko sareen egoera goiztiarra, geroz eta gehiago erabiltzen direnak, tesi honen bitartez aurre egin nahi diren erronkarik garrantzitsuenetarikoak dira.

Testuinguru honetan, tesiaren **helburu nagusia ac/dc mikrosareen** portaera dinamikoa hobetzen duten **kontrol estrategiak garatzea** da.

Helburu hau lortzeko lau lerro nagusi planteatu dira, besteak beste, mikrosareen topologia eta kontrol estrategia desberdinen identifikazio eta analisia, sare hauek konposatzen duten sistemen kontrol primarioaren funtzionamendu motak azterketa, eta azkenik, bai ac eta bai dc mikrosareendako nibel baxuko kontrol estrategia desberdinen garapena. Azken hauek generadore sinkrono klasikoetan oinarritu dira, modu autonomoan eta bananduan aritzeko gaitasuna emateaz gain, sareko perturbazioen aurrean erantzun inertziala ematea ahalbidetzen dielako.

Tesiaren ekarpenen artean, alde batetik, makina sinkronoen emulazioan datzan kontrol estrategien analisia eta konparaketa azpimarratu behar dira. Kasu honetan, teknika hauek hainbat perturbazioetarako ebaluatzen ditugu, eta Nyquisten kriterio generalizatuan oinarrituta estabilitatea aztertzen dugu. Korronte zuzeneko sareei erreparatuz, bestalde, kontrol teknika berriak proposatzen ditugu. Hauei kondentsadore-birtual izena ezarri diegu, elementu pasibo horien erantzun dinamikoa emulatzen dutelako. Hemen, teknika hauen erregimen iraunkorreko eta iragankorreko erantzuna aztertzen dugu, soilik kontrol parametro batzuk aldatuta egokitu daitezkela frogatuz. Hortaz gain, sistema hauen estabilitatea aztertzen dugu berezko balio dominanteen (*eigenvalue*-en) analisi parametrikoak eginez.

Resumen

La sociedad actual se enfrenta a varios retos importantes en materia energética, entre los que destacan la gran dependencia de los combustibles fósiles, el constante aumento del consumo energético y los problemas medioambientales que estos factores conllevan. La integración de sistemas de generación distribuida—principalmente de origen renovable—combinadas con sistemas de almacenamiento de energía, se presenta como la solución más interesante para hacer frente a estos retos.

Sin embargo, la mayor parte de estos sistemas se conectan a la red a través de convertidores electrónicos que controlan el intercambio de potencia de manera activa. Este hecho hace que la transición desde un modelo eléctrico principalmente dominado por máquinas síncronas, hacia un modelo donde la electrónica de potencia comienza a cobrar protagonismo—hasta el punto de llegar a ser dominante en algunos casos—acarree diversos problemas que prácticamente no se han manifestado desde los orígenes de las redes eléctricas. La falta de respuesta inercial y reserva primaria, las inestabilidades debidas a la interacción de los sistemas electrónicos de potencia o la prematura situación de las redes de corriente continua, cada día utilizadas en mayor medida, destacan como algunos de los retos más importantes a los que se quiere dar respuesta a través de esta tesis.

En este contexto, el **objetivo principal** de la tesis es el **desarrollo de estrategias de control de microrredes ac/dc** que mejoren el comportamiento dinámico del sistema.

Para la consecución de este objetivo se han planteado cuatro líneas principales que constan de la identificación y análisis de diferentes topologías y técnicas de control de microrredes, el estudio de los modos de operación del control primario de los sistemas que las componen, y finalmente, el desarrollo y evaluación de diversas técnicas de control de nivel bajo tanto para microrredes ac como dc. Las estrategias de control de nivel bajo desarrolladas en la tesis se basan en el concepto de operación de los generadores síncronos clásicos, lo que les permite operar de manera distribuida y autónoma, aportando a su vez respuesta inercial ante perturbaciones en la red.

Entre las contribuciones de la tesis destacan, por un lado, el análisis y comparativa de técnicas de control de emulación de máquinas síncronas para redes ac, donde evaluamos su comportamiento ante diferentes tipos de perturbaciones y examinamos su estabilidad aplicando criterios generalizados de Nyquist. En el ámbito de las redes dc, por otra parte, proponemos nuevas técnicas de control que son análogas a las analizadas para las redes ac, y que denominamos como condensadores-virtuales puesto que emulan el comportamiento dinámico de estos elementos pasivos conectados a la red. En este caso, estudiamos en detalle su comportamiento dinámico y en régimen permanente, demostrando que se pueden adaptar simplemente variando parámetros de control, y analizamos su estabilidad llevando a cabo análisis paramétricos de sus valores propios dominantes.

Acknowledgement

Nire inguruan egon den jende guztiagatik ez balitz, ez zinateke tesi hau irakurtzen egongo. Horregatik, nahiz eta ezinezkoa den parrafo batzuetan nigan eragina eduki duten pertsona guztiak aipatzea, lerro hauen bitartez guztioi eskerrak ematea gustatuko litzaidake.

Alde batetik, Mondragon Unibertsitateari tesi hau egiteko aukera emateagatik, eta bereziki Jon Andoni Barrenari, bai atal teknikoan eta bai bizitzako beste hainbat arlotan eskainitako ezagutza guztiengatik. Lehenengo egunetik lankide eta lagun sentiarazteak izugarri erraztu du tesiaren garapena eta egunerokotasuna, eta ezingo dut ahaztu urte hauetan mentore bezala erakutsitako guztia, milesker Jonan!

Hortaz gain, Canales, Iosu eta Unai modu berezian eskertu nahiko nituzke, berez ikertzeko neukan grina indartu eta, behar izan nuenean, nire gidak izan zirelako.

Nirekin bulegoa, otorduak eta galdu ezin daitezkeen kafe orduak partekatu duen jendea ere ezin dut ahaztu, eta hortaz eskerrak ematea da egin dezakedan gutxienekoa: Txef, Iratxo, Oier, Jugón, Argiñe, Olmo, Teki, Laura, Erik, Carlos, Christian, Ordoño, irakasle, doktoregai, ikasle eta langile guztiak, amaitu ostean unibertsitatea utzi zutenak... Aipamen berezia merezi dute Eduk eta Txejok, tesiko momentu hobeenetan zein txarrenetan alboan edukitzeak ez daukalako preziorik, eskerrik asko lanegunei “saltsa” jartzeagatik. Eta nola ez Julen, beraren laguntza eta motibazioagatik ez balitz ezinezkoa izango litzatekelako hemen aurkeztutako lana gauzatzea.

I would also like to show my most sincere gratitude to Prof. Marta Molinas, which hosted me at NTNU Trondheim and made me feel a part of her team since the very first day. I will always remember the enriching discussions, amazing barbecues, walks and trips, coffee breaks and last-day chocolate cakes I shared with Marta, Amin, Jing, Vicky, Benni, Paula, Atle, Max, Noe and Jon Are. I feel very fortunate to have shared all these moments and to learn so much from you, and I hope we meet sometime soon.

Kuadrillakoak ere, “Monjetakuak”, bereziki agurtzea gustatuko litzaidake, azkenaldian gutxi ikusi banaute ere beti hor egon izan direlako deskonektatzeko beharra izan dudanean. Alatz, Dani, Xabi, Larra, Unai, Beitxi, Gorka, Zangi, Ibon, Urru, Erik, eskerrik asko!!

No me gustaría olvidarme del aita y la ama, Iñigo y Toñi, que han hecho que todo esto sea posible gracias a su incesante esfuerzo, trabajo, cariño y comprensión. Si no os tuviese como ejemplo no sería como soy y si no fuese por vosotros no estaría aquí, por lo que no tengo palabras suficientes para agradeceros todo lo que habéis hecho por mí. Y cómo no mencionar a Unai, con quien he compartido gran parte de mi vida y especialmente los momentos de locura y risas que alegran el día a día.

Me gustaría mencionar también al resto de miembros de la familia (amama Antoni, tíos y tías, primos y primas...), a Arantza, Joserra, Idoia y amama Felisa, que desde el primer momento me han acogido como a uno más, y a todos los que nos han dejado por el camino pero que también están reflejados en esta tesis, especialmente a amama Tina, con quien siempre mantuve un vínculo especial.

Amaitzeko, ezin ditut parrafo hauek amaitu nire bizitzako pertsona garrantzitsuenetarikoa aipatu gabe. Zuri, Maialen, eskerrak eman behar dizkizut eskainitako maitasunagatik, pertsona bezala hazten lagundu nauzulako, momentu on eta txarretan beti alboan eduki zaitudalako eta, batez ere, zoriontsu egiten nauzulako. Espero dot orain datorkigun etapa berri hontan, beti bezala, zure alboan irribarrez beteriko askoz abentura gehiago bizi ahal izatea.

Contents

Abbreviations

APC Active Power Controller

AVR Automatic Voltage Regulator

CCVSM Current-Controlled Virtual Synchronous Machine

DG Distributed Generation

DRF Dynamic Reference Frame

DVC Direct Virtual-Capacitor

ESS Energy Storage System

FFT Fast Fourier Transform

GM Gain Margin

GNC Generalized Nyquist Criterion

GRF Global Reference Frame

HVDC High-Voltage DC

IE Inertia-Emulation

LRF Local Reference Frame

MAS Multi-Agent Systems

MGCC Microgrid Central Controller

MPPT Maximum Power Point Tracking

MTDC Multi-Terminal DC

PI Proportional-Integral

PLL Phase-Locked Loop

PM Phase Margin

PV Photovoltaic

PWM Pulse-Width Modulator

RES Renewable Energy Sources

RoCoF Rate of Change of Frequency

RoCoV Rate of Change of Voltage

RPC Rective Power Controller

SCADA Supervisory Control And Data Acquisition

SM Synchronous Machine

SME Synchronous Machine Emulation

SoC State of Charge

SST Solid State Transformer

SV Synchronverter

VC Virtual-Capacitor

VC2 Voltage-Controlled Virtual-Capacitor

VCVSM Voltage-Controlled Virtual Synchronous Machine

VSC Voltage Source Converter

VSM Virtual Synchronous Machine

WP Wind Power

Symbols: AC Systems

C_f converter output filter capacitance

ψ SM stator flux linkages in dq-domain

γ state of the PI regulator

H per unit mechanical inertia

$\mathbf{i}_c$ converter current in dq-domain

i_{fd} SM damping winding current

i_{kd} SM amortisseur d-axis current

i_{kq} SM amortisseur q-axis current

$\mathbf{i}_o$ output current in dq-domain

$\mathbf{i}_s$ CCVSM virtual winding current in dq-domain

$\mathbf{i}_{sm}$ SM output current in dq-domain

J mechanical inertia

K SV RPC constant

K_D damping factor constant

K_i integrator gain of PI regulator

K_ω frequency droop gain

K_p proportional gain of PI regulator

K_q voltage droop gain

L_f converter output filter inductance

L_{fd} SM damping winding inductance

L_{kd} SM amortisseur d-axis inductance

L_{kq} SM amortisseur q-axis inductance

L_m SM mutual inductance

L_s SM stator winding inductance

L_v VCVSM virtual-impedance inductance

$\mathbf{m}$ modulation index in dq-domain

$\mathbf{m}_{pwm}$ modulation index after PWM delay in dq-domain

ω_b base frequency

ω_f reactive power filter cut-off frequency

ω_g grid frequency

ω_m SM frequency

ω_{pll} PLL frequency

ω_{ref} reference frequency

ω_{sv} SV frequency

ω_{vsm} VSM frequency

p measured active power

p_e electrical power

p_m mechanical power

$p_{m_{\text{ref}}}$ mechanical power reference

p_{ref} constant active power reference

q measured reactive power

q_f filtered reactive power

q_{ref} constant reactive power reference

R_f converter output filter resistance

R_{fd} SM damping winding resistance

$\boldsymbol{\rho}$ PWM states in dq-domain

R_{kd} SM amortisseur d-axis resistance

R_{kq} SM amortisseur q-axis resistance

R_s SM stator winding resistance

R_v VCVSM virtual-impedance resistance

S_b base power

τ_e electrical torque

τ_m mechanical torque

T_{ex} exciter delay time

T_{gt} governor and turbine delay time

θ_c controller angular position

θ_g grid voltage angular position

θ_{pll} PLL angular position

θ_{sm} SM rotor angular position

θ_{sv} SV angular position

θ_{vsm} VSM angular position

T_s PWM delay time

$\hat{\mathbf{v}}_{\text{ref}}$ voltage amplitude reference

V_b base voltage

$\mathbf{v}_c$ converter output voltage in dq-domain

V_{dc} converter dc bus voltage

v_{fd} SM exciter voltage

$\mathbf{v}_g$ grid voltage in dq-domain

$\mathbf{v}_o$ filter capacitor voltage in dq-domain

$\hat{\mathbf{v}}_{rpc}$ RPC reference voltage amplitude

$\mathbf{v}_{sm}$ SM output voltage in dq-domain

Symbols: DC Systems

C_f output filter capacitance

C_{V} virtual-capacitance

d_{PWM} buck-boost duty cycle after the PWM delay

γ state of the PI regulator

H_{dc} per unit virtual-capacitance

i_{VC} VC current

i_c converter current

i_g grid current

i_{L_c} buck-boost inductance current

L_c buck-boost inductance

L_f output filter inductance

r parasitic resistance

S_b base power

T_s PWM delay time

v_{VC} VC voltage

V_b base voltage

v_c converter voltage

v_{C_i} buck-boost input capacitor voltage

v_{C_o} buck-boost output capacitor voltage

R_{V} virtual-resistance

v_g grid voltage

v_i buck-boost input voltage

Z_{V} virtual-impedance

Chapter 1

Introduction

In this chapter we talk about the situation of the current energy model and how its evolution is causing some requirements that have not been noticed since their origins.

Under this context, we point out some of the most important challenges that have arisen in the last decades and which are our main objectives with this thesis.

Apart from that, we summarize the contributions made throughout the thesis and show the outline of the document.

1.1 Background

The concerns about environmental issues caused by the high dependency on fossil fuels, the constant increment of the global power consumption or the lack of reliable energy sources—primarily on developing countries—are driving one of the most severe transformations of the electric infrastructure since its creation in the beginning of the XX-th century.

Classically, the energy has been generated at high-scale power plants and then transmitted to consumption areas through long-distance transmission and distribution lines, which are interconnected through low-frequency transformers (Figure 1.1). These top-down topologies are mainly dominated by the synchronous generators employed to generate energy at power plants—e.g. hydroelectric power plants, thermal plants fuelled by coal or gas, nuclear plants, etc. This means that no matter where a power perturbation occurs, these generators share the power deviations by opposing to frequency disturbances, so the dynamic behaviour of the grid is primarily defined by synchronous generators and their inherent mechanical inertias (highlighted as J in Figure 1.1).

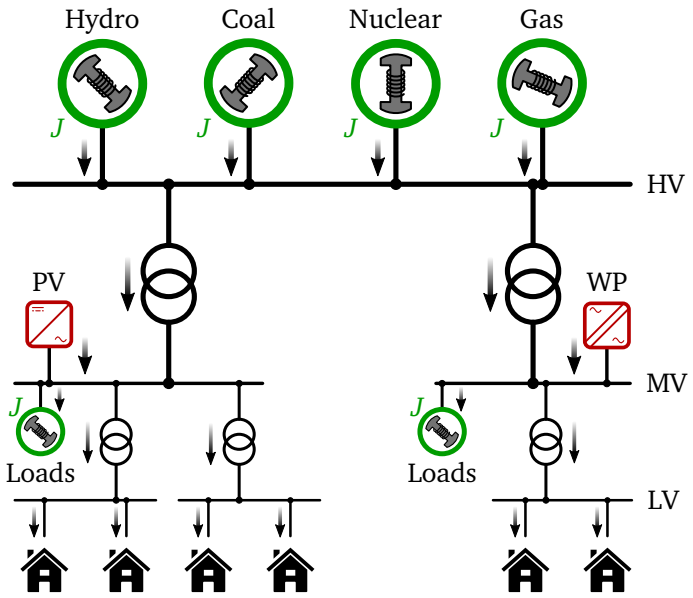

Figure 1.1: Configuration of classical synchronous-machine-dominated electric grids.

In the last decades, however, electric grids are undergoing different modifications in their structure. On the one hand, there is an increasing trend to locate generation systems near consumption areas—also known as distributed generation (DG)—which shifts the structure of electric grids towards more distributed topologies. On top of that, the evolution of power electronics, and semiconductor and information technologies is enabling the massive integration of power electronic converters in the grid [1], for instance for the interconnection of asynchronous ac grids through high-voltage dc (HVDC) links, the active control of power flow

in the grid, or the integration of DG systems (Figure 1.2).

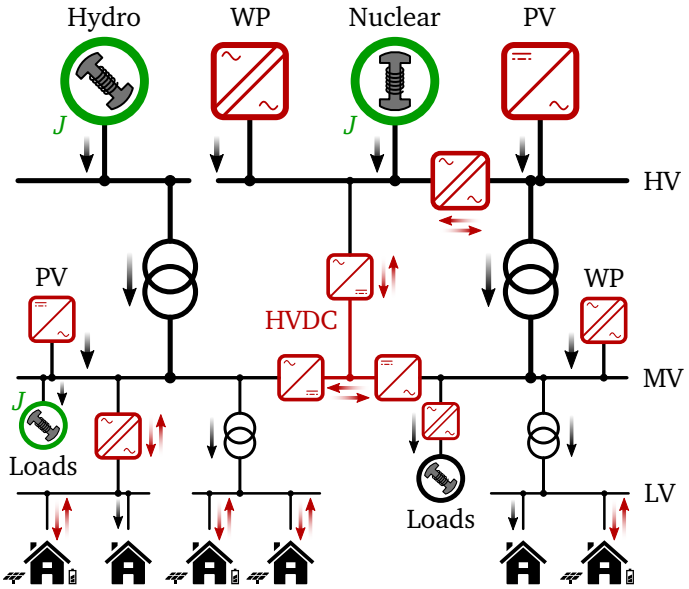

Figure 1.2: Configuration of modern converter-dominated distributed electric grids.

Although this transformation might seem ideal to increase the flexibility of the grid and improve the quality of the energy supply, it brings about several challenges, as the electric grid was not originally designed to handle distributed and variable generating systems and to operate with a high number of interconnected power electronic converters.

In this context, **microgrids** are emerging as one of the key players to cope with these challenges [2, 3], as they efficiently integrate different types of DG systems thanks to the energy storage system (ESS) and advanced control strategies they incorporate (Figure 1.3). Moreover, they can operate either connected or islanded from the main grid, improving the overall flexibility of the grid.

Microgrids usually operate on ac, taking advantage of the existing grid infrastructure and the knowledge gained over the years related with voltage conversion transformers and protection devices. Several companies of recent creation such as Tesla[1] or Sonnen[2] are already demonstrating the viability and usefulness of ac microgrid deployment in the current grid infrastructure through the installation of distributed ESSs. In addition, there are several fields where microgrids already play a key role, such as electric transportation—vessels, aircraft, trains, etc.—or the integration of renewable energies.

However, thanks to the evolution of power semiconductor technologies and power electronics in general, dc-based microgrids are becoming a competitive solution at different applications. Among the advantages of dc grids we can highlight the lack of reactive power circulation, the reduction of conversion stages in systems that operate in dc or systems that

[1] https://www.tesla.com/
[2] https://www.sonnen-batterie.com/

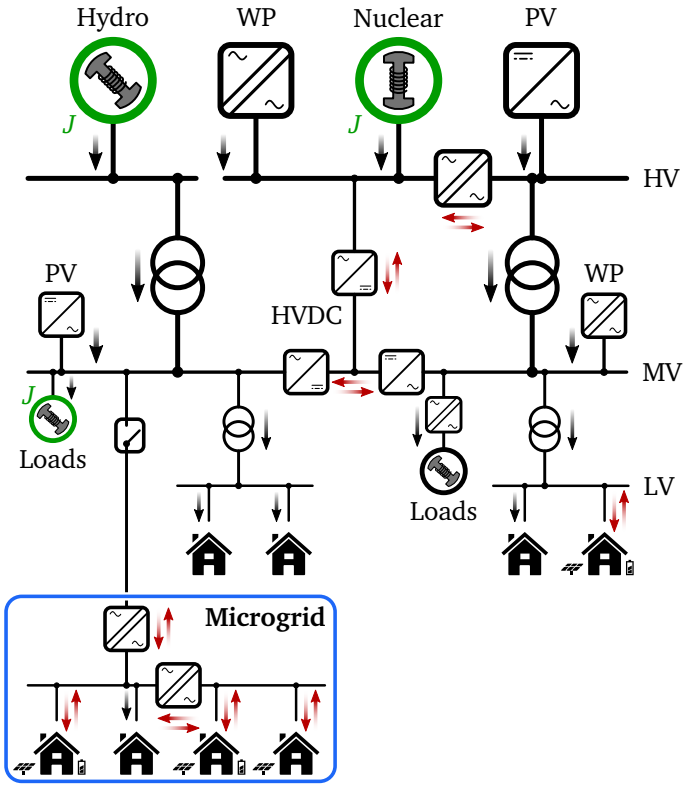

Figure 1.3: Concept of a microgrid integrated in an ac grid.

require a dc stage to operate—such as photovoltaic (PV) panels, electronic devices, elevators, washing machines, wind power (WP) systems—or the fact that devices do not have to be synchronized to connect to the grid.

Even though most dc microgrids are developed for research purposes and have not been yet expanded to real applications, there are other fields in which the direct current has been already employed.

In the **high-voltage range**, most of the systems use dc links for transmitting energy between two ac grids, in point-to-point configurations. There are multiple examples of these type of HVDC links worldwide, such as the Jinping-Sunan[3] ±800 kV link in China or the Interconnexion France-Angleterre (IFA)[4] that connects the French and British transmission systems. In the last decades, these links are evolving to interconnect more than two dc terminals through meshed dc grids, also known as multi-terminal dc (MTDC) grids, which are an interesting solution for instance to transfer energy from offshore wind mills to the ac grid.

In the **medium-voltage range**, the research about dc grids is mainly focused on isolated distribution systems such as the ones that could be found in vessels or aircraft. In vessels, for example, the most conventional propulsion solutions make use of an ac distribution system

[3] http://new.abb.com/systems/hvdc/references/jinping—sunan
[4] http://www2.nationalgrid.com/About-us/European-business-development/Interconnectors/france/

composed by synchronous ac generators, which at the same time are associated to diesel motors operating at fixed speed in order to provide fixed voltage and frequency (50 Hz or 60 Hz). The fact that these generators have to operate at fixed speeds implies very poor efficiencies at highly varying loads, so dc distribution is an appealing solution to operate these generators at variable speeds while keeping the bus at the rated value. In this context, there are several examples of vessels operating in dc, such as the Onboard DC Grid[5] developed by ABB or research projects such as EDSOMA[6] carried out between Ingeteam and Ulstein to develop these type of systems.

Moreover, medium-voltage dc grids are also used for the integration of PV or WP plants through MTDC systems. Among some of the projects that are being carried out in this line of research are DC-Direkt[7], BestPaths[8] or LIFE Factory Microgrid[9].

In the **low-voltage range** the number of real application facilities is very low but it is being widely researched for the integration of DG, ESSs and loads operating in dc or containing a dc stage in their power converters. In this context, we can find various project examples that develop different technologies for low-voltage dc grids such as the DC C+G Project[10] or the Intelligent DC Microgrid Living Lab[11] from Aalborg University. In addition, the association named EMerge Alliance[12] composed by multiple academic and industrial partners is developing standards so that dc distribution grids can be integrated in commercial and residential buildings.

All these examples demonstrate that future electric distribution grids will not be exclusively on ac, but rather a combination of both ac and dc at all voltage levels, forming hybrid ac/dc grids. Moreover, the integration of DG and ESS will enable the disconnection and autonomous operation of certain parts of these hybrid grids in the form of microgrids. According to a report developed by Navigant Research (Figure 1.4), the microgrid market capacity and implementation revenue will increase significantly in the following decade [4].

This growth is being also driven by an intense research activity, which is clearly reflected in the constant increment of publications, new journals and conferences held in the last decade. Figure 1.5 shows for example the number of publications related to the control and management of microgrids since the year 2000.

[5] http://new.abb.com/marine/marine/systems-and-solutions/power-generation-and-distribution/onboard-dc-grid

[6] https://goo.gl/rXu4sF

[7] http://www.acs.eonerc.rwth-aachen.de/cms/E-ON-ERC-ACS/Forschung/Forschungsprojekte/Gruppe-Control-of-Special-Purpose-Grids/ lctf/DC-Direkt/?lidx=1

[8] http://www.bestpaths-project.eu/

[9] http://www.factorymicrogrid.com/es/index.aspx

[10] http://www.dcc-g.eu/

[11] http://www.et.aau.dk/research-programmes/microgrids/activities/intelligent-dc-microgrid-living-lab/

[12] http://www.emergealliance.org

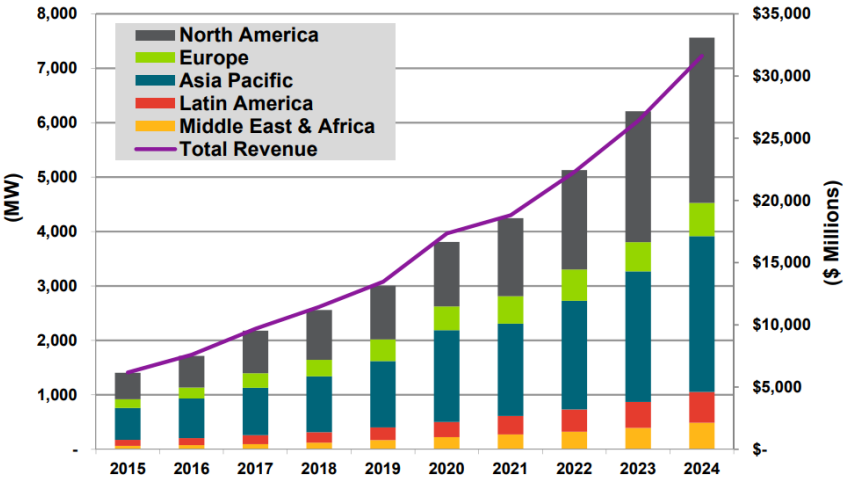

Figure 1.4: Annual Total Microgrid Market Capacity and Implementation Revenue by Region, World Markets: 2015–2024 (source: Navigant Research, *Market Data: Microgrids* [4]).

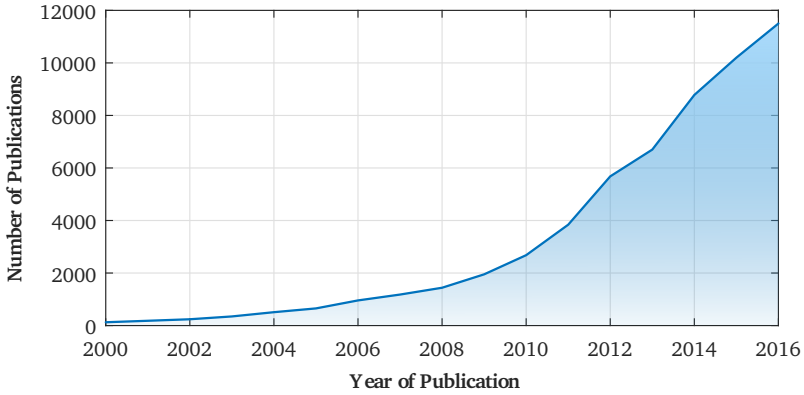

Figure 1.5: Number of publications obtained from Google Scholar for the query: *microgrid AND (control OR management)*.

1.2 Key Challenges

Although the technologies related to microgrids are improving rapidly, there are still several barriers that need to be addressed.

Premature Stage of DC Grids

Even though there are multiple examples in which dc grids are being used nowadays, most of the systems are used in high-voltage applications, and the grids that are being integrated in the medium- or low-voltage range are mainly research facilities and not final industrial systems. Therefore, there is a clear necessity to research different aspects of low-scale dc grids—for instance microgrids—from various points of view, such as their topologies or control/management strategies.

Inertial Response

Some of the **main challenges** related to microgrids still reside in their **control and management**, especially when they operate islanded or decoupled—through power converters—from the main grid. Being converter-dominated systems, microgrids have a very weak inertial response compared to classical grids. In the latter, the inherent inertia of rotating synchronous generators reacts instantly over power disturbances, and usually hierarchical control structures are employed to recover the frequency and voltage to their rated values (Figure 1.6).

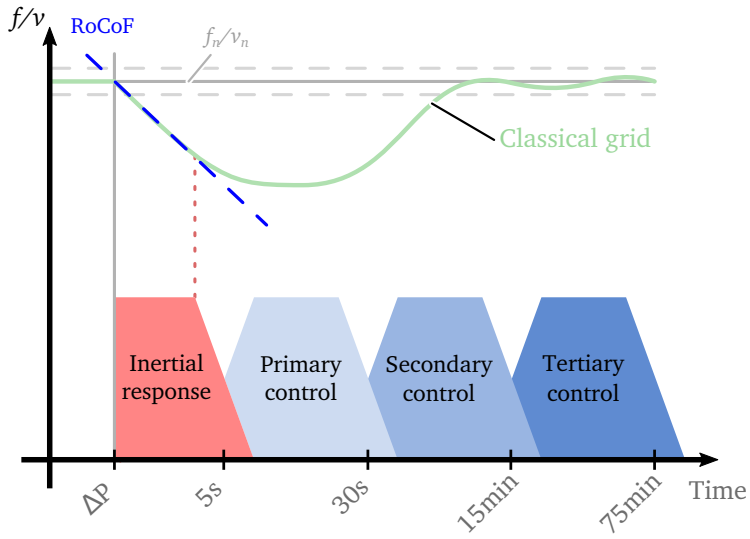

Figure 1.6: Participation of inherent inertia and the hierarchical control in the regulation of frequency at a classical grid.

At microgrids, the mode of operating of classical grids is reproduced by integrating hierarchical control structures in power electronic converters. In this case, as shown in Figure 1.7, the inertial behaviour is provided by the lower-level regulators integrated in these controllers to avoid a very steep rate of change of frequency (RoCoF). By doing that, secondary controllers—which operate in larger scales of time—have more time for restoring the frequency to their rated values, which is carried out by adjusting the steady-state point of operation of the systems regulating the grid frequency.

Nowadays, some grid operators such as **Hydro Québec TransÉnergie** [5] require that newly installed wind mills or photovoltaic parks provide inertial response under certain conditions to ensure the frequency remains under the required boundaries. This is fundamental in order to avoid blackouts as the one happened in south Australia in September of 2016 [6].

In this context, the European Network of Transmission System Operators for Electricity (also known as ENTSO-E) has recently published two reports named “Need for synthetic inertia (SI) for frequency regulation” and “High Penetration of Power Electronic Interfaced Power Sources (HPoPEIPS)” whose aim is to provide guidance on synthetic inertia to European elec-

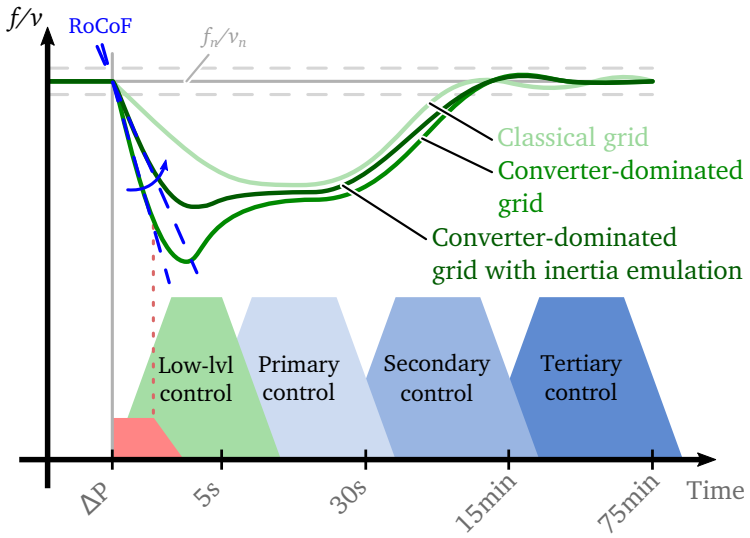

Figure 1.7: Participation of inherent inertia and the hierarchical control in the regulation of frequency at a microgrid.

tric system operators, so that they can develop different network codes for newly-installed grid-connected systems [7, 8].

These facts show that there is still a high necessity to research the inertial behaviour of converter-dominated grids and to provide solutions to improve the operation of weak grids through the control and management of these converters. Even though the vast majority of research activity about this topic has been focused on ac distribution grids, there is a clear necessity to analyse these issues also in dc-based systems.

Spinning Reserve

In addition to the issues related to the lack of inertia, there are other **challenges associated with reserves of primary regulation capability**, also known as "spinning reserve" or "primary reserve". This reserve has to be designed to handle the maximum difference between generated and demanded power in the grid, and is classically done with synchronous machine-based generators.

However, ensuring the minimum spinning reserve is specially complicated at converter-dominated grids with very distributed and variable generation systems. Therefore, generation systems, energy storage systems, and even loads, must participate in the primary regulation of microgrids to avoid large frequency and voltage deviations. In this context, designing the adequate modes of operation of these devices is still a challenge that needs to be researched more in detail.

Stability

The interaction of converters on a converter-dominated grid brings about other challenges that might deteriorate the power quality. In addition to a weak inertial response, microgrids can suffer instability problems due to the different control methods and physical characteristics of the converters that participate in the regulation of the grid. Kundur *et al.* provide in [9] an interesting synthesis of the most common stability types in power systems, and classify them on three main groups, namely rotor angle-, frequency- and voltage-stability (Figure 1.8).

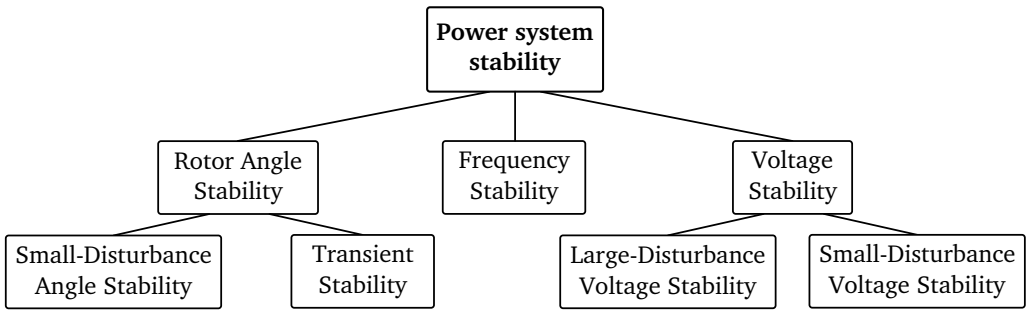

Figure 1.8: Classification of power system stability, adapted from [9].

However, this classification is oriented to power systems and needs to be adapted to the field of microgrids, which are mainly dominated by power electronic converters.

1.3 Goals of the Thesis

Inspired by the identified challenges, the **main goal** of the thesis is to **develop and analyse primary and low-level control strategies for ac and dc microgrids that ensure their adequate operation in terms of dynamic and steady-state response and stability**.

In order to reach this goal, we have set the following specific objectives:

[O1] Identify and analyse different types of microgrid topologies and control methods that do not require communication networks to integrate distributed generation systems.

[O2] Study the modes of operation of primary controllers for generation and storage systems, loads and other agents participating in the regulation of microgrids.

[O3] Develop control techniques for ac as well as dc microgrids that contribute in the inertial response of the system and ensure a stable operation.

1.4 List of Contributions

The most relevant technical contributions of this thesis can be summarized as follows:

- A **review of** the most employed **topologies of hybrid ac/dc microgrids** from the point of view of the nature of their current and their interconnection with the main grid, and a review of their most interesting **control strategies**.
- The generalization of **mode-adaptive, droop-based primary regulators** for generation, energy storage systems, loads and interlinking converters based on local measurements of frequency or voltage.
- A performance and impedance-based stability analysis of **synchronous machine emulation techniques** for converter-dominated ac grids, compared to the behaviour of a classical synchronous generator.
- A **methodology** for the analysis and comparative evaluation of synchronous machine emulation techniques.
- Novel **virtual-capacitor techniques for dc grids** emulating the principles of operation of SME controllers to contribute in the inertial behaviour of these grids.
- An adaptation of **low-level techniques to control systems with different dynamic behaviours** and take advantage of their inherent transient or steady-state response types.

Some of these contributions have been published in the form of conference proceedings, journal papers, book chapters or tutorials. Below there is a summary of these publications:

Journal Papers

[J1] E. Unamuno, M. Amin, A. Rygg, M. Molinas and J. A. Barrena, "Synchronous Machine Emulation Techniques: Comparative Evaluation of Performance and Stability," *IEEE Trans. Power Electron.*, 2017. → **Under revision**

[J2] A. Rygg, M. Molinas, E. Unamuno, C. Zhang and X. Cai, "A simple method for shifting local *dq* impedance models to a global reference frame for stability analysis," *IEEE Trans. Power Electron.*, 2017. → **Under revision**

[J3] E. Unamuno and J. A. Barrena, "Equivalence of Primary Control Strategies for AC and DC Microgrids," *Energies*, vol. 10, no. 1, p. 91, Jan. 2017.
DOI: 10.3390/en10010091

[J4] E. Unamuno and J. A. Barrena, "Hybrid ac/dc microgrids—Part I: Review and classification of topologies," *Renew. Sustain. Energy Rev.*, vol. 52, pp. 1251–1259, Dec. 2015.
DOI: 10.1016/j.rser.2015.07.194

[J5] E. Unamuno and J. A. Barrena, "Hybrid ac/dc microgrids—Part II: Review and classification of control strategies," *Renew. Sustain. Energy Rev.*, vol. 52, pp. 1123–1134, Dec.

2015.
DOI: 10.1016/j.rser.2015.07.186

Book Chapters

[B1] E. Unamuno and J. A. Barrena, "Hybrid AC/DC Microgrid Mode-Adaptive Controls," in *Development and Integration of Microgrids*, W.-P. Cao and J. Yang, Eds. InTech, 2017, pp. 255–273.
DOI: 10.5772/intechopen.69026

Conference Papers

[C1] E. Unamuno, M. Amin, A. Rygg, M. Molinas and J. A. Barrena, "Impedance-Based Stability Evaluation of Virtual Synchronous Machine Implementations in Converter Controllers," in *International Power Electronics Conference IPEC-Niigata 2018 -ECCE Asia-*, 2018.
→ **Under revision**

[C2] E. Unamuno and J. A. Barrena, "Design and Small-Signal Stability Analysis of a Virtual-Capacitor Control for DC Microgrids," in *2017 19th European Conference on Power Electronics and Applications (EPE'17 ECCE Europe)*, 2017.
DOI: 10.23919/EPE17ECCEEurope.2017.8098923

[C3] J. Paniagua, E. Unamuno, and J. A. Barrena, "Experimental Test Bench for Testing DC Microgrid Control Strategies," in *2017 IEEE International Workshop of Electronics, Control, Measurement, Signals and their application to Mechatronics (ECMSM)*, 2017, pp. 1–6.
DOI: 10.1109/ECMSM.2017.7945872

[C4] E. Unamuno and J. A. Barrena, "Equivalence of primary control strategies for AC and DC microgrids," in *2016 IEEE 16th International Conference on Environment and Electrical Engineering (EEEIC)*, 2016, pp. 1–5.
DOI: 10.1109/EEEIC.2016.7555729

[C5] E. Unamuno and J. A. Barrena, "Primary control operation modes in islanded hybrid ac/dc microgrids," in *IEEE EUROCON 2015 - International Conference on Computer as a Tool (EUROCON)*, 2015, pp. 1–6.
DOI: 10.1109/EUROCON.2015.7313681

Tutorials

[T1] J. A. Barrena, G. Abad, J. J. Valera-García, E. Unamuno, and A. Alacano, "DC distribution grids: Providing comprehensive tools for a more efficient and reliable design," in *2017*

19th European Conference on Power Electronics and Applications (EPE'17 ECCE Europe), 2017[13].

1.5 Thesis Outline

Figure 1.9 depicts the structure of the thesis showing how the proposed objectives and contributions relate to each chapter.

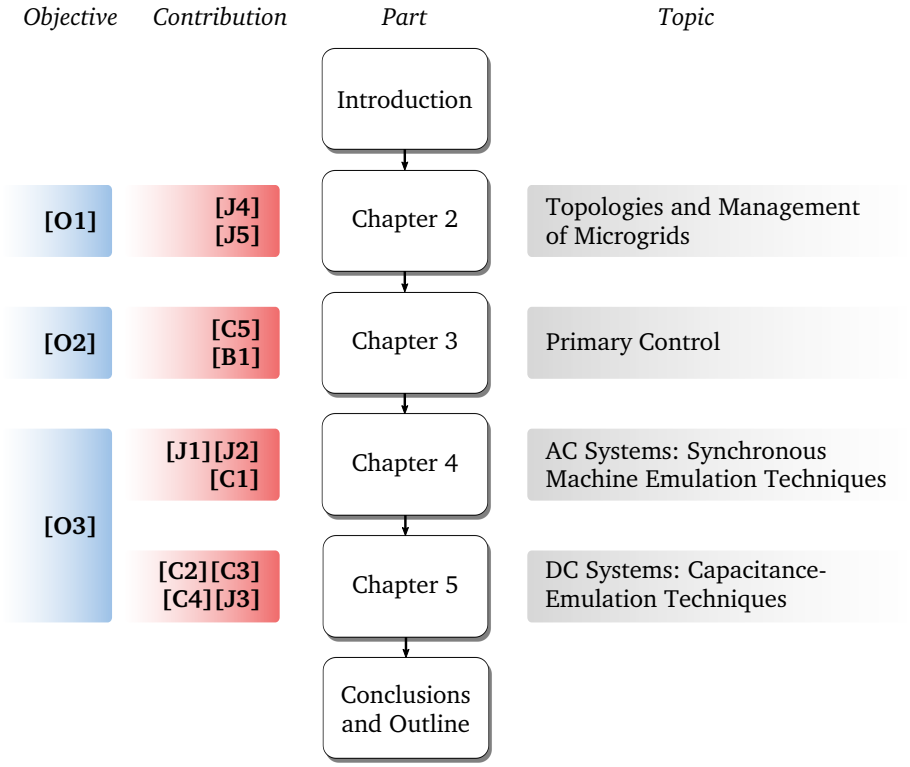

Figure 1.9: Structure of the chapters of the thesis and their relation to the specific objectives and main contributions.

As illustrated in the figure, the aim of **Chapter 2** is to carry out a revision of some of the most relevant topologies and management strategies related to microgrids. In the first part of this chapter we elaborate a more in depth study of the configurations of microgrids in terms of the nature of their current, highlighting their main advantages and drawbacks. Similarly, in the second part, we revisit hierarchical control structures—which are widely employed at classical ac grids—showing some of the most interesting approaches at each control level. In this chapter we pay special attention to distributed control techniques that do not require any communication infrastructure, as they are the basis for the strategies studied in the thesis.

In **Chapter 3** we focus on primary controllers and their modes of operation depending on

[13] http://www.epe2017.com/public/userfiles/epe2017/tutorials/docs/T8-DC-Distribution-Grids.pdf

the type of system they are controlling—generation, energy storage, loads, etc. The study carried out throughout this chapter is a generalization of mode-adaptive controllers considering all the agents that could participate in the regulation of a hybrid ac/dc grid and their different roles in the primary regulation of the grid.

Our purpose in **Chapter 4** and **Chapter 5** is to focus on control techniques below primary regulators—i.e. low-level strategies—that contribute in the inertial response of converter-dominated microgrids. Unlike primary control techniques—which can be similarly applied to ac- or dc-based devices—low-level regulators are dependent on the nature of the current. For this reason, we focus **Chapter 4** and **Chapter 5** on the analysis of techniques oriented to ac and dc microgrids, respectively.

In **Chapter 4** our purpose is to study the behaviour of synchronous machine emulation (SME) techniques for power converters—which reproduce some characteristics of classical synchronous generators—in terms of performance and stability when connected to the grid.

Based on the previous study, in **Chapter 5** we carry out an analysis highlighting some of the most important analogies of ac and dc grids. This equivalences are employed afterwards to propose low-level control techniques for dc microgrids that reproduce the same principles of operation of SME strategies and classical synchronous generators. In this chapter we also analyse the dynamic behaviour and stability of the proposed controllers.

In the last part of the thesis, **Chapter 6**, we collect some of the most relevant remarks and propose different research lines following the work done throughout the thesis.

Chapter 2

Topologies and Management of Microgrids

The operation principle of microgrids—and electrical grids in general—is tightly influenced by their topological structure and the management strategy that is employed. Therefore, this chapter aims to review some of the most interesting configurations and control methods typically employed in the literature.

Topologies are mainly studied in terms of the nature of the current flowing through the power lines, i.e. ac, dc or hybrid ac/dc. In addition, we include a brief discussion about hybrid ac/dc configurations from the perspective of their connection to the main ac grid and the type of connection between their subgrids.

The review about management strategies is focused on hierarchical structures inspired by classical grids. In this part we pay special attention to the role of each device in the regulation of frequency and/or voltage, as it will be basis for the rest of chapters of the thesis.

2.1 Topologies

One of the most important factors that defines the way a microgrid operates is its configuration or topology. As it happens with classical electric grids, there is a wide variety of possibilities to define the configuration of microgrids depending on the scale or the requirements of the application, for instance:

- *Current nature:* ac, dc or hybrid ac/dc.
- *Grid coupling:* galvanic isolation, decoupling of ac subgrids, power flow management capability.
- *Connection configuration:* radial, ring, meshed.
- *Link configuration:* single-/three-phase, monopolar, homopolar, etc.
- *Type of construction:* overhead, underground.

Among these factors, one of the most important ones is the nature of the current flowing through the microgrid. Not only does it define the way power is transmitted, but it also determines the type of devices that have to be employed and the characteristics of the management strategy. In this context, in the following sections we overview some of the most relevant features of ac, dc and hybrid ac/dc microgrids.

2.1.1 AC Microgrids

AC microgrids are by far the most employed topology, as they are the most straightforward solution to integrate DG systems based on the current grid infrastructure. Figure 2.1 illustrates the configuration of a typical microgrid composed by different types of generation, energy storage systems and loads.

One of the reasons for employing ac grids is that since their early stages, several devices have been based on ac and therefore can be directly connected to the grid. A clear example are the classical synchronous generators employed for energy generation in nuclear, thermal or hydroelectric power plants.

The principal advantages of ac grids can be summarized as follows:

- *Voltage level transformation:* the conversion of voltage levels can be easily achieved by the use of transformers. The high maturity of this field has led to very efficient and reliable devices at very low costs, enabling their use in very diverse applications apart from electric grids.

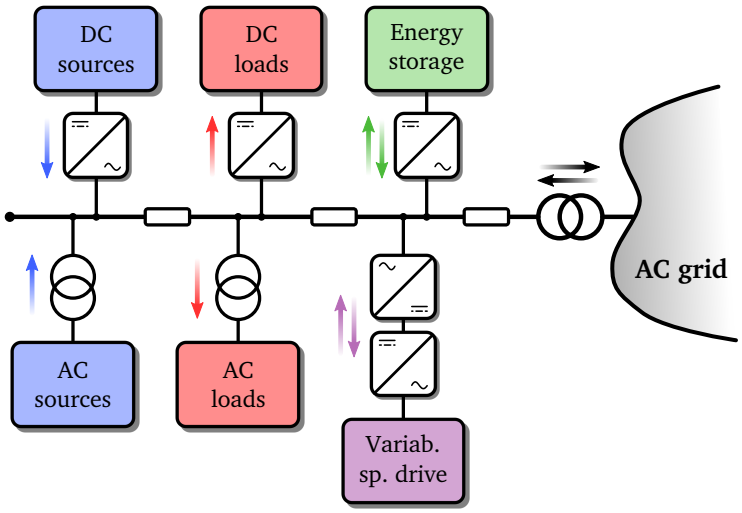

Figure 2.1: Configuration of an ac grid.

- *Protection:* the knowledge gained over the years over ac systems has facilitated the development of different types of protection devices oriented to all kind of applications. Moreover, the zero-crossings of the ac current suppose an advantage in comparison to dc grids, as they allow the opening of faulty lines when the current is nearly zero.

- *Maintenance:* according to Hossain *et al.* the maintenance of ac grids is easier and less expensive than dc ones [10].

- *Inertial devices:* synchronous machines directly connected to ac grids—used either for generating power or as loads—provide inertial response under power perturbations, which improves the dynamic response and hence the stability of ac grids.

2.1.2 DC Microgrids

Even if most distribution grids operate in ac, the evolution of semiconductor technologies and power electronics during the last decades has enabled the use of dc grids as a competitive alternative for the integration of DG systems. Figure 2.2 shows the same type of devices as in the previous section connected to a dc microgrid.

The main reasons for considering the use of dc grids instead of classical ac ones are summarized below:

- *Integration of devices:* in the last decades the number of devices based on dc or that require a dc stage—e.g. photovoltaic based DG, li-ion batteries or supercapacitors, LED lighting or variable speed drives—has increased significantly. By employing dc grids the quantity of ac-dc conversions are reduced, providing a more efficient and robust way of integrating DG, ESS or loads.

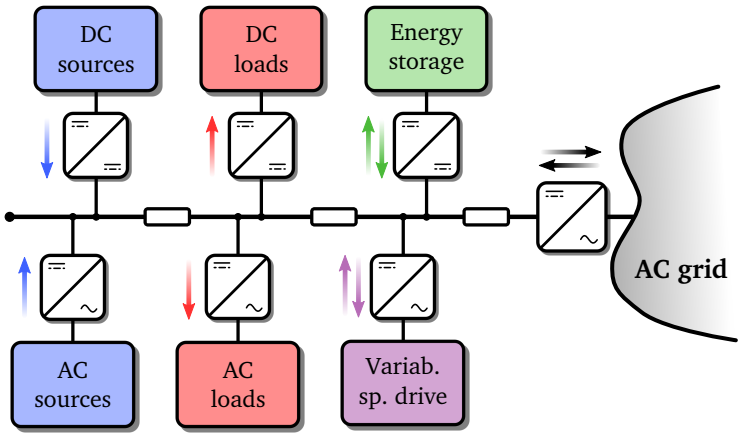

Figure 2.2: Configuration of a dc grid.

- *Synchronization:* unlike at ac based distribution networks, in dc there is no need to synchronize the output current of devices before being connected to the grid. The lack of synchronizing algorithms in the controllers such as phase-locked loops (PLLs) simplifies the control and reduces the risk of a system becoming unstable under certain grid conditions [11, 12].

- *Reactive power:* as the current circulating in this kind of grids is dc, there is no reactive current, which means no reactive power circulation. This is directly reflected in the overall efficiency of the system, as electrical losses are reduced. Moreover, there is no need to include additional regulators in the control strategies of devices connected to dc grids, simplifying their design and dynamic behaviour.

- *Power transmission capacity:* usually ac cables must be designed for the peak voltage value, but the transferable power is determined with the root mean square value of this voltage. This is $\sqrt{2}$ times less power that if we employed dc current, so at a dc microgrid we could either transfer more power in a conductor of the same diameter, or reduce the size of the conductor for the same power transmission.

DC microgrids provide several advantages over ac-based systems and therefore, as we mentioned before, are being already used at different applications such as HVDC links, renewable energy generation park power collectors through MTDC networks or electric traction systems (vessels, trains, elevation, etc.).

However, the substitution of the current grid infrastructure to use a purely dc distribution system would be unfeasible, so the future of the electric grid resides in a combination of ac and dc systems forming a hybrid ac/dc grid.

2.1.3 Hybrid AC/DC Microgrids

Hybrid ac/dc (from now on hybrid) microgrids are an interesting alternative because they enable the integration of dc-based systems through a dc subgrid while maintaining the current ac infrastructure. By doing this, the advantages of ac as well as dc grids can be combined towards an efficient and reliable integration of DG systems. In Figure 2.3 we have integrated the same devices as in the previous sections in a hybrid microgrid to illustrate a typical configuration.

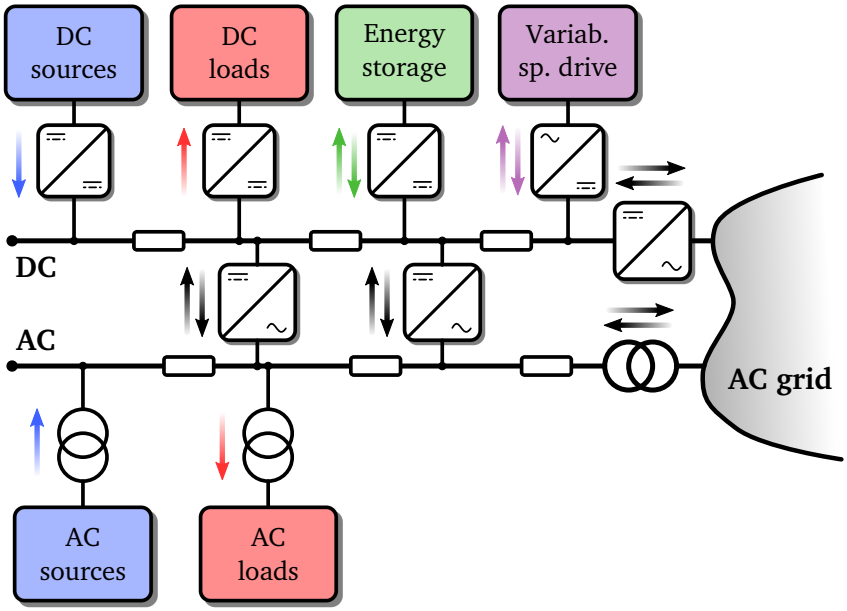

Figure 2.3: Configuration of a hybrid ac/dc grid.

In addition to the particular advantages of ac or dc microgrids, hybrid ac/dc systems improve even more the integration of ac- or dc-based devices, because they are directly connected to the network with the minimum number of interface elements, reducing the conversion stages and therefore the energy losses. Moreover, the integration of interlinking ac-dc converters through the grid increases the degrees of freedom in the management and regulation of the overall grid, enabling the active control of power flows—which cannot be done with passive low-frequency transformers—and providing auxiliary services such as dynamic response support, active fault management, and power quality or stability improvement.

Configurations of Interlinking Converters

Hybrid microgrids can be further classified depending on the type of connection of interlinking converters with the main ac grid and between ac and dc subgrids [J4]. As summarized in Figure 2.4, these connections can be divided into two main subgroups, namely coupled and decoupled configurations. The former correspond to hybrid microgrids whose ac subgrids are

connected through a transformer to the main ac grid, whereas the latter refers to topologies whose ac subgrids are decoupled via power converters—which would enable for instance the interconnection of asynchronous ac grids.

Moreover, these connections can be subdivided depending on whether they are completely or partially isolated from the main grid through a transformer and the stages of the power converter.

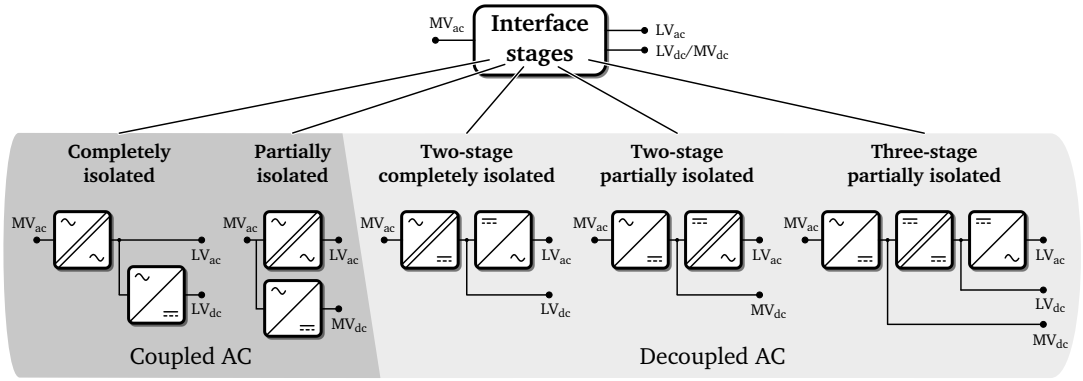

Figure 2.4: Hybrid ac/dc microgrid interconnection types.

For a thorough analysis of these topologies and the advantages and drawbacks of each one we refer the reader to the review we carry out in [J4].

2.2 Management Structures

As demonstrated in the previous section, the structure of microgrids can be very different depending on the application or the scenario where they operate, and so can be their management structure [J5]. At classical grids, distributed systems are equipped with local controllers to provide certain functions predefined by the manufacturer, such as constant power supply/-demand or maximum power point tracking (MPPT) to extract as much energy as possible from sources.

Taking into account that the operation of microgrids depends on these distributed systems, their controls need to be more advanced compared to conventional devices. In this context, the management and control of microgrids is a challenging field that is being widely researched, and a vast number of publications can be found in the literature as previously shown in Figure 1.5.

Identifying and classifying the strategies adopted by most authors is a challenging task, but many times they can be represented in a hierarchical structure, similar to the one employed in classical grids [13, 14]. Hierarchical strategies are composed by various cascaded control levels—i.e. low-level, primary, secondary and tertiary—which are responsible for different functions in the management of the grid (Figure 2.5).

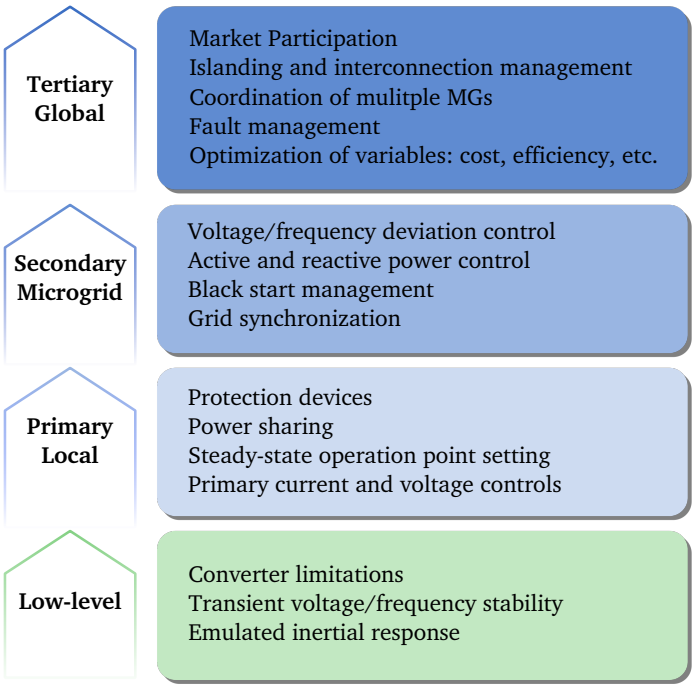

Figure 2.5: Main functions of the control levels of a hierarchical control architecture.

The dynamic behaviour of each level in a hierarchically-controlled microgrid can be observed in Figure 2.6 for a perturbation in the grid.

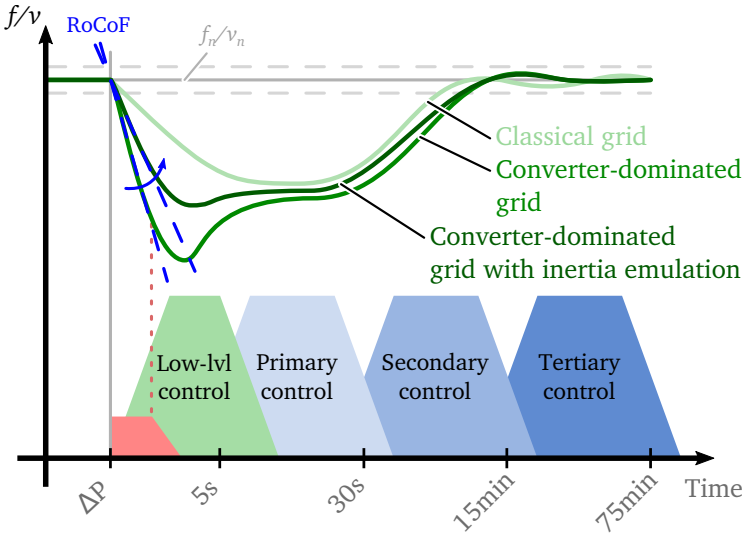

Figure 2.6: Participation of inherent inertia and the hierarchical control in the regulation of frequency at a microgrid.

Based on this structure, we have carried out a classification and analysis of the most interesting techniques that are used in the literature at each control level [J5].

In Figure 2.7 we illustrate this classification and we highlight in red the approaches in

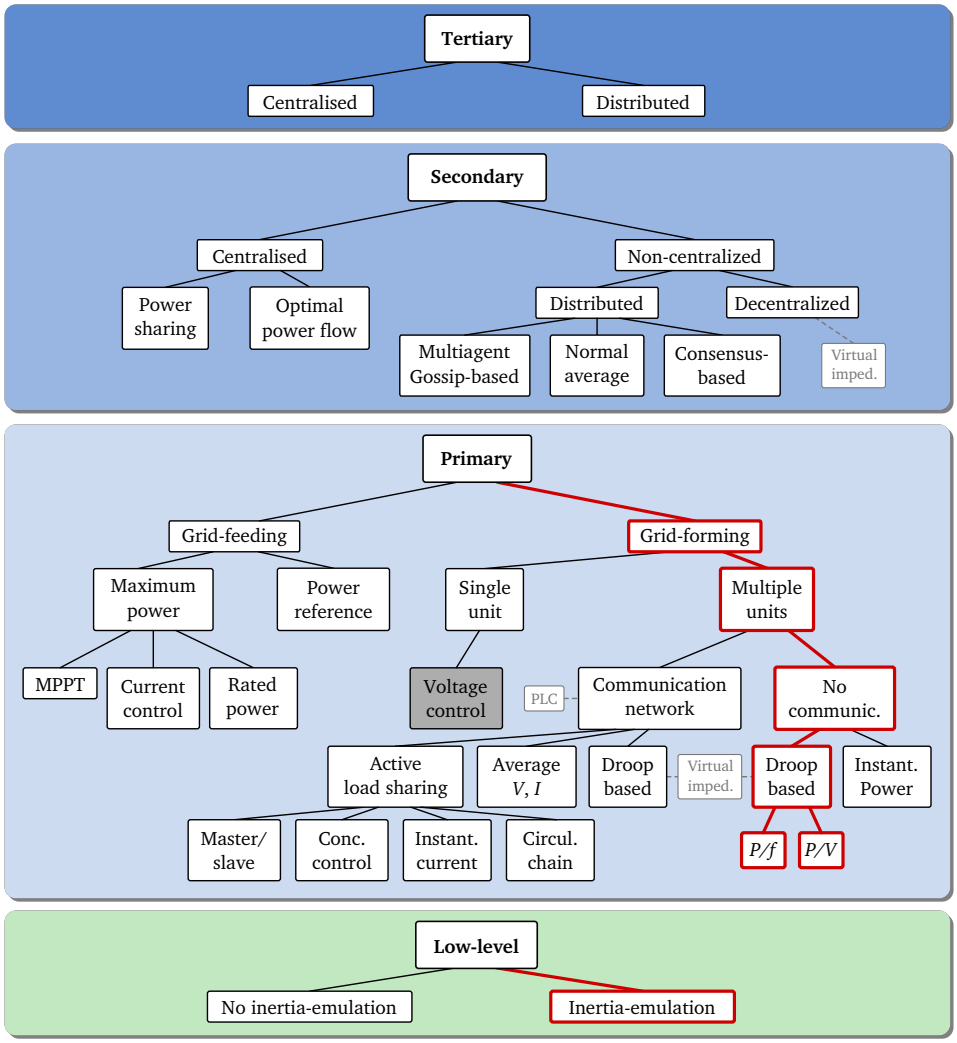

Figure 2.7: Classification of microgrid control strategies based on a hierarchical structure. The techniques highlighted in red denote the focus of this thesis.

which this thesis is focused.

In the following sections the characteristics of these control levels are addressed and the features of some of the specific techniques are analysed.

2.2.1 Low-level control

Low-level control techniques are completely dependent on the nature of current of the system that is being controlled, but generally we can follow two main approaches in its design.

In the classical approach, where there is no emulation of inertia, this control stage is composed by one or more cascaded proportional-integral (PI) regulators that are tuned to follow the reference value provided by upper-level controllers, e.g. a voltage or a power reference. In this case, the regulators do not provide any inherent response over variations in the grid,

and are mainly designed to control the system so that it reaches the reference value as fast as possible. Blaabjerg *et al.* and Palizban *et al.* review in [15] and [16] some of the most relevant low-level control strategies for DG systems connected to ac grids, respectively. In these studies, control techniques are distinguished based on their control reference frame type: synchronous (dq), stationary ($\alpha\beta$) and natural (abc). In the case of dc grids, the classical control is more simple because the variables to be controlled are not rotating vectors.

Apart from these, other approaches have been recently proposed where lower-level regulators are designed to provide a certain inertial response—i.e. transient response—under voltage and frequency variations. These regulators are designed to mimic the behaviour of classical synchronous generators through power converters that control DG, ESSs and loads.

In the case of ac-based grids, SME techniques such as virtual synchronous machines (VSMs) or synchronverters have been widely employed for different applications [17–23]. By integrating electromechanical models of synchronous machines in the control strategies, this inertial response can be provided. In addition, some types of SME techniques are self-synchronized and hence do not require any PLL, which improves the overall stability of the controlled system [11, 12]. Other very recent techniques for providing inertial behaviour through power converters are virtual-oscillators, which consist of implementing the differential equations of non-linear oscillators in the control strategy [1, 24, 25].

Regarding dc grids, the studies we carry out in [C2], [J3] and [C4] show that a similar response to VSMs in ac systems can be emulated by employing virtual-impedances in the control strategy. In this case, instead of controlling the frequency as in VSMs, the variable we control is the voltage in order to emulate the behaviour of a capacitor connected to the bus.

The detailed analysis of techniques that provide inertia emulation is one of the main contributions of the thesis, and is covered in Chapter 4 and Chapter 5 for systems connected to ac and dc microgrids, respectively.

2.2.2 Primary control

The main purpose of primary controllers is to set the steady-state operation point of power converters connected to the microgrid. Due to the dispersed nature of microgrids, primary controllers are usually autonomous and operate based on local measurements of the device they are controlling. Moreover, primary controllers do not vary depending on the nature of the current of the microgrid, which means that unlike low-level techniques, primary controllers can be equally employed for ac or dc systems.

In the literature there are different approaches to distinguish the types of primary controllers. Some authors separate them in three main groups, namely **grid-forming**, **grid-following** and **grid-supporting** controllers [26, 27]. According to these authors, the roles of each type are as follows:

- *Grid-forming:* they establish the frequency/voltage of the grid to a predefined value. An example of this type of controller would be a voltage control with PI regulators or a classical droop controller as will be shown afterwards.

- *Grid-following:* they do not contribute in the frequency/voltage regulation of the microgrid and operate based on the reference provided by an upper control level or based on a reference internally calculated.

- *Grid-supporting:* they contribute in the regulation of the bus frequency/voltage and share the power deviations occurring in the microgrid to decrease bus variations.

Other authors simplify this classification by reducing the number of primary control strategies to **grid-forming** and **grid-following** ones [28]. In this case, grid-supporting strategies are integrated in these two groups because they can be employed either at systems that *follow* the grid with a synchronizing algorithm or at devices that establish or *form* the grid. For the sake of simplicity, in this thesis we follow this second classification.

Grid-following control

Classically, most of the systems that do not include a synchronous generator directly connected to the grid have been controlled by grid-following techniques, because the voltage and frequency is already established by these rotating generators.

Grid-following techniques do not react over frequency or voltage deviations, which means they do not participate in the primary regulation, and carry out other functions for instance to extract as much power as possible from energy resources—e.g. MPPT mode in wind turbine or photovoltaic systems, rated power operation in diesel/biomass generators, etc. [28].

Other approaches include non-optimal points of operation—out of the maximum power range—for example when the references are set by upper control levels. Usually the purpose of this approach is to optimize the power sharing strategy of the network [27].

Grid-forming control

At grids dominated by power converters the capacity to carry out the primary regulation is significantly reduced, requiring the participation of power converters in the regulation of voltage and frequency to ensure an adequate operation. This primary reserve can be either positive or negative, and is provided by employing grid-forming control techniques.

Depending on the type and scale of the application and its requirements, the systems connected to the microgrid might have different modes of operation [28]. For instance, the voltage and frequency of the microgrid can be regulated either by a single converter or by multiple converters connected in parallel.

At low-scale applications where power variations are low compared to the rated power, a usual approach is to employ a single converter that establishes the frequency and voltage of the grid—i.e. in grid-forming mode—while the rest of devices remain in grid-following mode. This grid-forming unit can be controlled either as a voltage-controlled voltage source or with a droop controller. In the former the frequency and voltage are tightly controlled to a predefined value that does not depend on power variations in the microgrid—making very difficult the addition of more grid-forming converters in parallel. In the latter, a droop slope defines the steady-state value of the power to be supplied or absorbed depending on the frequency and voltage deviation in the microgrid and the rated power of the device. This second approach has been widely employed for the parallel interconnection of grid-forming converters and will be explained more in detail afterwards.

In many cases a single grid-forming unit is not sufficient to handle the power variations of the system and therefore multiple devices need to contribute in the primary regulation—i.e. a system composed by multiple grid-forming units. Some clear examples are converter-dominated electric grids, critical applications where reliability and redundancy of devices is fundamental—e.g. aircrafts or vessels—or power converters with multiple branches in parallel.

Approaches under this category can be distinguished depending on whether converters carrying out the primary regulation in parallel are interconnected by a communication network or not [14, 29, 30].

- *Communication between devices:* these strategies are usually based on active load sharing, and include master/slave, central or concentrated control, instantaneous current sharing or circular chain approaches, among others [16, 30]. The main disadvantage of these techniques is that the communication network can become extremely complex in highly extended microgrids, and it can cause failures in the control strategy if any part of the network has a fault, which makes the system vulnerable. Moreover, *plug-and-play* capability is not ensured, which complicates the integration of newly integrated devices.

  There are other solutions where communication between grid-forming devices is employed but no communication network is necessary. These approaches are based on the communication through the power lines of the microgrid, which is also known as power line communication (PLC) or power line signalling (PLS). An example of this strategy can be observed in [31], where signals of different frequencies are sent through the power line so as to synchronize the converters connected to the grid. Although this strategy does not require any additional communication network, the control signals that circulate through the microgrid pollute the voltage and frequency of the networks. Moreover, the integration of new generation or storage units in the microgrid is more complex as the range of frequencies where the signals can be injected is reduced when the number

of devices already connected is high.

- *No communication:* droop control, which is a proportional (P) type of control, is one of the most employed and studied strategies where no communication between devices is required [30, 32–36]. This technique has been originally used in the control of synchronous machine based generators because of its simplicity to share power perturbations between all the parallel generators carrying out the primary regulation. During the last decade, a lot of research effort has been focused on adapting this method for the control of microgrids due to the advantages it provides over other control alternatives: *plug-and-play* capability, power sharing, less faults due to the lack of a communication network, control simplicity, etc. Basically, the purpose of droop control is to proportionally vary the power references of the device depending on the grid side frequency and voltage deviations—i.e. based on local measurements. This way the power sharing between devices is carried out autonomously.

  Under this category, Guerrero *et al.* propose in [13] some primary droop-based control strategies for ac and dc microgrid architectures. According to the authors, even if conventional droop techniques have several advantages over other alternatives, they also present some drawbacks: no capability for non-linear load sharing, load-dependent frequency deviation or a trade-off between the voltage regulation and the current sharing between the converters, among others.

  In this context, Bidram and Davoudi also carry out an extensive comparative evaluation of several droop control strategy variants for ac microgrids, and collect their most relevant advantages and disadvantages [14].

  Although the above-mentioned studies focus on ac or dc microgrid droop controls independently, they can be also implemented in hybrid microgrids with slight modifications. As an example, Loh *et al.* and Baharizadeh *et al.* combine both strategies for their operation in a hybrid microgrid by the use of interlinking converters [33, 37].

  The modes of operation of droop-based control techniques of devices connected to microgrids is discussed more in detail in Chapter 3.

  Virtual-impedances

  In order to enhance the behaviour of droop-based techniques, many authors introduce the concept of the virtual-impedance in the control strategy [13, 38]. These virtual-impedances are control tools mainly used to provide active stabilization and disturbance rejection or to provide ancillary services to the microgrid.

  Shi *et al.*, for example, introduce an adaptive virtual-impedance in the control strategy in order to perform the voltage and frequency regulation of the ac microgrid [39]. Moreover, Li and Kao use a virtual-impedance in order to decouple the control of the

active and reactive power of converters, and they state that the reactive power control and sharing accuracy is significantly improved [40].

An ancillary service provided by virtual-impedances can be to avoid circulating power flows between converters connected in parallel, as studied by Kim *et al.* in [41] or by Zhang *et al.* in [42]. The latter study, for example, contemplates the interconnection of six three-stage solid state transformer (SST) converters in parallel, and employs an adaptive virtual-impedance to mitigate currents circulating between them.

Other ancillary services such as state of charge balancing of ESS [43] or soft-start techniques for wind turbines [13] can be also seen in the literature.

In some cases hybrid control solutions are also used, although they are not as common as the above-mentioned approaches [30]. An example of a hybrid control strategy can be observed in [44], where a communication-based and an autonomous control strategy are mixed. In this case, the autonomous control is used for DG converter blocks that are physically apart, and it is based on the droop control technique. On the other hand, the converters inside each block, which are near to each other, are controlled with a dynamic power distribution technique. The authors state that this strategy improves the system efficiency while ensuring balanced power sharing.

2.2.3 Secondary control

As we have shown previously, the primary control level handles power disturbances by sharing them among the grid-forming units and defines the steady-state point of operation of each device. Despite the simplicity of this regulation, depending on the control type employed—e.g. droop control—the frequency and voltage of the grid might stabilize at a point different from their rated value. The main purpose of the secondary control level is to recover the frequency and voltage, reducing their deviations towards zero [13, 45]. This regulation is carried out at a slower time-scale so that secondary and other control levels do not interact dynamically and are decoupled in terms of design.

Depending on the architecture and the state of the microgrid, the control levels adopt different grades of responsibility. For instance, when operating in islanded mode, the secondary control strategy is the higher control level in the microgrid, so it must also ensure features such as black-start management and resynchronization on the transition from islanding to grid-tied mode of operation.

Secondary control strategies are primarily categorized as centralized or non-centralized [46–48].

Centralized management

In centralized approaches (Figure 2.8), the management of the microgrid is performed from a central controller located at a single global control level, usually named as microgrid central controller (MGCC). In order to do so, variables such as active and reactive power are collected from DG, ESS and critical loads; moreover, market conditions, security issues and requests coming from upper control units—e.g. the supervisory control and data acquisition (SCADA) of the utility grid—are taken into account [46]. This means that a low-bandwidth communication network links all the hierarchical control levels.

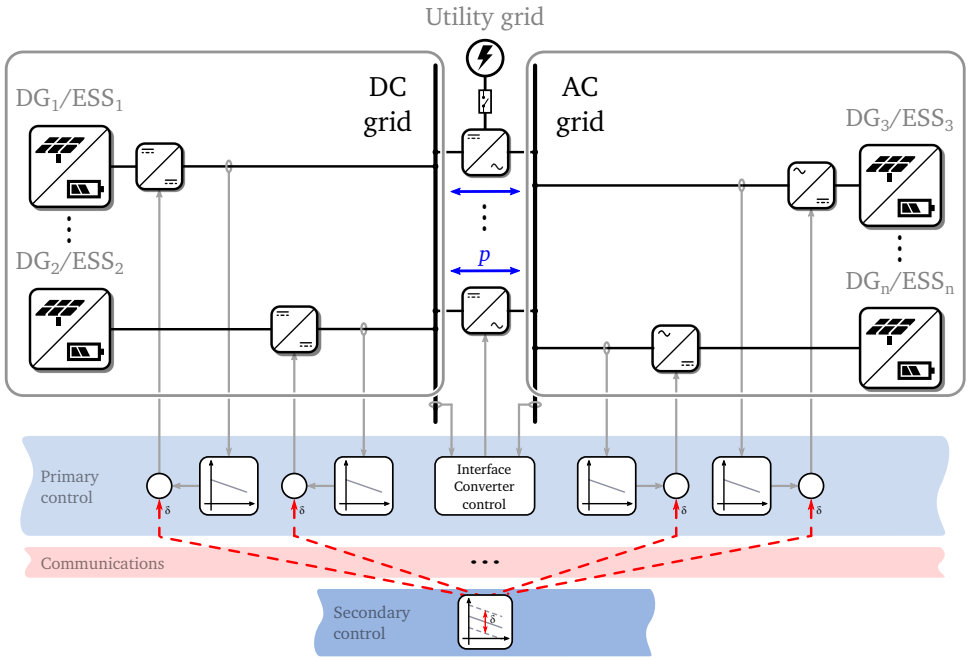

Figure 2.8: Concept of the centralized secondary control.

Centralized control strategies become significantly complex when a high amount of devices are connected at dispersed locations. However, they are suitable for the management of small-scale microgrids where there is a single or reduced number of devices and owners, as they provide high *plug-and-play* capabilities [47].

This type of control compensates the deviations of voltage and frequency based on the references set by the upper tertiary control level when operating in the grid-tied mode. Alternatively, these references are internally generated when an islanding process occurs. The study performed by Guerrero *et al.* in [13], for instance, shows an example of this strategy. A similar approach is proposed by Shafiee *et al.* for dc microgrids in [45]. The authors study the integration of a control strategy that relies on a communication network for a proper operation and power sharing of generation and storage devices. They state that it is not possible to take advantage of this technique when there is an interconnection of microgrids, since power

sharing has to be ensured. Therefore, the adoption of a decentralized strategy is proposed for this operating mode.

Another approach of this control strategy can be observed in [49], where an optimal power flow algorithm is developed in order to find and generate the optimal reference values for voltages and active powers in a dc microgrid.

The integration of a secondary control strategy for the interface converter of a hybrid microgrid can be also seen in [50]. In this approach, Radwan and Mohamed employ a centralized strategy for the control of the interface converter whereas the management of the generation devices located at the microgrid is performed autonomously. According to the authors, the control of the interface converter operates successfully regardless of the mode DG units are managed.

Non-centralized management

In non-centralized control strategies, power management responsibilities recall in generation and storage devices. This means that instead of being implemented in the MGCC, they are integrated in the local controller, avoiding the communication network with upper level control strategies [51]. The main advantage of these management strategies is that in case a fault occurs, the rest of the microgrid can operate normally even if the faulty unit is disconnected.

The non-centralized control approach is envisioned as an attractive approach, as it simplifies the management of microgrids while providing *plug-and-play* connection of devices [47]. In this sense, two main variants can be found; one where a communication network is integrated between neighbour devices, also named distributed control [52], and another where there is no communication between units (DG, ESS, etc.), also known as decentralized control.

- *Distributed secondary control:* this is one of the most studied secondary techniques due to the good performance it provides and the relatively simple communication network it requires (Figure 2.9).

  Yazdanian *et al.* for instance perform a review of some of the suitable solutions—e.g. consensus or agent-based techniques—stating that they provide higher performance over decentralized or centralized approaches thanks to the interaction between units [52].

  Multi-agent systems (MAS) are one of the most typical solutions for the distributed management of microgrids. In this approach, each local controller acts as an agent, making decisions over the parameters of the DG or ESS unit that is controlling. An example of this alternative is explained and developed by Bidram *et al.* in [53] for ac microgrids. The authors propose a droop-based primary control strategy where the reference values are generated based on the parameters of adjacent devices. The validation in this case is performed by simulation, concluding that an adequate voltage control is ensured while

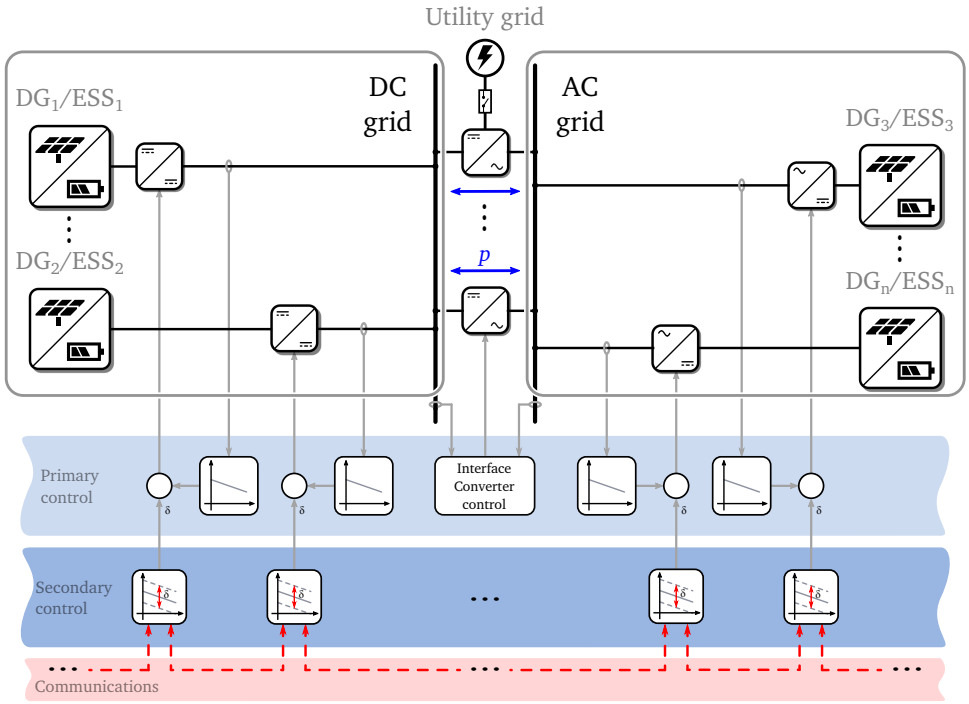

Figure 2.9: Concept of the distributed secondary control strategy.

carrying out a good power sharing between devices. In addition, Liang *et al.* show a MAS-based control algorithm that performs the communication between neighboring devices via wireless connections [54]. The authors state that even if the convergence of the microgrid is slower due to near interferences, this strategy improves previous MAS-based techniques by reducing multiagent coordination errors.

Apart from MAS-based techniques, other distributed strategies have been also identified in the literature. Shafiee, for instance, has proposed in cooperation with several other authors a wide variety of distributed secondary control strategies to provide frequency and voltage deviation controllability while ensuring reactive power sharing [51,55–57]. These strategies are divided into three main groups: normal averaging, gossip-based (a type of MAS technique) and consensus based techniques. As an example, a normal averaging control strategy can be seen in [51], which has been experimentally validated and compared to a centralized control structure afterwards. The conclusions are that a good performance is obtained with this strategy and the communication network is simplified considerably comparing to centralized configurations.

Regarding consensus-based secondary techniques, some examples can be seen in the literature such as the solution proposed by Guo *et al.* in [58]. In this paper, the authors state that this control strategy can restore voltage and frequency to their rated values while the power sharing is ensured between the connected devices.

- *Decentralized secondary control:* these control strategies are more suitable for converter-dominated systems such as microgrids, as they need no communication networks and therefore the *plug-and-play* connection of newly installed units can be guaranteed (Figure 2.10).

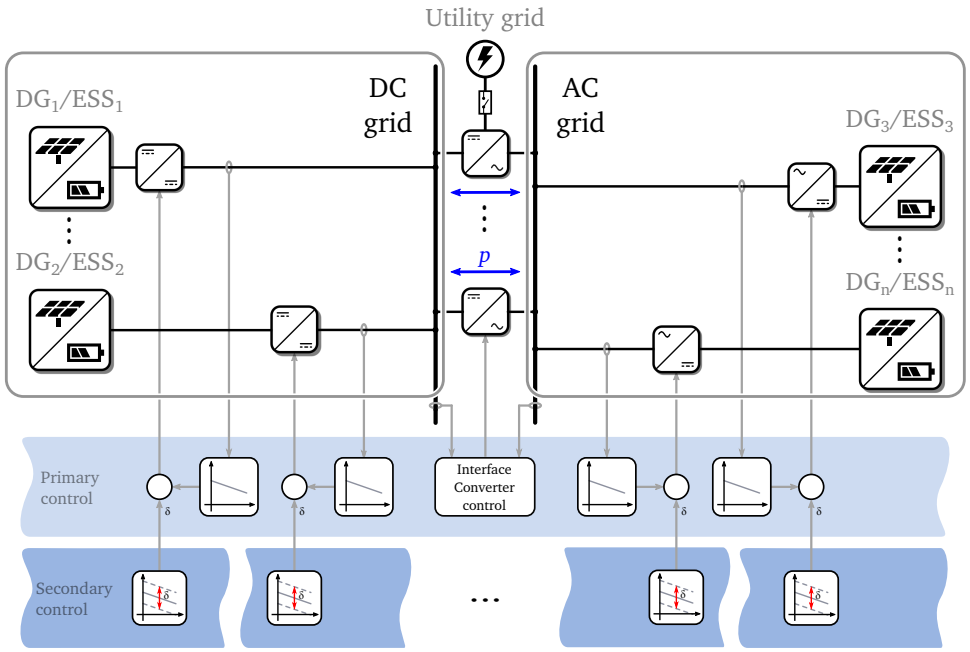

Figure 2.10: Concept of the decentralized secondary control.

Díaz *et al.*, for example, propose a secondary control strategy that merely uses local variables to perform the control of ESS units [59]. The authors mention that with this control technique, which is based on fuzzy inference, it is possible to adequately balance the state of charge of the ESS while ensuring small voltage deviations.

The concept of virtual-impedance has been also used by some authors to provide frequency and voltage compensation without any type of communication between devices [39].

A slightly different approach is employed by Wang *et al.* in [60], where the decentralized control strategy is used to control the DG and ESS systems located at the ac and dc network of a hybrid microgrid.

2.2.4 Tertiary control

When operating in grid-tied mode, the tertiary or global control level manages the active and reactive power flow between the microgrid and the utility grid by regulating the voltage and frequency of the microgrid. Similar to the secondary control level, this can be done in two ways: as a centralized strategy where the tertiary control level is located at the MGCC (which

can be the SCADA system), or employing a distributed technique so that the entire control is carried out locally at each device.

Centralized management

In centralized techniques, power values are measured at different grid nodes and they are compared to the desired values. *P/Q* reference values are obtained based on the power requirements of the microgrid and the market situation—i.e. energy cost, generation, storage and/or load forecasting, etc. This way, different variables can be optimized such as efficiency, economical aspects, control simplicity, power quality, etc.

An example of this control level can be seen in [13], where active and reactive power are compared to the desired values in order to generate the frequency and voltage references for the secondary level. The algorithms have been tested by simulation and show a good performance of the overall control strategy for the islanded/grid-tied modes and the transition between both modes of operation. Moreover, the authors mention that the management of multiple microgrids can be done with the proposed control.

A centralized tertiary control can be also seen in [61] for the energy management of a hybrid ac/dc microgrid. As well as ensuring an adequate voltage control, this strategy takes into account several factors such as the forecast of electricity price, generation and demand power profiles so as to optimize the overall system—grid interaction and ESS/DG interaction. According to the authors, this strategy reduces the operation cost of the microgrid. A similar approach is employed by Shi *et al.* in [62], where an optimal power flow problem is formulated in order to generate the schedule of the microgrid. The results in this case show that the proposed energy management strategy operates successfully in grid-tied and islanded modes.

Distributed management

Although the most common approach is to locate the tertiary control level in the main management structure of the grid there exist some approaches where this controller is deployed in a distributed manner. The authors in [63], for instance, propose a gossip-based tertiary control algorithm that is directly integrated in the local controllers. In addition, all the devices are interconnected via internet, increasing the reliability and efficiency of the system. A similar architecture has been used by Meng *et al.*, where the three hierarchical levels are integrated in the local controller [64]. In this approach, a consensus-based tertiary control strategy has been implemented, and two communication networks have been developed for the adequate operation of the microgrid: one for the communication between consensus-based controls and another one for the primary and secondary levels.

Even if these strategies significantly improve the flexibility of microgrids, the most common trend in the classical grid and the literature related to microgrids is to employ centralized

tertiary control strategies. The main reason is that the coordination of the devices attached to the microgrid is performed based on factors that are difficult to be integrated locally, for example the forecasting of generation and demand profiles, energy flow in the microgrid, energy market situation, etc.

Chapter 3

Mode-Adaptive Primary Control

From the previous chapter it is clear that the control and management of converter-dominated highly-dispersed grids, such as microgrids, is a challenging field that is being widely studied in the literature. We have also highlighted the key role of local controllers in the dynamic regulation of microgrids.

In this chapter our aim is to analyse more in detail droop-based primary control levels (Figure 3.1) from the perspective of the roles they can play in the primary regulation. Our purpose is to generalize this study so that it can be applied to different types of grids—multi-microgrids, hybrid ac/dc microgrids, etc.—regardless of the type of systems they are controlling—e.g. generation, energy storage systems, interlinking converters, etc.

In order to visualize the different modes of operation of these primary controllers, we carry out various simulations at a generic grid-connected hybrid microgrid scenario.

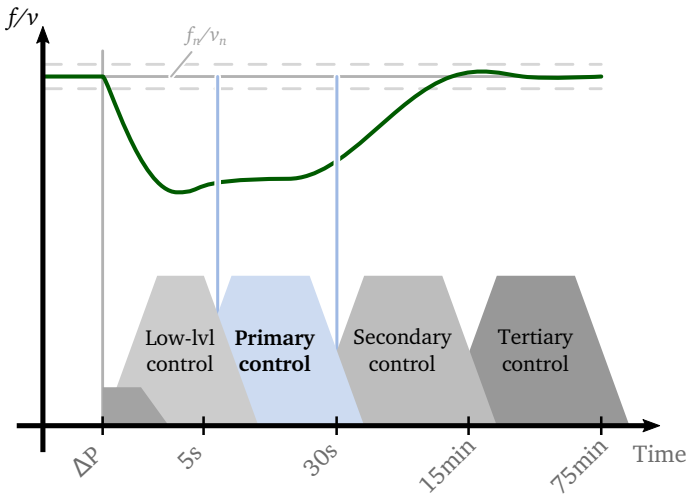

Figure 3.1: Operation range of the primary control in the hierarchical regulation of a microgrid.

In Section 2.2.2 we have shown that primary controllers can be configured to act as grid-forming devices—i.e. participating in the frequency and voltage regulation—or as grid-following devices that do not react over variations in the grid bus. The classical approach has been to define the control method depending on the type of system that is being controlled. For example, generators composed by synchronous machines have been typically equipped with grid-forming techniques, because they are adequate to carry out the regulation of the bus frequency and voltage. Similarly, renewable energy sources (RES)-based generators have been usually controlled with grid-following techniques to extract as much energy as possible via MPPT strategies.

The transition towards converter-dominated grids poses diverse challenges because the participation of these power converters in the primary regulation becomes fundamental to ensure enough primary reserve. This means that, unlike in classical grids, converter-interfaced systems must provide some type of primary regulation.

3.1 Operation modes

Converters interfacing generation, energy storage systems or loads do not have to operate constantly in the grid-forming or grid-following mode. Instead, they can be designed to change their mode of operation depending on some external condition—e.g. a command received from upper control levels or the conditions of the grid. In this sense, this type of strategy is also known as mode-adaptive control in the literature [32, 65].

As aforementioned, the most interesting alternatives for primary controllers are the distributed techniques that operate based uniquely on local measurements [32, 37, 65–68]—e.g. the device terminal frequency or voltage.

Following this concept, Figure 3.2 shows a possible configuration for a droop-based mode-adaptive primary control of the devices that compose a microgrid. We show as an example the controllers of generation, storage systems, loads and the converter interconnecting the microgrid to the main grid. In this case, positive sign means power is injected to the microgrid bus.

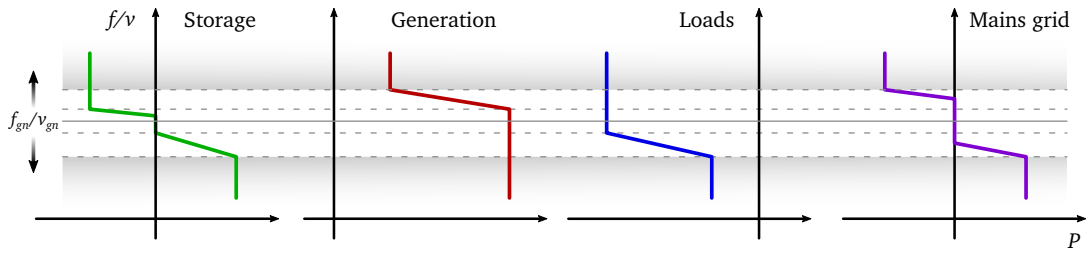

Figure 3.2: Example of adaptive primary controllers for systems connected to a microgrid.

As we can observe, the primary control of each type of device is configured to behave dif-

ferently depending on the value of the voltage or the frequency. At ac microgrids the usual approach would be to employ the grid frequency because it is directly related to the transmission of active power, whereas at dc microgrids we would have to use the bus voltage. In any case, the concept of operation of mode-adaptive primary control remains the same for both current natures.

Although in Figure 3.2 each device type carries out the primary regulation of a certain frequency/voltage range, in a real application the ideal approach would be to mix the type of devices doing the primary control of these ranges. The limits where each system starts participating in this regulation would be determined by grid codes based on different priority levels and market conditions. This way the system would become more robust and stable because power variations would be handled by a higher number of devices with different characteristics and dynamics.

In the following sections we describe the different modes of operation of each type of system that composes a microgrid.

3.1.1 Energy Storage Systems

ESSs are one of the most important agents in the microgrid regulation because they serve as an energy "buffer" to compensate generation and demand deviations during normal operation. We must design and size these systems in order to cope with the most severe conditions of the system; otherwise, a poor regulation would cause the malfunction or disconnection of devices.

Figure 3.3 shows the most important modes of operation of energy storage systems connected to a microgrid. Under a balanced operation (mode ①), the ESS does not exchange any power with the microgrid. This hysteresis range must be carefully determined so as to avoid an excessive cycling—which means ageing—of the ESS, but also to prevent the system from entering into a point of operation that is out of the required boundaries.

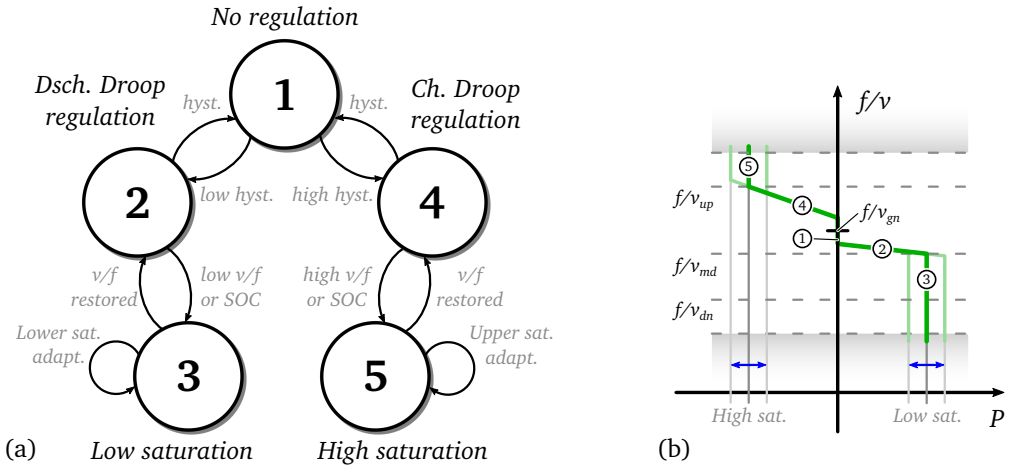

Figure 3.3: ESS primary controller operation modes.

When the generated power is higher than the demanded one the voltage or frequency of the microgrid increases over the hysteresis upper value and therefore the ESS absorbs power according to the charging droop slope (mode ④). This slope depends not only on the charging capabilities of the ESS but also on the sizing of its power converter.

When the voltage/frequency (from now on v/f) of the microgrid increases above the pre-established value or the state of charge (SoC) of the ESS is too high, the device turns to mode ⑤, where the power absorbed from the microgrid is kept constant regardless of the v/f deviation increment. As illustrated in Figure 3.3, if the SoC of the ESS continues to increase while in mode ⑤, the maximum power level value is decreased. The limit of this saturation would be when the SoC is on its upper limit and hence the ESS would not absorb power any more—i.e. the saturation line would be located in the vertical axis.

A similar behaviour is reproduced when there is an excessive demand in the microgrid and the voltage or frequency decrease below the hysteresis lower value (mode ②). At this point, the ESS supplies power to the microgrid according to its discharging droop slope.

The ESS remains in mode ② until the voltage or frequency reach their minimum value or the SoC of the ESS is too low. When any of these conditions takes place, the ESS jumps to mode ③ and supplies a constant power regardless of the v/f negative deviation. As in mode ⑤, the maximum power provided by the ESS will be decreased if the SoC decreases below the predefined levels. At some point, when the minimum SoC is reached, the ESS will not supply more power to the microgrid.

Even though these modes of operation are the most typical ones for ESS, there is an infinite number of possibilities to configure the behaviour of primary controllers depending on the conditions of the grid. For instance, we could design the charging and discharging droop slopes differently, for example depending on the rated charging and discharging current rates of the ESS, respectively.

As an example, Figure 3.4 illustrates three variants of mode-adaptive primary techniques based on the previously mentioned approach.

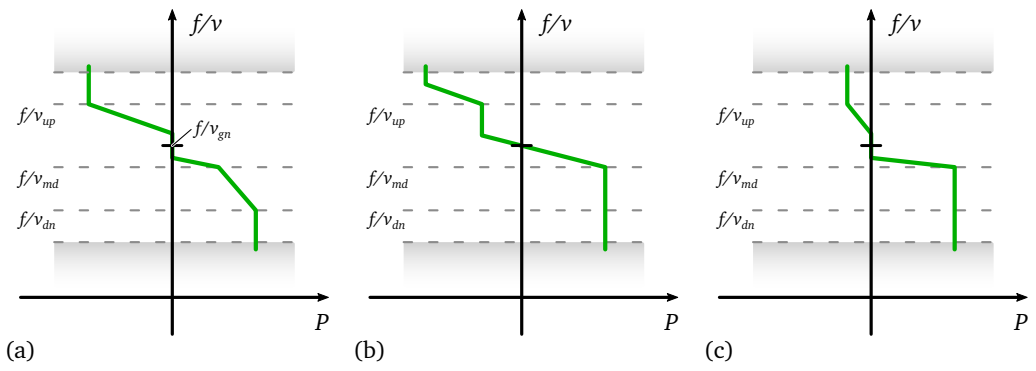

Figure 3.4: ESS primary controller variants.

We can implement different droop slopes in the discharge process (Figure 3.4 (a)), add more hysteresis ranges and a symmetrical droop slope for the charging and discharging stage (Figure 3.4 (b)) or drastically reduce the operation boundaries (Figure 3.4 (c)). Even though we do not mention it in the following sections, similar variants can be employed for other types of devices.

3.1.2 Generation Systems

Generation systems mainly operate in two different modes (Figure 3.5): maximum energy extraction/constant power operation and droop regulation. During normal operation in mode ①, as most DG systems are based on RES, the converters attached to generation systems are controlled to absorb as much energy as possible from energy sources. In the case of other types of DG systems such as diesel generators or classical synchronous generator-based systems, secondary level controllers determine their constant power reference.

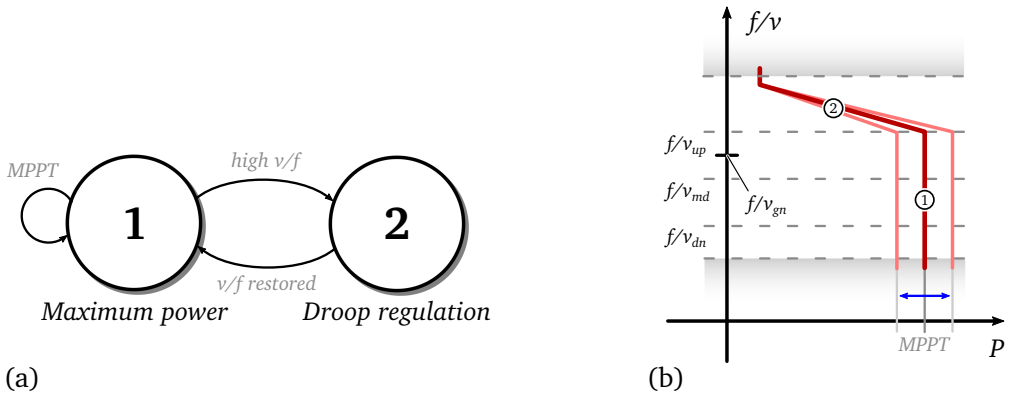

Figure 3.5: DG primary controller operation modes.

When the voltage or frequency of the microgrid increases above the pre-established level, DG systems shift out of their MPP to reduce the power amount they supply to the system. In this mode ②, DG systems contribute in the v/f regulation of the microgrid through a droop slope (Figure 3.5). The saturation point of this slope depends not only on the value of the voltage or frequency, but also on the MPP of the DG system. This means that depending on the available power that can be absorbed from the RES, the controllers will have to adapt their operation characteristics to meet the grid codes predefined by the system operator.

As we have mentioned previously, classically most converters associated to DG systems have been configured to exclusively operate on the MPP. However, the transition towards converter-dominated and distributed electrical systems and the associated regulatory changes will require the participation of these generators in the regulation of the grid.

3.1.3 Loads

Similar to DG systems, load converters operate normally in mode ①, absorbing the power required by the load. When generation systems are producing all the power they can, no power can be absorbed from the main grid, and energy storage systems are not able to provide more power, the voltage or frequency decreases below the predefined level and the power consumed by loads must be consequently decreased (mode ②) to avoid entering into the trip zone. In this case, as with DG systems, the droop slopes as well as saturation values are dependent on the instantaneous load (Figure 3.6b).

In the literature, this type of operation is a part of the so-called demand side management, as the loads actively participate in the regulation of the microgrid by reducing their consumed power when required. A high research activity has been carried out in the last years highlighting the importance of the participation of loads in the management of different types of electric systems [69].

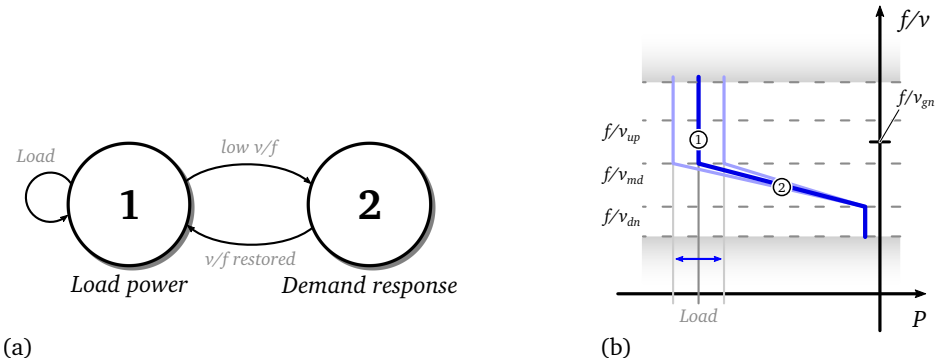

Figure 3.6: Load primary controller operation modes.

3.1.4 Connection to the Main Grid

Depending on the topology and type of microgrid, we can follow different approaches with respect to the connection to the main grid. On a classical approach, the connection to the main grid can be employed to contribute in the regulation of the microgrid for the entire voltage range [J4]. Another solution would be to use the link to the main grid at specific cases where the voltage or frequency levels are above the maximum or below minimum levels, avoiding the malfunction or disconnection of other devices.

Figure 3.7 shows the five main operation states of this last approach; as it can be seen, this link only operates when the v/f levels are out of some predefined values. If the voltage or frequency goes above or below boundaries, we employ the link to the main grid to support the regulation of the system. An example of this situation is an excess of generated energy that causes an increment in the voltage or frequency; as our purpose is to extract as much energy as possible from RES, we could employ the connection to the main grid to send this

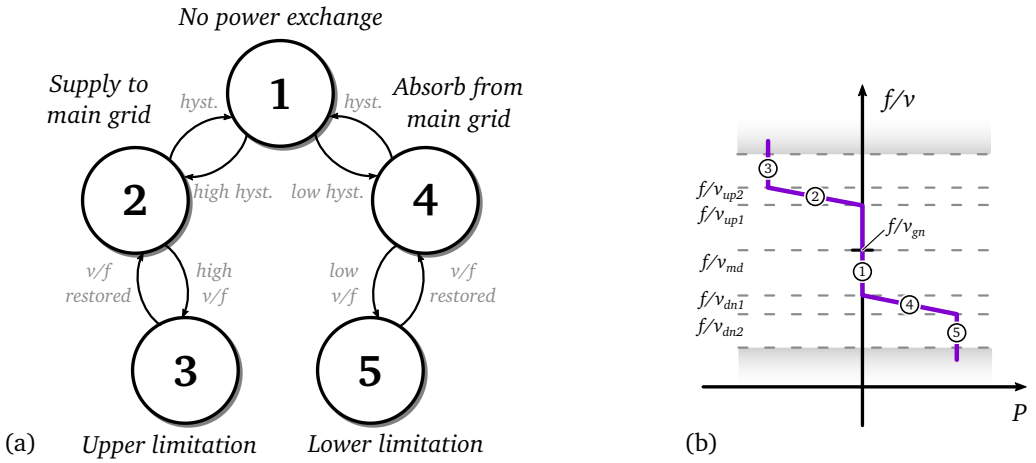

Figure 3.7: Grid connection primary controller operation modes.

extra power to the grid with a droop controller in the mode ② shown in Figure 3.7. Note that in this case, following the notation mentioned at the beginning of the chapter, positive power of the converter connected to the main grid means we are absorbing power from the grid and injecting it in the microgrid bus, and vice-versa.

3.1.5 Interlinking Converters

Interlinking converters located throughout microgrids provide extra degrees of freedom in the management of individual subgrids, as we can control them to carry out diverse operations. The most typical approach would be to employ these converters to compensate the v/f deviations in ac and dc subgrids [C5], [33, 37]. The converters would transfer power from one subgrid to the other in order to equalize the excess of generated or demanded power at both systems. This principle of operation does not have to be exclusively between ac and dc subgrids, as it can be also applied to systems with the same nature of current but different voltage levels or frequency values.

As illustrated in Figure 3.8, interlinking converters might carry out the power transfer between the different subgrids of a hybrid microgrid with a droop controller. Unlike classical approaches, this droop is based on the difference between the frequency deviation in their ac subgrid and the voltage deviation in their dc subgrid.

Whenever there is a mismatch between these deviations, ac-dc converters located in the hybrid microgrid will transfer power to balance them. Modes ② and ③ correspond to the maximum power that ac-dc systems can transfer in both directions.

It has to be mentioned that although interlinking converters and the links to the main grid provide local primary regulation, if we look to the overall picture, they cannot be taken into account as a part of the primary reserve. This is because they do not supply or absorb power from a source or a load, but rather they interchange power between different grids.

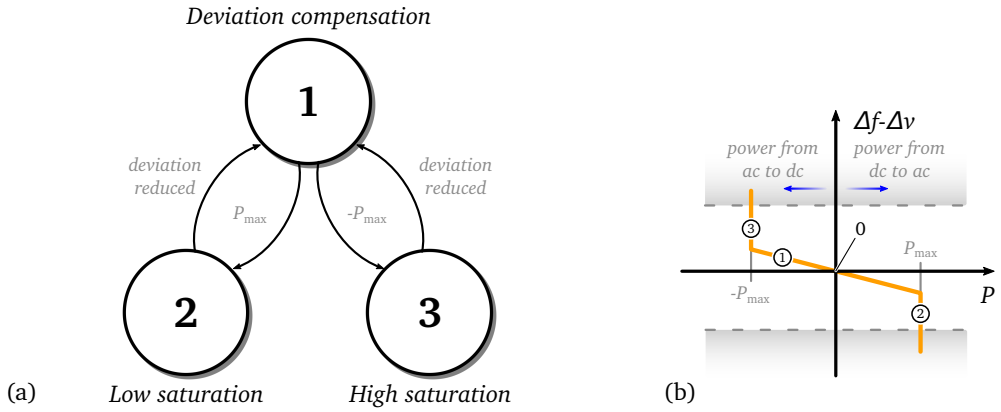

Figure 3.8: Interlinking converter primary controller operation modes.

However, there are some special cases in which these interlinking converters contribute in the primary regulation of their both sides, for instance when one of the subgrids has an exceeding generation of power and an adjacent system has a high demand of power. In this case, interlinking converters contribute in the regulation of both systems by transferring power from one to the other. However, if two subgrids have an excessive demand or generation of power and interlinking converters carry out the deviation compensation, one subgrid will be benefited with the primary regulation whereas the second will suffer a higher deviation.

In this context, and according to the study we have developed in [C5], other techniques can be employed in the control of interlinking converters integrated at microgrids such as state of charge balancing of ESSs or the improvement of the energy quality.

3.2 Simulation Results

In this section the concept of operation of the modes presented in the previous section are verified by simulation at a hybrid ac/dc microgrid scenario composed by an ac and dc subgrid. The simulation environment employed for these tests is Matlab/Simulink®.

3.2.1 Simulation Scenario

The ac and dc subgrids of the hybrid microgrid are composed by a generation system, an energy storage system and a load, and they are linked by an interlinking converter (Figure 3.9). In this case we have also included a connection interface between the subgrids and the main grid to observe their behaviour. As shown in the following sections, the islanded operation is a particular case of microgrids connected to the main grid; the difference is that islanded microgrids do not exchange any power with this grid. Although the following analysis is carried out for a hybrid microgrid, this process can be equally reproduced for other configurations of microgrids, as the modes of operation of primary controllers would be the same.

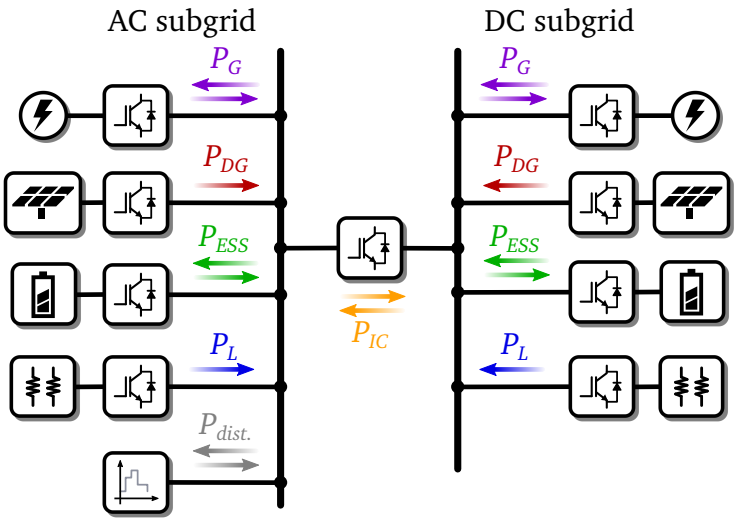

Figure 3.9: Simulated hybrid ac/dc microgrid scenario.

As we want to evaluate the concept of operation of mode-adaptive primary controllers, the simulation models employed in this chapter are simplified and do not consider the dynamics of the inner loop current or voltage regulators.

In order to evaluate the behaviour of the different devices connected to the proposed scenario, we introduce a power disturbance in the ac subgrid of the microgrid. Taking into account that the results would be equivalent if we introduced the disturbance in the dc part, we do not contemplate this case.

Figure 3.10 shows the specific primary control slopes employed for ESSs, DG systems, loads and the connection to the main grid. As the purpose is to validate the operation modes of the different agents participating in the regulation of the microgrid, we have made no distinction in the configuration of systems located in the ac and dc subgrid. The interlinking converter between these subgrids operates reducing their frequency and voltage deviations as shown in Section 3.1.5.

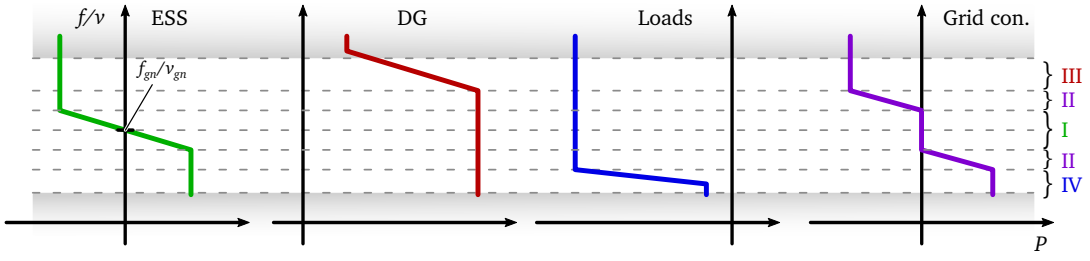

Figure 3.10: Primary controllers of the simulated scenario.

In the proposed configuration, if the demanded and generated power are balanced, all systems remain in an equilibrium state and ac and dc buses remain at their rated values (State 0). When the voltage or frequency are out of their rated values, ESSs carry out the regulation

of the bus based on a predefined droop curve as shown in Figure 3.10 (State I). For simplicity in this case we do not consider any hysteresis operation range.

When storage systems reach their boundary, the microgrid exchanges power with the main ac grid to carry out the primary regulation (State II). For instance, when the voltage or frequency reaches a certain upper boundary, instead of taking DG systems out of their maximum power point, the exceeding power is supplied to the main ac grid. This is a key aspect of systems connected to the main grid because energy from RES is not wasted and could be beneficial from the point of view of the electric market.

A similar situation occurs when the voltage or frequency falls below the limit; instead of reducing the power consumed by loads—that could lead to a malfunction or under-performance of the load—this lack of power is covered by absorbing power from the main grid (State II).

Usually the exchange of power with the main grid is limited—either by technical or economical limitations—so when the voltage or frequency reach the next upper or lower limit, generation systems and loads are employed to contribute in the power regulation. Therefore, State III occurs when the upper boundary is exceeded and DG systems are out of their MPP and controlled by a droop curve to regulate the power they generate. State IV, on the other hand, relates to the situation where loads reduce their consumed power.

On an islanded system, where no power can be exchanged with the main grid, if storage systems reach their upper or lower boundaries of operation, DG systems and loads enter directly in the regulation state. This means there would not be any State II, and the system would directly enter into the State III or IV.

3.2.2 Response Under Disturbances

In order to reproduce the states mentioned in previous sections, we have simulated three different power disturbances. The first two consist of a positive and a negative step-shaped profile, respectively; in the third simulation we have implemented a dynamic disturbance that would be closer to a real system. All the variables of the following simulations are normalized and shown in per unit (p.u.) values to facilitate the analysis [70].

Positive Power Disturbance

The aim of this simulation is to observe the modes of operation of ESS, DG systems and the grid connection for positive power disturbances occurring in the microgrid.

Figure 3.11 shows the most relevant variables of the hybrid ac/dc microgrid during the simulation.

In summary, we illustrate the following parameters:

- *AC subgrid:* we show the frequency of the subgrid and the powers of the DG, ESS, load and the connection to the grid. The sign of powers is determined based on whether

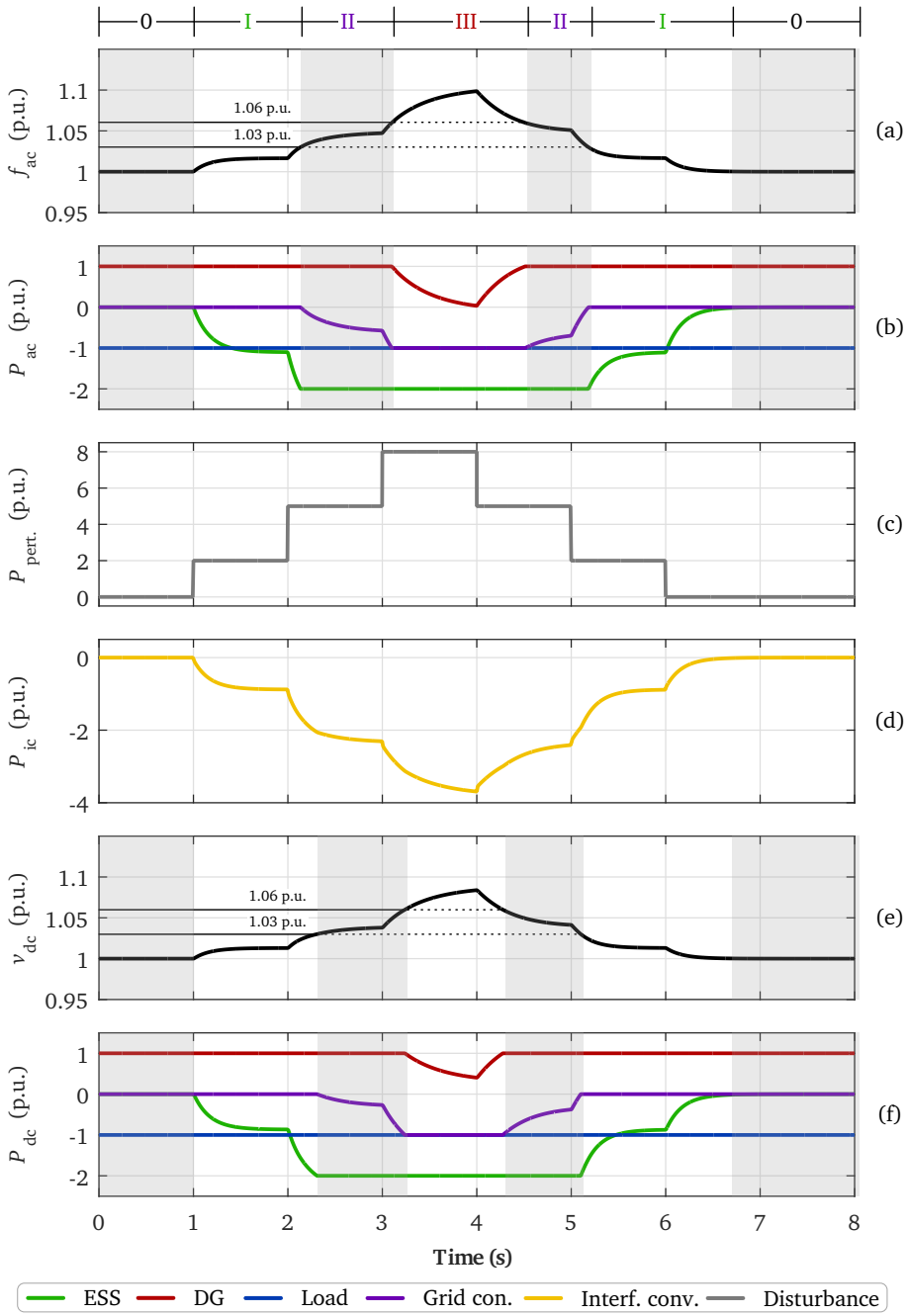

Figure 3.11: Microgrid response under positive power disturbances: (a) ac bus frequency, (b) ac subgrid power values, (c) disturbance power, (d) interlinking converter power, (e) dc bus voltage and (f) dc subgrid power values.

the device supplies (positive sign) or absorbs (negative sign) power from the ac bus. Therefore, the power of DG systems has a positive sign whereas we represent load power with negative sign.

- *Disturbance power:* this disturbance is located in the ac subgrid and its sign is defined as

in the previous point.

- *Interlinking converter:* we illustrate the power transferred between the ac and dc subgrid, where positive sign means the power is transferred from the ac subgrid to the dc one, and vice versa.

- *DC subgrid:* as in the ac subgrid, we represent the voltage amplitude and powers of DG, ESS the load and the connection to the grid. The sign of these powers are determined following the same rule as in the ac part.

In the figure we can distinguish different stages during the simulation, based on the values of the frequency and voltage of the hybrid ac/dc microgrid.

The system begins at an equilibrium state with no power disturbance, which in this case is named State 0. At this stage, the demanded and generated power are balanced so the ac and dc buses remain at their rated values (1 p.u.).

At the instant $t = 1$ s a positive power step is introduced in the ac subgrid and therefore the ESS starts regulating the bus by absorbing power, entering into State I. In this case the interlinking converter transfers power to the dc subgrid so as to compensate v/f deviations in the system, which causes an increment in the bus voltage. Due to this voltage deviation, the ESS located in the dc subgrid begins absorbing the power transferred by the interlinking converter. In conclusion, it can be corroborated that the power disturbance is shared among all the devices carrying out the primary regulation thanks to the control type used in the interlinking converter.

At $t = 2$ s a higher power disturbance is introduced in the system and ESSs continue regulating the bus in State I until they reach their maximum power value. When this boundary is exceeded ($v/f = 1.03$ p.u.), the system enters in the State II and the exceeding power is supplied to the main ac grid.

Similarly, at $t = 3$ s the power disturbance is increased and the microgrid continues supplying power to the main grid in State II until the maximum exchangeable power is reached. After exceeding this limit ($v/f = 1.06$ p.u.), the power supplied to the main grid is fixed and DG systems begin regulating the system (State III).

After the instant $t = 4$ s the disturbance is reverted and the system recovers its original equilibrium state in the opposite sequence.

Negative Power Disturbance

In the following simulation, the main purpose is to observe the mode of operation of loads when lower limits of v/f are reached. Therefore, in this case we have reversed the power disturbance employed in Section 3.2.2 emulating different values of demanded power.

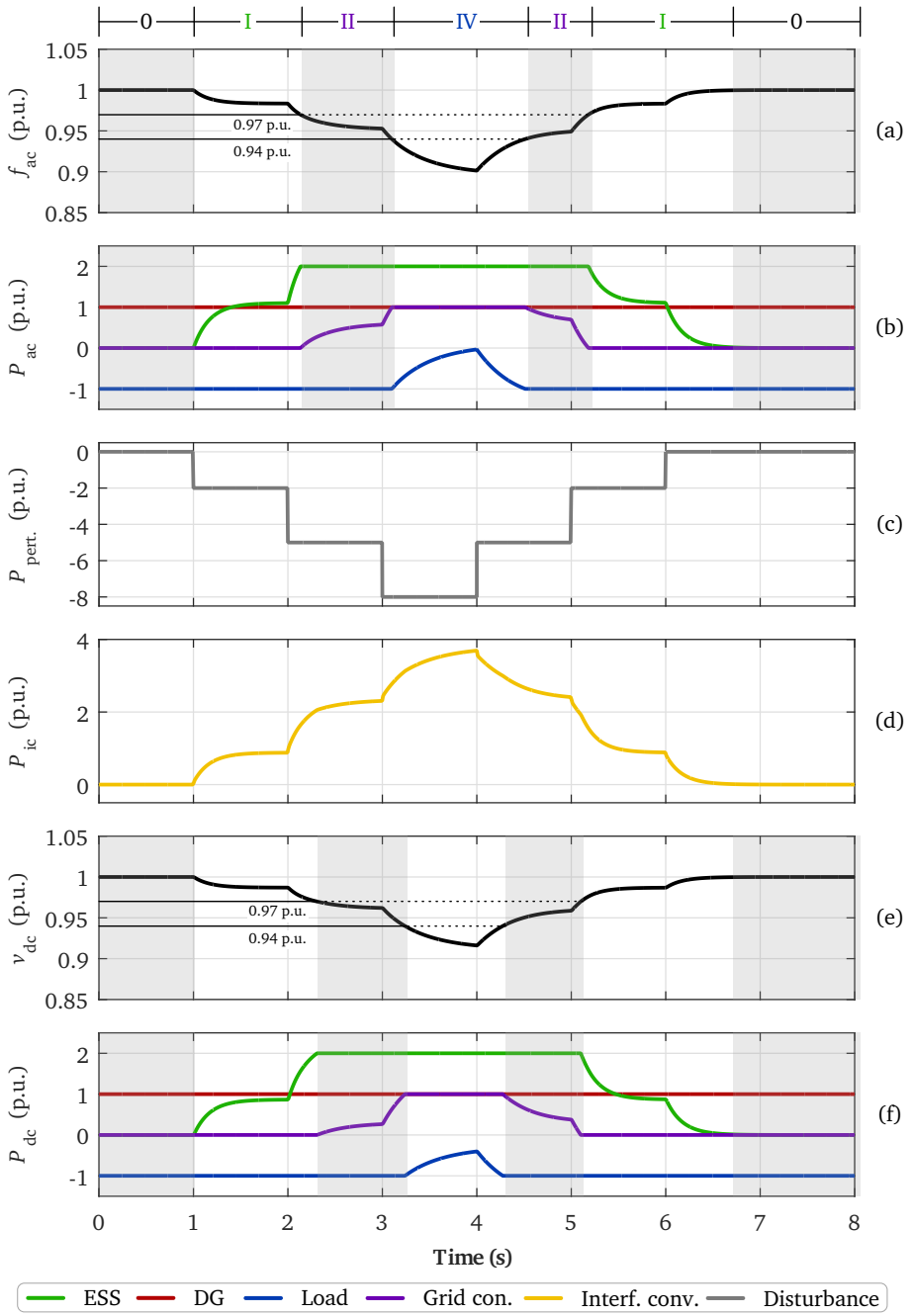

Figure 3.12: Microgrid response under negative power disturbances: (a) ac bus frequency, (b) ac subgrid power values, (c) disturbance power, (d) interlinking converter power, (e) dc bus voltage and (f) dc subgrid power values.

In this case we show again the most relevant parameters of the hybrid ac/dc microgrid (Figure 3.12). As we can observe, the system goes through a very similar process as in the previous case. The difference is that the voltage as well as frequency decrease instead of increasing due to the negative power disturbance.

In this context, the system begins in State 0 at an equilibrium point and enters into State I when the first negative power step is introduced. Afterwards, with the second power step the microgrid reaches the $v/f = 0.97$ p.u. limit and enters into State II, where the lack of power is handled by absorbing power from the main grid. Finally, with the third negative power step the system reaches the $v/f = 0.94$ p.u. limit and, as no more power can be absorbed from the grid, loads begin to reduce their demanded power (State IV).

In the proposed configuration, we can conclude that all the systems attached to the hybrid microgrid participate in the regulation of the system at some extent.

Dynamic Disturbance with Mixed Operation Modes

Although the previous simulations facilitate the analysis of the mode-adaptive control concept, the step-shaped power disturbances do not represent a real variation in a microgrid. In addition, in a more realistic environment the most optimal approach would be to take advantage of the disperse characteristics of ESSs, DG systems, loads and interlinking converters to design a primary control strategy composed by a mix of these systems for the entire v/f range.

In this context, in the following simulation we have modified the droop slopes of the devices connected to the hybrid microgrid so that they overlap as illustrated in Figure 3.13.

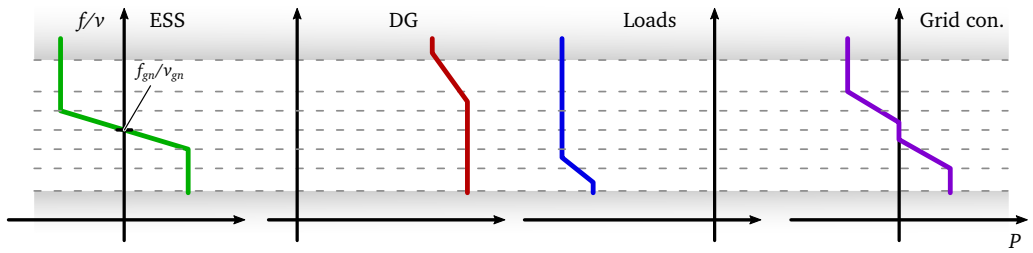

Figure 3.13: Primary controllers of the simulated scenario for a dynamic perturbation profile.

Moreover, we have simulated a more realistic perturbation profile to observe the behaviour of converters carrying out the primary regulation and the evolution of the frequency and voltage of the ac and dc subgrids, respectively.

Figure 3.14 shows the results of this simulation, represented as in the previous two cases. As expected, ESSs located in the ac and dc subgrid are the most relevant devices in terms of primary regulation because they react under any frequency and voltage variation. When perturbations are more severe the exchange of power with the grid becomes more significant and it is not until the frequency or voltage deviate notably that DG systems and loads reduce their performance in order to contribute in the primary regulation. In addition, we can notice from the variation of frequency and voltage that their deviations from rated values are lower thanks to the mix of devices sharing power disturbances. This means that the more systems

are integrated that contribute in the primary regulation, the better will be the quality of the frequency and voltage of the system.

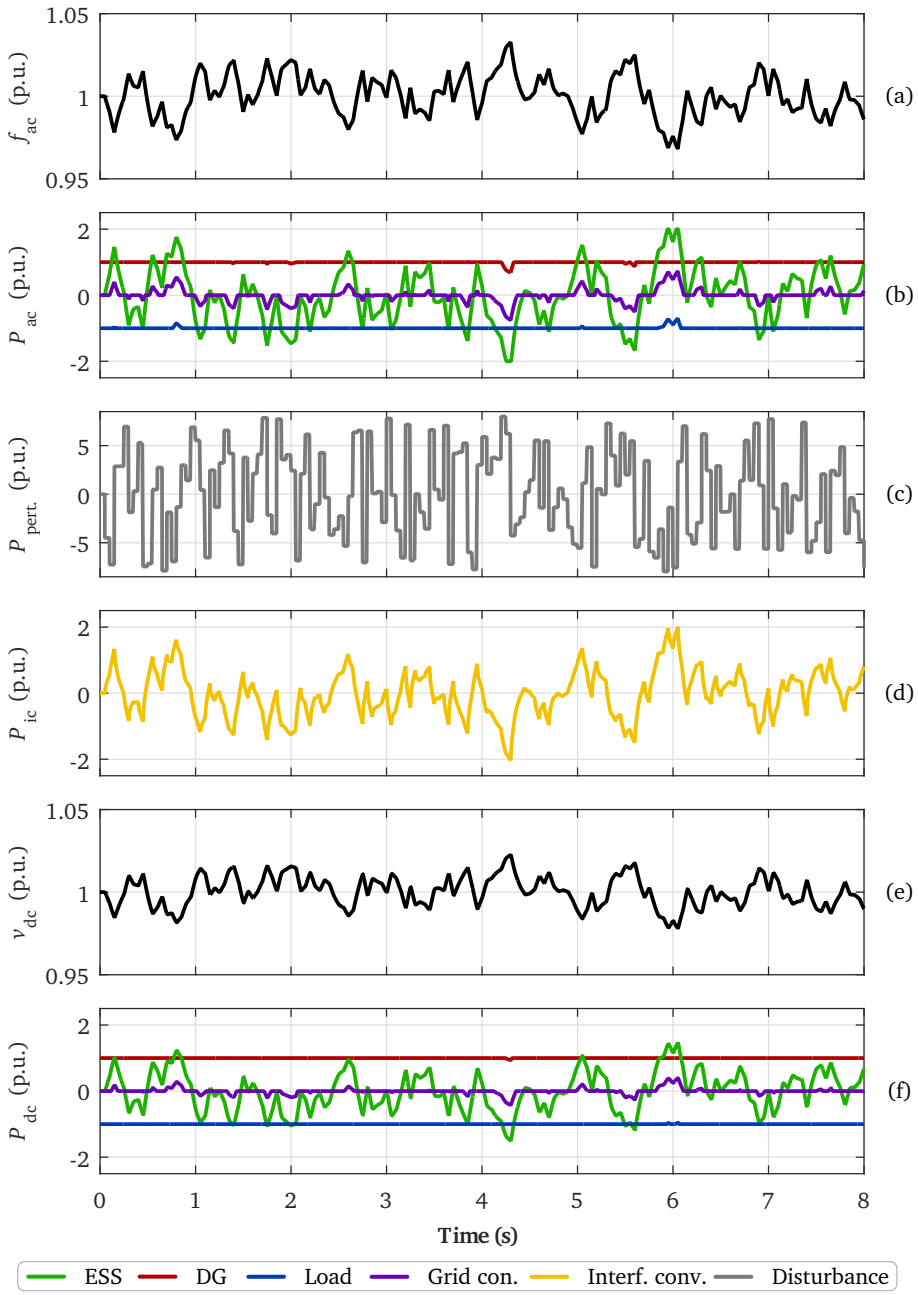

Figure 3.14: Microgrid response under dynamic power disturbances: (a) ac bus frequency, (b) ac subgrid power values, (c) disturbance power, (d) interlinking converter power, (e) dc bus voltage and (f) dc subgrid power values.

Chapter 4

AC Systems: Synchronous Machine Emulation Techniques

Up to this point we have shown that one of the most important challenges regarding microgrid control is to ensure enough primary reserve to handle power variations in the grid. Another challenge associated to the control of converter-dominated grids is to provide sufficient inertial response through the devices regulating the grid frequency and voltage to avoid large deviations.

The aim of this chapter is to carry out a comparative evaluation of classical synchronous machines and some of the most interesting low-level control techniques for power-electronic converters that provide inertial response at ac microgrids (Figure 4.1), based on the synchronous machine emulation concept. The analysis is focused on their dynamic performance under perturbations and their stability characteristics when connected to the grid.

This operation concept is used afterwards as the basis for Chapter 5, where inertia emulation techniques are developed for dc microgrids.

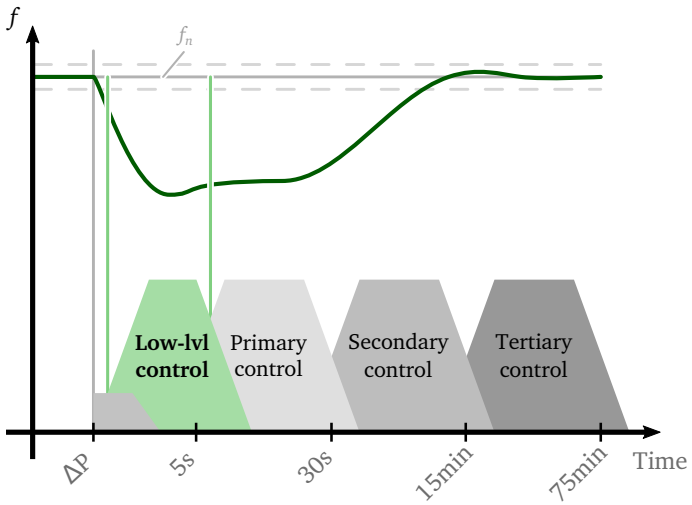

Figure 4.1: Operation range of the low-level control in the hierarchical regulation of an ac microgrid.

We have already mentioned that a higher amount of converter-interfaced systems on an electric grid may cause large deviations and instabilities in the voltage or frequency because, unlike classical synchronous machines (SMs), they do not provide any inherent inertia over power variations [1]. Therefore, these converters must be controlled by more advanced techniques not only to participate in the primary regulation as shown in the previous chapter but also to support the grid by providing this inertial behaviour.

In this context, in the last decades, synchronous machine emulation (SME) control strategies have arisen as one of the most interesting alternatives. These techniques not only provide synthetic inertia to the grid, but they are also capable of operating in a distributed manner as classical SMs, which makes them suitable for grid-connected or islanded systems. By employing only local measurements, SME controlled converters share power variations occurring in the grid without any extra communication network. Furthermore, some SME control types provide better flexibility when connecting to electric grids by eliminating the dedicated synchronization unit—e.g. a PLL.

In the following sections we first revisit the concept of operation of SMs and then introduce some of the most relevant non-augmented SME techniques employed in the literature. Then, we carry out a comparative evaluation in terms of performance and stability considering classical SM-based systems as the benchmark system.

4.1 Classical SM Operation

SME techniques, which are explained in detail in the next section, are inspired by the concept of operation of conventional electric grids. In such systems, as shown in Figure 4.2, the generated electrical active power matches the consumed power and the losses of the grid.

When a sudden load or generation change occurs in the grid, parallel-connected SMs share these variations to keep the power balance:

$$\sum p_{gen} = \sum p_{load} + \sum p_{loss} \tag{4.1}$$

The dynamic behaviour of each SM-based generator—and hence the grid, which is dominated by these machines—under such variations is primarily determined by its mechanical properties, and can be represented as the combined inertia J of the SM and the prime mover (Figure 4.3).

The expression of this mechanical system can be written as:

$$J\frac{d^2\theta}{dt^2} = \tau_m - \tau_e = \frac{p_m}{\omega} - \frac{p_e}{\omega} \tag{4.2}$$

where θ is the angular position of the machine.

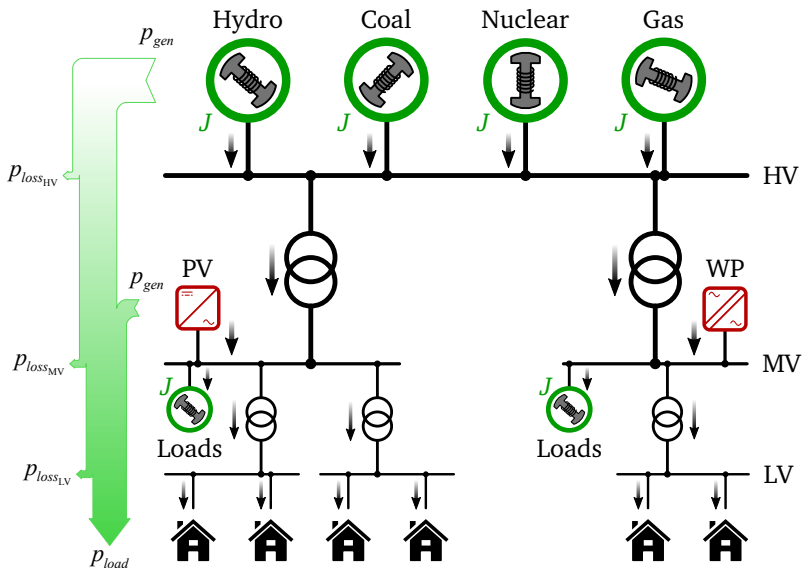

Figure 4.2: Power transmission and distribution in a conventional SM-dominated electric grid.

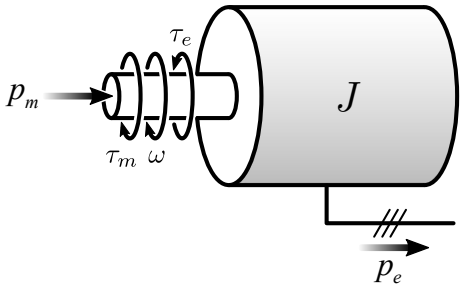

Figure 4.3: SM mechanical system diagram.

If we include an additional damping term in (4.2), rewrite the equation in p.u. and consider δ as the the angular position of the rotor with respect to a synchronously rotating reference, we obtain the so-called *swing equation*, which represents the swings in the machine rotor angle during perturbations [70]:

$$\boxed{2H\frac{d^2\delta}{dt^2} = \frac{p_m}{\omega} - \frac{p_e}{\omega} - K_D\Delta\omega} \tag{4.3}$$

where

$$H = \frac{1}{2}\frac{J\omega_b^2}{S_b} \tag{4.4}$$

This expression represents the dynamic behaviour of SM-based systems under perturbations and is the basis of the SME control, as will be explained in the next section.

At steady-state, SMs' mechanical power, p_m, and electrical power, p_e, are equal and there-

fore the machine has no angular acceleration and rotates at a constant speed.

When there is an active power variation in the grid p_e changes and, if the mechanical power is kept constant, the rotating speed of the SM—and hence the system frequency—decreases. As we can deduce from (4.2), considering small variations in the angular speed, the angular acceleration is directly proportional to power variations and inversely proportional to the inertia J.

In order to avoid the deceleration of the machine, SM-based generators are equipped with primary controllers such as the droop techniques analysed in the previous chapters, to restore their speed to the rated value by modifying the fuel coming into the turbine connected to the shaft of the SM (Figure 4.4).

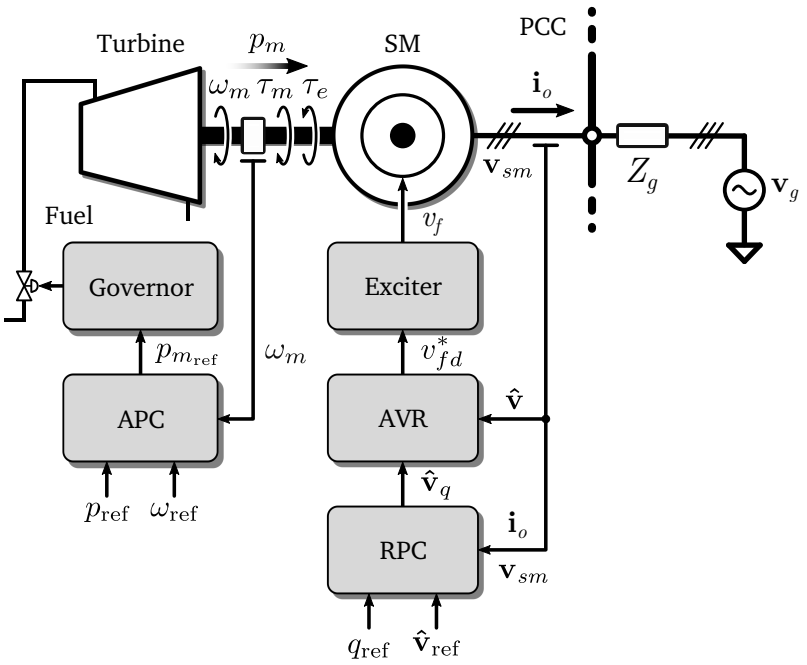

Figure 4.4: Configuration of a synchronous machine-based generator connected to the grid.

As shown in the figure, the control of SMs is usually composed by two main parts, the already mentioned primary controller usually named active power controller (APC) with the governor of the turbine, and the rective power controller (RPC) with the automatic voltage regulator for the exciter of the SM rotor.

Most of the times the APC includes an external power reference added to the output of a frequency droop regulator. As explained before, the droop control measures the SM frequency and, comparing it to the reference value, calculates through a proportional gain how much power must the turbine supply to reduce this frequency deviation (Figure 4.5).

The obtained power reference $p_{m_{\text{ref}}}$ is sent to the governor so that it adjusts the flow of fuel going to the turbine.

The RPC, on the other hand, usually consists of a voltage amplitude reference and a droop

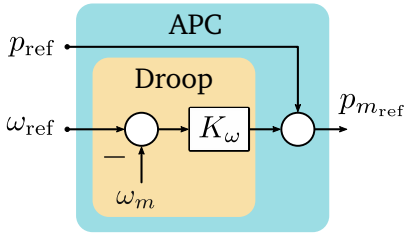

Figure 4.5: Active power controller of classical SMs.

controller that adds a certain voltage value depending on the difference between the reference and measured reactive power (Figure 4.6).

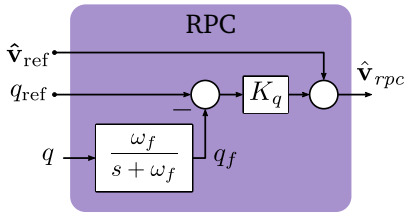

Figure 4.6: Reactive power controller of classical SMs.

The voltage signal generated by the RPC is then employed in the automatic voltage regulator (AVR), by comparing it to the measured voltage amplitude, to set the dc voltage reference of the exciter. As illustrated in Figure 4.7, in this case the reference is calculated through a classical PI regulator.

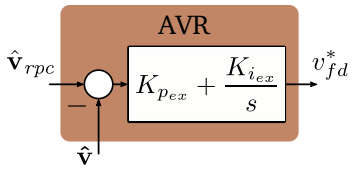

Figure 4.7: Automatic voltage regulator of classical SMs.

The above-mentioned controllers are responsible for defining the steady-state operation point of each SM by setting active power and voltage amplitude references. In this context, and following the nomenclature explained in previous chapters, these regulators would be encompassed under the primary control category, operating the SM as a grid-forming system regulating the voltage and frequency of the grid.

4.2 SME Control

Synchronous machine emulation consists fundamentally on integrating the *swing equation* and droop regulators of classical SMs in the control algorithms of power-electronic converters.

Figure 4.8 illustrates a typical grid-connected voltage source converter (VSC) with its output filter and the controller with the pulse-width modulator (PWM).

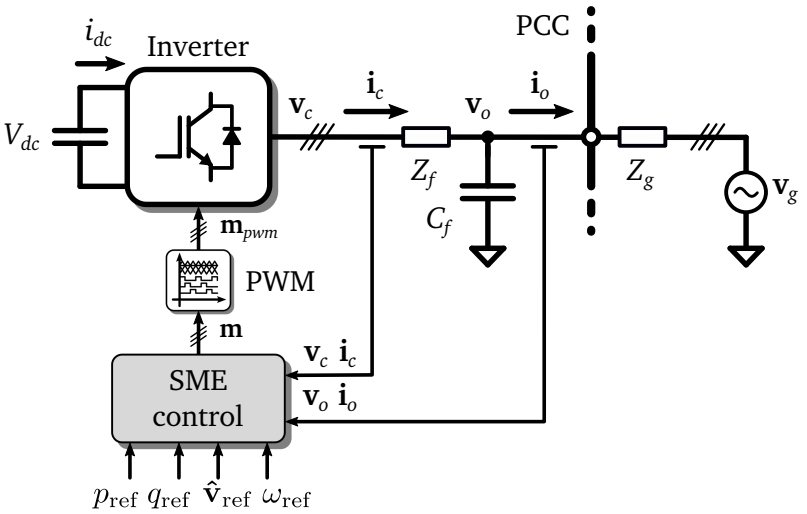

Figure 4.8: Configuration of a power electronic converter-based system connected to the grid.

In the literature there is a wide variety of SME techniques, and some of them have been already reviewed for instance by D'Arco *et al.* or Bevrani *et al.* in [71] and [72], respectively. In this case we distinguish them based on their control configuration and the approach they follow to model the *swing equation* of SMs, and we categorize them in four main groups:

- Synchronverter (SV) [12, 19, 73–77]
- Inertia-emulation (IE) [78–85]
- Current-controlled virtual synchronous machine (CCVSM) [86–90]
- Voltage-controlled virtual synchronous machine (VCVSM) [21, 91–94]

These techniques have been already employed for different applications, such as the integration of photovoltaic [74, 95–98] or wind-power [12, 76, 81, 99] generation systems, vehicle-to-grid applications [21], microgrids [19, 73, 75, 89, 92, 100] or HVDC systems [12, 82, 101, 102].

In the following subsections we analyse each group of SME techniques more in detail.

4.2.1 Synchronverters

This technique was first proposed by Q.-C. Zhong and G. Weiss in [103], and is the simplest technique among the analysed SME control strategies.

The non-augmented version of a synchronverter mainly consists of a frequency regulation and a reactive power control part as shown in Figure 4.9.

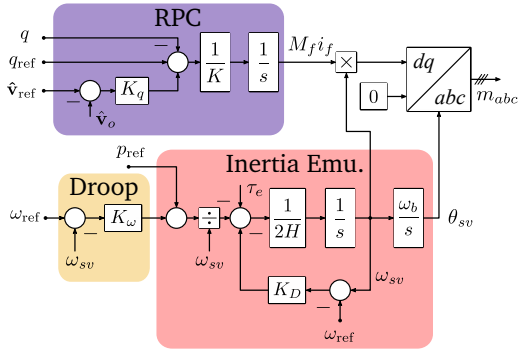

Figure 4.9: Synchronverter control diagram.

The former reproduces the concept of operation of SMs by integrating a droop frequency control and the *swing equation* to mimic the evolution of the SMs' output frequency. Many times, the frequency droop and the emulated damping are combined in a single term as in [77]; in this case we separate both terms to facilitate the comparison with other SME techniques.

The RPC is very similar to the one employed at SMs, as it includes a reactive power reference with a voltage droop regulator. The difference resides in that SV control usually includes a $1/K$ gain and an additional integrator in the RPC to obtain the magnetic field and current term $M_f i_f$ [18, 77].

One of the most important characteristics of SV control is its simplicity to be implemented in the controllers of power-electronics converters, which is a key factor in the manufacturing of commercial devices. Moreover, the need of a synchronization unit such as a PLL can be avoided by slightly modifying the basic SV technique [104]. This feature not only simplifies even more the control of the system but also avoids oscillations and instabilities that might appear due to the synchronization delay [12].

On the contrary, the lack of any current regulator in the control technique means that SVs do not have any inherent current limitation, which could be problematic for instance under fault conditions. Even though we could implement a current limitation for example employing an external loop, the SV technique would become more complex and therefore it would be more similar to other types of SME strategies. In addition, the fact that SVs are so simple implies that there are not so many control parameters—and hence degrees of freedom—to adapt the dynamic response of the converter.

4.2.2 Inertia-Emulation

The concept of operation of IE techniques is slightly different from the rest of techniques discussed in this chapter, because the *swing equation* is used inversely to calculate the power reference from the frequency (Figure 4.10). This technique has been widely employed in the project called VSYNC [105], and is a common approach to provide inertial behaviour

for example at photovoltaic or wind power plants [98, 99] to meet the requirements of grid operators.

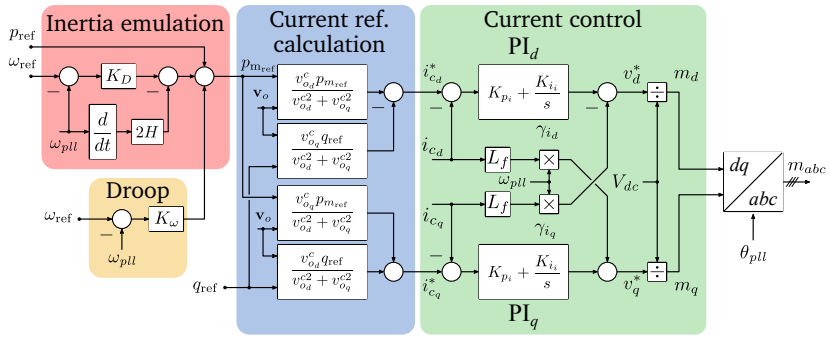

Figure 4.10: Inertia-emulation control diagram.

Apart from the *swing equation* to reproduce an inertial response with converters, the IE control is usually composed by a droop controller and a current control loop. The current references are calculated with active and reactive power references and measured voltages at the output of the converter. In this case, a voltage droop could be also implemented to carry out the reactive power regulation, but we have not included to keep it as in the revised studies.

Even though this technique is not as simple as SVs, it is still not so complex as it only includes a current regulator and the references are directly calculated from power and measured voltages. IE techniques are therefore simple to be implemented in a converter controller and are capable of limiting the current of the converter with the current regulator.

Nevertheless, IE strategies require a PLL to synchronize with the grid, which makes the control more complex. Moreover, the employed inverse *swing equation* contains a derivative term that could cause very steep variations in the control strategy under sudden frequency deviations.

4.2.3 Current-Controlled Virtual Synchronous Machines

From the studied SME techniques, CCVSMs are the closest to classical SM-based systems, because, in addition to the components of SVs—e.g. the active and reactive power controllers with inertia emulation—they implement the electrical model of a SM in the control strategy. This approach has been recently studied by Mo *et al.* in [86], where two different SM electrical models are compared: a dynamic electrical model and quasi-stationary model. Figure 4.11 illustrates the control employed by these authors with the dynamic electrical model.

As it can be observed, the active and reactive power controllers are very similar to the ones employed at SVs. One of the differences in the APC is that in this case, instead of estimating the frequency of the grid with a PLL, the frequency is generated by filtering the value obtained in the *swing equation*, assuming that it will vary very slowly. Another difference resides in the

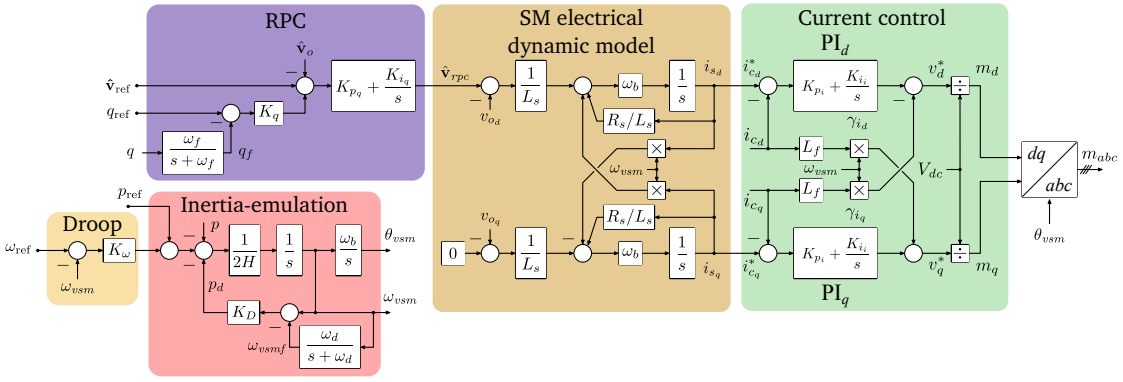

Figure 4.11: Current-controlled virtual synchronous machine control diagram.

fact that the RPC includes a PI regulator to establish the voltage amplitude reference in the *d* axis.

Apart from these controllers and the dynamic model of the SM, CCVSMs include a current control as in IE techniques.

The main advantage of this control is that it increases the flexibility to adapt the behaviour of the converter by varying not only the virtual-inertia but also the virtual windings of the SM model. In addition, the current controller provides a current limitation as in IE techniques, and there is no need to employ any synchronizing algorithm because the frequency is internally generated.

The most remarkable drawback might be the fact that the SM dynamic model must be carefully designed to ensure an adequate dynamic behaviour of the converter.

4.2.4 Voltage-Controlled Virtual Synchronous Machines

As shown in Figure 4.12, VCVSM techniques are the most complex among the four SME approaches. They have been widely employed in the literature, specially by D'Arco *et al.* for different applications such as microgrids or electric vehicles [92, 93].

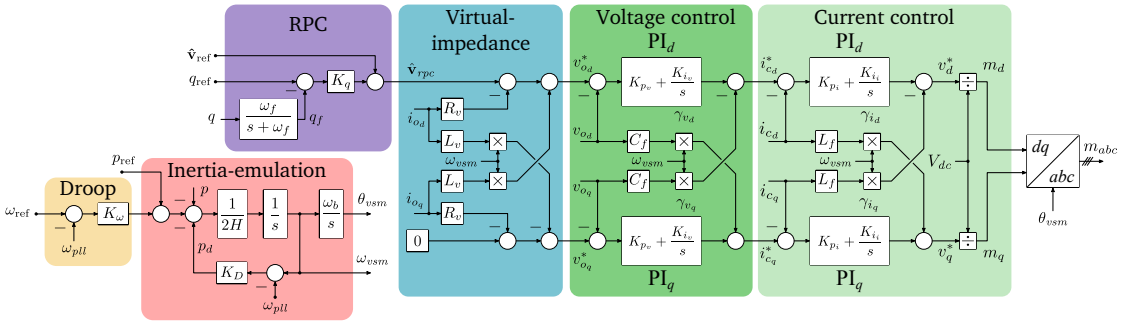

Figure 4.12: Voltage-controlled virtual synchronous machine control diagram.

The configuration illustrated in Figure 4.12 is composed of a cascaded current and voltage

controller, a virtual *RL* impedance and similar active and reactive power controllers as in previous techniques.

One of the advantages of this technique is that the cascaded current and voltage loops enable the current limitation and the accurate control of the voltage at the output of the converter. In addition, the included virtual-impedance provides more degrees of freedom to adjust the dynamic behaviour of the converter.

However, this approach brings about some drawbacks. On the one hand, the high number of cascaded controllers significantly increases the complexity of the technique, making the tuning and configuration of parameters a challenging task. In addition, the strategy shown in Figure 4.12 requires a synchronizing algorithm to capture the frequency of the grid. Even though this could lead to oscillations or stability issues due to the delay of the PLL, it might be possible to follow the approach of the CCVSM to generate this frequency internally and avoid the us of a PLL. As in this case we are analysing the technique proposed in [92], we have kept the PLL in the control strategy.

4.3 Comparative Evaluation

The comparison of the SM operation and SME-controlled power converters is done in two different ways.

On the one hand, we evaluate their dynamic behaviour under different disturbances. These simulations serve not only to observe the response of each analysed system but also to verify the analytical model by comparing it with the non-linear simulation model.

On the other hand, our purpose in this chapter is to observe the characteristics of each approach in terms of stability, as it is one of the key factors in converter-dominated grids such as microgrids. Despite the fact that we can find in the literature a wide variety of methods for determining the stability of such systems, several challenges arise due to their non-linear properties. Therefore, in this case we adopt the impedance-based stability analysis, which is one of the most used methods to determine the stability of power electronics-based power systems [11, 106–109]. One of the most interesting advantages of this method is that we can determine the stability of a real grid without knowing the characteristics of the devices connected to it, by simply injecting a signal on the point in which we want to evaluate the stability.

4.3.1 Methodology and Simulation Conditions

In order to carry out the above-mentioned performance and stability comparative evaluation, we have developed a methodology that is summarized in Figure 4.13.

In this approach, we first derive the differential equations that define the dynamics of the analysed system, including physical elements as well as control algorithms.

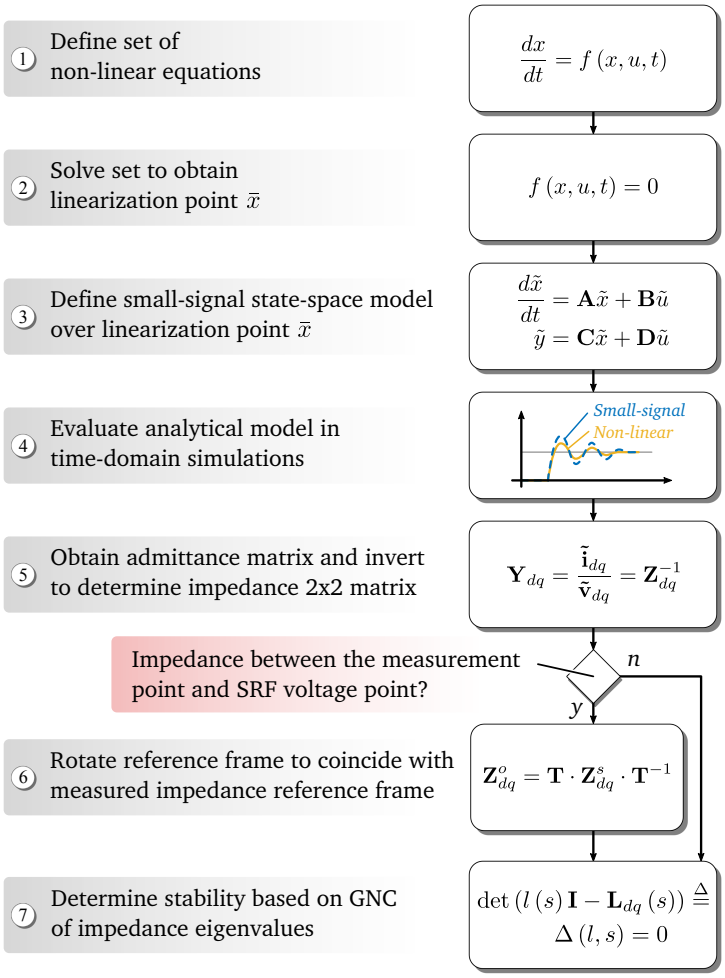

Figure 4.13: Methodology for the analytical derivation of *dq* impedance matrices and stability analysis.

Taking into account that some of the differential equations are non-linear, we solve the system to obtain the linearisation point $\bar{x}$. This is equal to the steady-state point of operation, and is computed by eliminating the derivative terms and solving the set of equations for specific input values. We then obtain the small-signal state-space model linearised over $\bar{x}$ employing Taylor series expansion, which enables the use of linear techniques for stability analyses.

In order to verify the small-signal model and observe its dynamic performance, we compare it with the non-linear model in time-domain simulations for different disturbances.

Once the model is verified, we obtain the analytical and measured impedance of each system and analyse the stability applying the generalized Nyquist criterion (GNC) [11, 110].

In this chapter all the equations employed to model the SM and SME-controlled converters are represented in rotating reference frames—i.e. in the *dq* domain—by applying the amplitude-invariant Park transform. In the SM-based generator as well as in SME-controlled VSCs we can distinguish three main rotating reference frames:

1. Global reference frame (GRF): the d axis of the GRF is aligned with the grid voltage vector $\mathbf{v}_g$, and the q axis, as in the rest of rotating reference frames, leads the d axis by 90°.

2. Local reference frame (LRF): the d axis of the LRF is aligned with the output voltage vector $\mathbf{v}_o$. In the case of the SM, this voltage corresponds to the terminal voltages of the machine, $\mathbf{v}_{sm}$, whereas in SME-control systems it represents the voltage at the capacitor of the output LC filter of the converter.

3. Dynamic reference frame (DRF): the DRF is slightly different from the previous two and is aligned differently for the SM-based generator and SME-controlled systems. In the first case the d axis of this reference frame is aligned with the **rotor** of the SM with an angle θ_{sm}, so we use the superscript "R". On the contrary, in the case of converters, this rotating reference frame is aligned with the **control** frequency—so we denote it with superscript "C"—and has an angle θ_c that can be either the angle of the PLL, θ_{pll}, or the angle generated by the VSM, θ_{vsm}, depending on the control technique. If the DRF is aligned with the angle generated by the PLL, in the steady-state this rotating reference frame will be the same as the LRF, because the PLL calculates the angle of the output voltage $\mathbf{v}_o$. Therefore, it can be said that in this specific case the LRF and the DRF will be different only during transients.

Figure 4.14 and Figure 4.15 represent the phasor diagrams of the SM-based system and SME-controlled converters, respectively. In addition, these figures illustrate the location where each rotating reference frame is aligned.

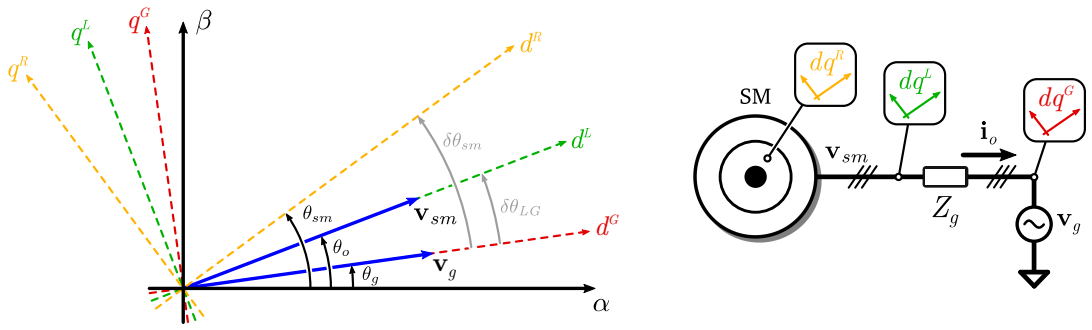

Figure 4.14: Phasor diagram of SM-based system rotating reference frames.

In relation to these rotating reference frames, special care must be taken when comparing the impedances obtained from the analytical equations and the simulation model. Usually, the latter is obtained by injecting a perturbation signal—either voltage or current—at the output of the converter and calculating the impedance matrix by dividing the voltage and current. These variables are measured in the *abc*-domain, and are transformed into the LRF through a fast Fourier transform (FFT). If there is no impedance between the analysed system—either a

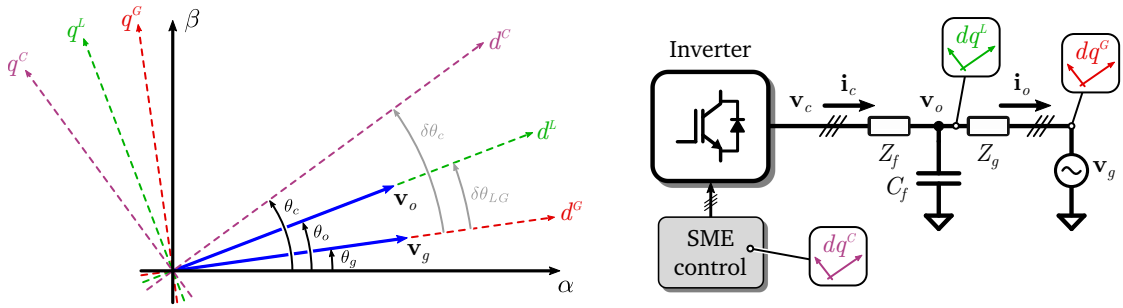

Figure 4.15: Phasor diagram of SME-controlled system rotating reference frames.

SM or a converter—and the grid, or if the power transmission between these two systems is zero, the LRF and the GRF are completely aligned. This means that the impedances referenced to any of these two rotating reference frames can be directly compared.

However, when these two conditions are not met, the two rotating reference frames are not aligned any more due to the voltage drop in the impedance. As analytical impedances are most of the times referenced to the GRF, a rotation must be applied to one of the impedances so as to compare them in the same reference frame (step ⑥ in the proposed methodology). This is even more relevant when carrying out the impedance-based stability analysis of a system composed by multiple interconnected devices, as they must be all referenced to a common reference frame [J2].

For the sake of simplicity and readability, we have included the entire analytical development of the previously shown grid-connected SM and SME-controlled converters in Appendix A and Appendix B, respectively. Moreover, we have determined the following conditions for the simulations carried out in the next sections:

1. The reactive power controllers are disabled by setting the reference q_{ref} and the droop gain K_q to zero in all cases, in order to carry out a fair comparison between SM-based generators and all SME-controlled converters.

2. No power stabilizer is included in the SM configuration and no active damping loops are added in the control algorithms of converters, as they would influence their performance and stability characteristics. This means the analysis is done for non-augmented techniques, considering only their inherent behaviour.

3. All the analysed systems begin the simulation from a steady-state point of operation of $p = 0.5$ p.u. to reproduce a more realistic point of operation.

In addition, we must mention that the most relevant parameters of the following sections are gathered from [86, 92, 111] and kept as similar as possible to carry out fair comparisons.

In this sense, in Table 4.1 we collect the parameters that are common for the SM-based generator and SME-controlled converters, such as the base values for the per unit calculations

or the reference values for the controllers.

Table 4.1: Parameter values that are common for the analysed systems connected to ac grids.

Parameter	Value	Parameter	Value
S_b	2.75 MVA	p_{ref}	0.5 p.u.
V_b	690 V	q_{ref}	0 p.u.
ω_b	$2\pi 50$ rad	$\hat{\mathbf{v}}_{\text{ref}}$	1 p.u.
$\mathbf{v}_g$	1 p.u.	Z_g	$0.01 + j0.2$ p.u.
ω_{ref}	1 p.u.	K_ω	20

Similarly, in Table 4.2 we show the parameter values that are specific to each of the analysed systems.

Table 4.2: Parameter values that are specific for each of the analysed systems connected to ac grids.

	SM	SV	IE	CCVSM	VCVSM
L_f	–		0.08 p.u.		
R_f	–		0.03 p.u.		
C_f	1μ p.u.		0.074 p.u.		
L_s	0.05 p.u.	–	–	0.25 p.u.	–
R_s	0.001 p.u.	–	–	0.1 p.u.	–
L_v	–	–	–	–	0.2 p.u.
R_v	–	–	–	–	0
H	1 s		0.025 s	1 s	
K_D	0	20	2	40	400
K_{pi}	–	–		0.085	
K_{ii}	–	–		4.69	
K_{pv}	–	–	–	–	0.59
K_{iv}	–	–	–	–	736
T_s	–		0.1 ms		
T_{ex}	0.1 s	–	–	–	–
T_{gt}	0.5 s	–	–	–	–

4.3.2 Dynamic Performance Under Perturbations

We analyse the dynamic behaviour of the SM and SME-controlled converters for two different perturbation types:

1. *Active power reference variation:* in this case we apply a step change in the active power reference, transitioning from $p_{\text{ref}} = 0.5$ p.u. to 0.6 p.u. The purpose of this simulation is to observe the response of the converter avoiding the effect of the frequency droop controller.

2. *Grid frequency variation:* the frequency of the grid begins at its rated value of 50 Hz and we apply a negative step variation of 0.2% of the rated frequency. This way we can study not only the dynamic behaviour but also the steady-state primary regulation of each system.

Active power reference variation

Figure 4.16 shows the output power and frequency response of the SM for a 0.1 p.u. variation of the power reference $p_{m_{\text{ref}}}$.

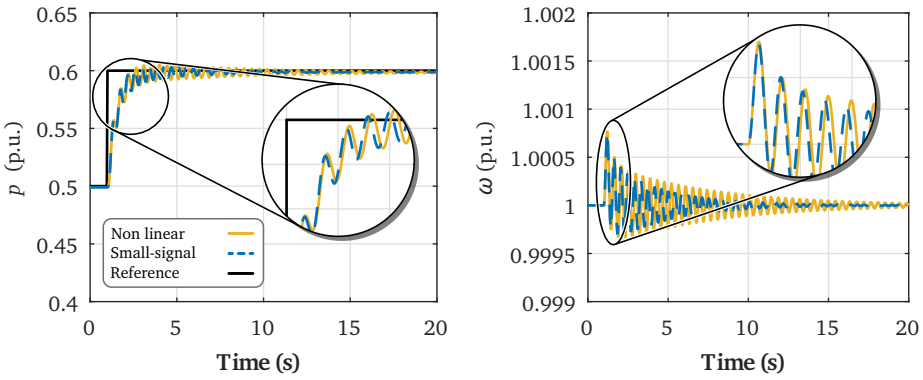

Figure 4.16: Dynamic response of a grid-connected SM over a power reference variation: output power in the left and machine frequency in the right.

Although the curves show that the small-signal state-space model and the original non-linear model have a very similar response for this perturbation, a slight difference can be observed from the instant 2 s on. The SM has a low frequency oscillation with a different frequency in the small-signal model and the original one, which causes the curves to differ slightly from each other. This difference could be caused by the information lost during the linearisation of the system, as some non-linearities of the machine might not be represented properly with the small-signal model in this range of frequencies, or by the time-varying characteristics of the system, which are not considered in the small-signal model.

Apart from that, we can see that the output power of the SM stabilizes at 0.6 p.u. after the oscillatory transient, which demonstrates that the active power of the machine is correctly controlled to the reference value. Regarding the frequency, we can notice that it has a small oscillation that begins when the power reference is modified and whose amplitude decreases over time.

Figure 4.17 shows the same curves as before but in this case for the four types of SME control.

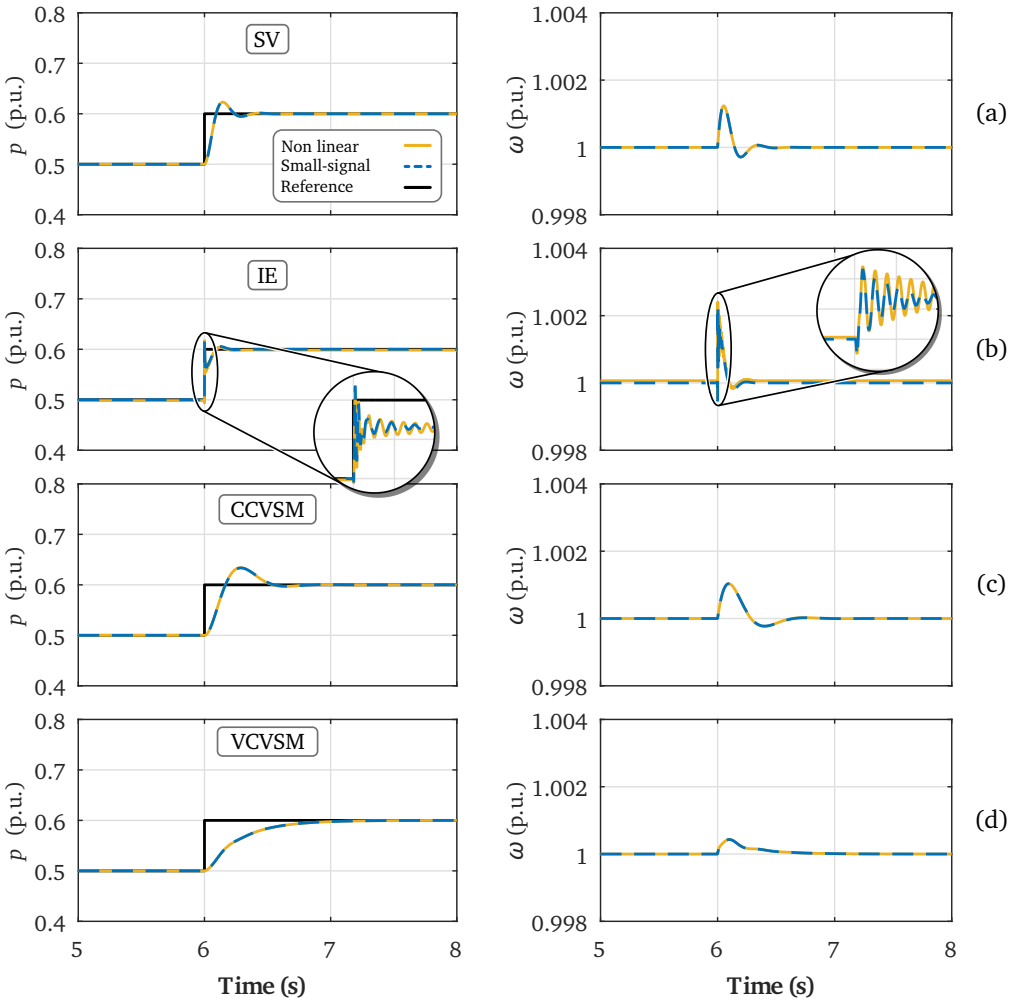

Figure 4.17: Dynamic response of grid-connected SME-controlled converters over a power reference variation: output power in the left and frequency of the output capacitor voltage in the right.

The curves in this case show a very good accuracy between the non-linear and small-signal models developed in the four cases. Moreover, from these results we can conclude that SME-controlled converters do not have the oscillatory behaviour observed in the SM, and their response over a reference power variation is much smoother in comparison.

The SV, CCVSM and VCVSM show a similar behaviour; the difference resides in their overshooting and the time they require to reach the steady-state operation. However, this can be adapted by varying the emulated inertia and damping factor of the *swing equation* included in their control strategies.

As expected, the IE algorithm has a different transient response compared to the previ-

ous three strategies. In this case, when we apply the power reference step variation, the IE-controlled VSC suddenly increases its output power. This is also reflected in the frequency of the controller, which in this case corresponds to the frequency of the PLL. This instantaneous variation occurs because of how the *swing equation* is employed. In the previous three approaches the power reference is added to the output of the frequency droop and then this value is fed into the inertia-emulation algorithm containing the *swing equation*. On the contrary, in the IE strategy this equation is reversed and hence the reference power is directly fed to the part where current references are calculated. As this calculation is immediate, the step variation of the power reference is directly reflected on a step variation of the current reference. Taking into account that the current loops are usually fast compared to other regulators, we can see how this sudden reference variation is reproduced in the output power of the converter.

Therefore it is important to note that SV, CCVSM and VCVSM control provide inertial behaviour when the power reference is changed, whereas IE techniques reproduce almost instantaneously—i.e. without inertial behaviour—this variation in the output of the converter.

Grid frequency variation

In this case we evaluate the SM and SME-controlled converters for a 0.2% grid frequency variation. Figure 4.18 shows for instance the dynamic response of the SM-based generator output power and rotor frequency for this perturbation.

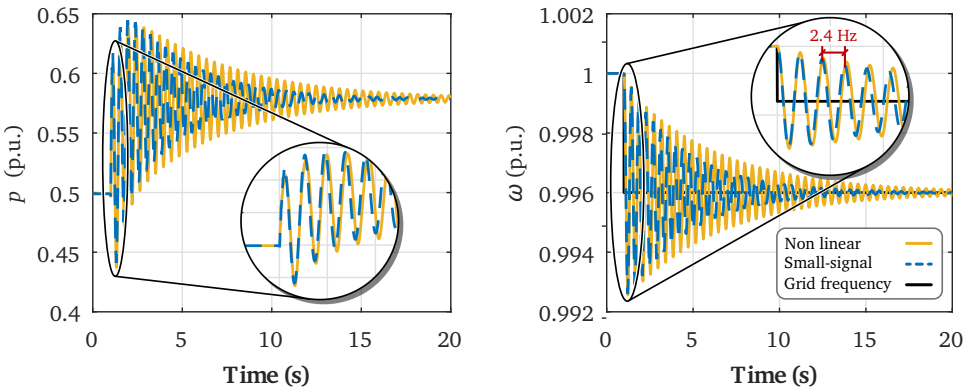

Figure 4.18: Dynamic response of a grid-connected SM over a grid frequency variation: output power in the left and machine frequency in the right.

Both curves show a very oscillatory response (of approximately 2.4 Hz), which means that the frequency of the grid has a strong influence over some weakly-damped dominant eigenvalues of the system. This phenomenon can be also identified by looking at the location of the dominant eigenvalues of the small-signal state-space model of the SM in the imaginary

plane (Figure 4.19).

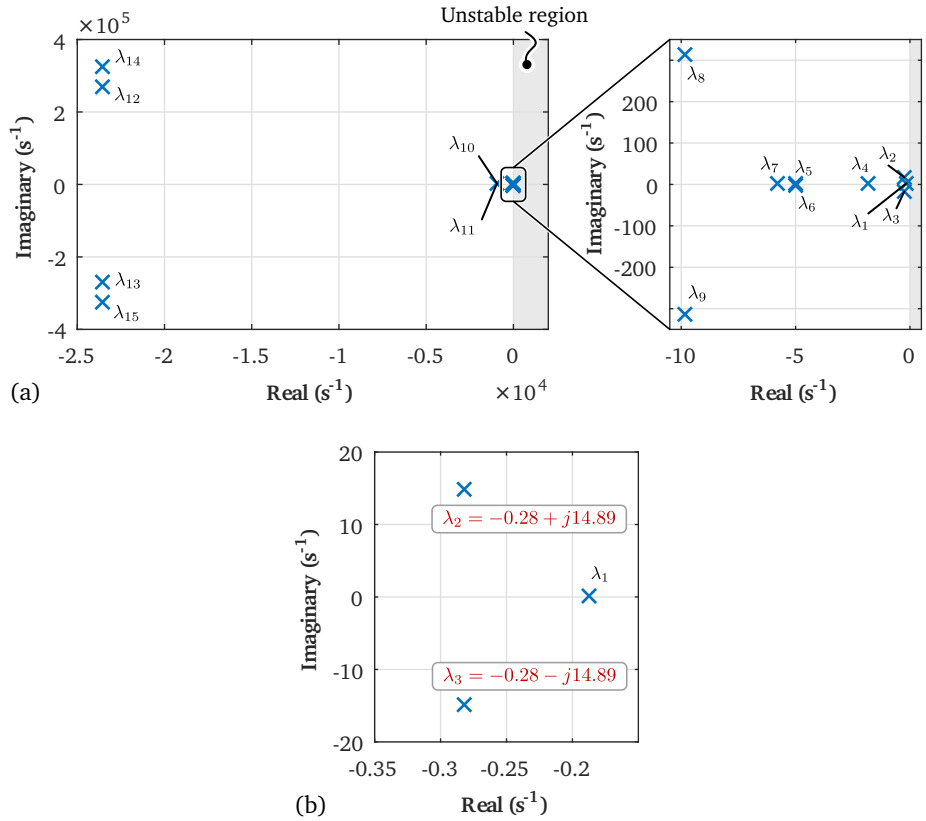

Figure 4.19: Root locus and zooms of the eigenvalues of the SM-based generator.

From this figure we can conclude that the natural frequency of eigenvalues λ_2 and λ_3, which are the dominant eigenvalues due to their proximity to the vertical axis, correspond to the frequency of the oscillation identified in Figure 4.18: $14.89/2\pi = 2.37$ Hz.

Regarding SME-controlled converters, in Figure 4.20 we have shown their dynamic response under the same grid frequency variation.

In this case the four control types provide inertial behaviour under the frequency perturbation. The SV, and VCVSM techniques have some overshooting and a small oscillation under the step variation, but they reach the steady-state approximately in 0.5 s. On the other hand, CCVSM has a very high overshoot ($\sim$ 30%) with no oscillation afterwards. Even though this can be problematic, CCVSM-controlled converters are very flexible and their response can be adapted by varying several control parameters. Moreover, despite its high overshooting the CCVSM technique is the one that provides most inertia among the studied approaches for the same H, which can be clearly noticed from the RoCoF of the curves shown at the right part of Figure 4.20.

The results also demonstrate that IE control techniques' purpose is to provide inertial behaviour under grid frequency variations.

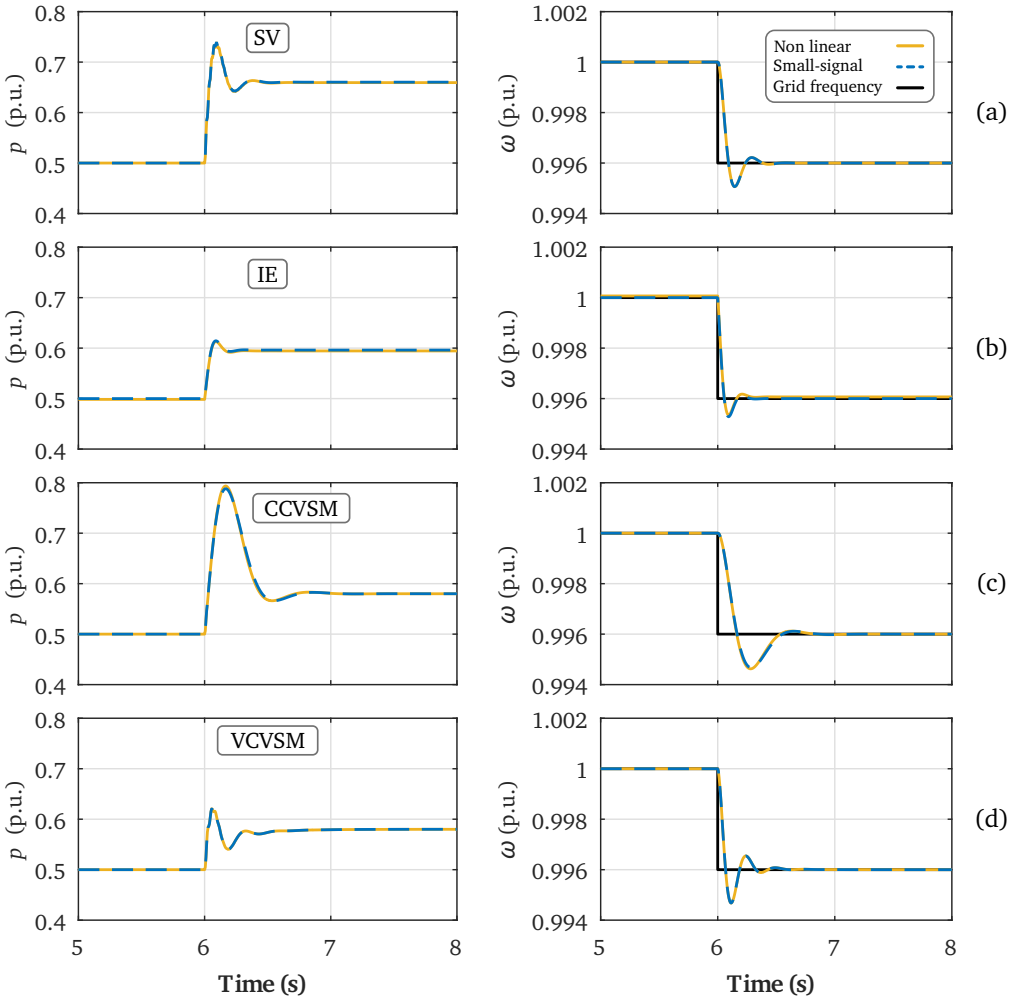

Figure 4.20: Dynamic response of grid-connected SME-controlled converters over a grid frequency variation: output power in the left and frequency of the output capacitor voltage in the right.

4.3.3 Integration of Different-Dynamic Systems

One of the most interesting characteristics of SME techniques that to the best of our knowledge has received no attention in the literature, is that the transient and steady-state behaviour of converters can be designed separately. As we have mentioned previously, the transient response of the converter is dependent on the virtual-inertia, whereas the steady-state point of operation is defined by the droop regulator. In this context, we can say that these characteristics are decoupled, and therefore can be adapted independently.

This is a very interesting feature of SME strategies because it enables the integration of systems with diverse dynamic characteristics, such as different technologies of ESSs.

Consider for instance the system with two converters in parallel depicted in Figure 4.21, and suppose that the first converter is controlling an electrochemical battery pack and the

second one a supercapacitor module.

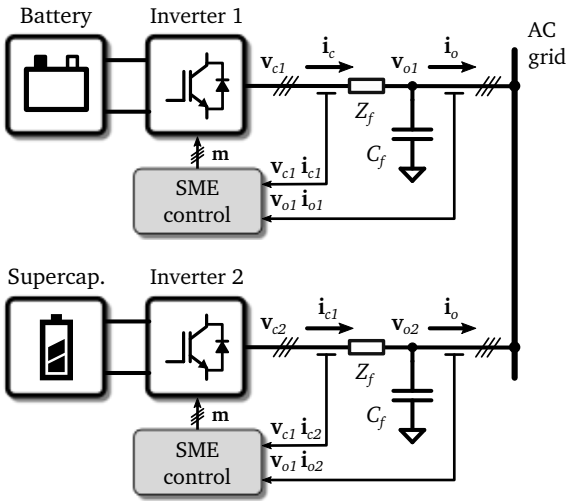

Figure 4.21: Different-dynamic SME-controlled inverters connected in parallel.

In this scenario, we can define the control parameters of each converter so that the first one provides power during steady-state periods whereas the second one handles the transient power variations happening in the grid. This way, we would take advantage of the dynamic characteristics of supercapacitors to reduce the ageing of battery-powered systems due to cycling.

Figure 4.22 shows a simulation of this configuration employing the SV control in both inverters for a sudden power variation in the grid. In this case, the controller of the battery is configured with a very low synthetic inertia ($H = 1$ s) and a high frequency droop gain ($K_\omega = 100$) in comparison to the controller of the supercapacitor, which has a H of 100 s and a $K_\omega = 0$.

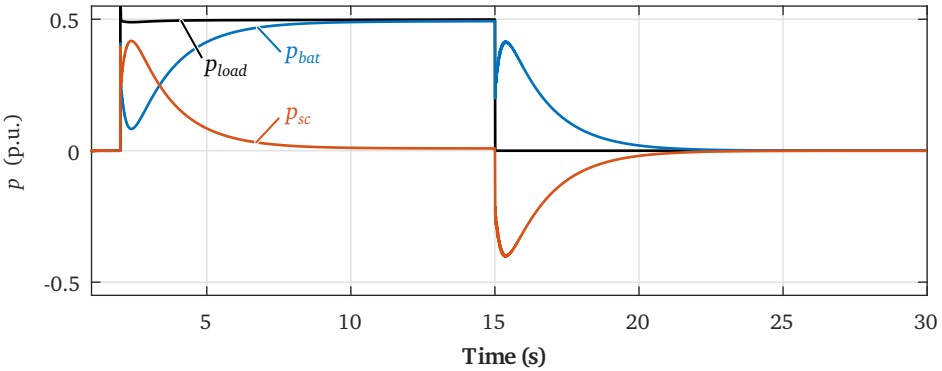

Figure 4.22: Different-dynamic SME-controlled inverters connected in parallel.

The figure shows how the system that emulates the highest inertia—in this case the inverter controlling the supercapacitor module—provides most of the power during the transient

period. Moreover, the power of this inverter is reduced automatically after the transient until it reaches the zero value, which is expected because we have set its $K_\omega = 0$. On the contrary, the inverter associated to the battery provides less power during the transient but becomes the dominant system in the steady-state period, supplying all the power demanded by the load.

As we have already said, this is a very interesting and useful feature of SME strategies because we can integrate generation, storage systems or even loads of different dynamics in the grid by simply varying their control parameters. Taking into account that the proposed techniques rely solely on local measurements, this integration can be done in a *plug-and-play* manner, which improves significantly the flexibility in the operation of the grid.

4.3.4 Review of SME Technique Features

Based on the previous analysis, in this section we carry out a brief review of the most relevant features of SME control. In this sense, we have developed the Table 4.3 including the advantages and disadvantages of each studied SME technique.

Table 4.3: Review of SME technique characteristics.

SME Technique	Advantages	Drawbacks
SV	Very simple technique to tune and implement in a real controller. Does not include a grid-synchronizing technique (PLL).	No direct current limitation and low flexibility to adapt the dynamic behaviour of the converter.
IE	Simple technique and includes a direct current limitation. More flexible than SV to adapt the dynamic behaviour.	Requires a PLL for synchronization, which might cause instability issues and includes a derivative term in the control that can cause sudden variations. Does not provide inertial behaviour for power reference variations.
CCVSM	Quite simple technique and includes a direct current limitation. Very flexible to adapt the dynamic behaviour of the converter and does not require any PLL.	The parameters of the virtual SM they include must be carefully defined to avoid excessive overshoots under power variations.
VCVSM	Includes a direct current limitation and is very flexible to adapt the behaviour of the converter.	Requires a PLL for synchronization and is a very complex technique to tune and implement.

4.3.5 Impedance-Based Stability Analysis

Once we have verified the small-signal models in time-domain simulations and we have proven their performance under different types of perturbations, the next step is to study the stability of each system.

As we have already mentioned, in the literature there is a wide variety of methods to determine the stability of power electronic systems connected to ac. In this case we have decided to employ the GNC following the process employed by Belkhayat in [112] and by Burgos *et al.* in [110], which are based on the GNC theorem proposed by MacFarlane and Postlethwaite in [113] and [114]. With such method the stability of a closed-loop system can be determined by studying the location of the open-loop poles and encirclements of the $(-1+j0)$ point by the eigenvalues $\{\lambda_1, \lambda_2\}$ of the return-ratio matrix $\mathbf{L}_{dq}(s)$ (for the sake of simplicity in the following expressions the function of s is omitted in the notation, simplifying to $\mathbf{L}_{dq}$). By recalling the theorem of MacFarlane in [113]:

Theorem 1 *Let the multi-variable feedback system shown in Figure 4.23 have no open-loop uncontrollable and/or unobservable modes whose corresponding characteristic frequencies lie in the right-half plane. Then this configuration will be closed-loop stable if and only if the net sum of anti-clockwise encirclements of the critical point* $(-1+j0)$ *by the set of characteristic loci of* $\mathbf{L}_{dq}$ *is equal to the total number of right-half plane poles of* $\mathbf{Z}_{S_{dq}}$ *and* $\mathbf{Z}^{-1}_{L_{dq}}$.

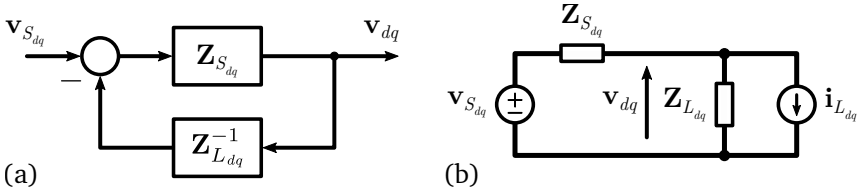

Figure 4.23: Representation of an ac source and load in the dq-domain.

The return-ratio matrix $\mathbf{L}_{dq}$ is given by [110]:

$$\begin{aligned}\mathbf{L}_{dq} &= \mathbf{Z}_{S_{dq}}\mathbf{Z}^{-1}_{L_{dq}} \\ &= \mathbf{Z}_{S_{dq}}\mathbf{Y}_{L_{dq}} \\ &= \begin{bmatrix} Z_{S_{dd}} & Z_{S_{qd}} \\ Z_{S_{dq}} & Z_{S_{qq}} \end{bmatrix} \begin{bmatrix} Y_{L_{dd}} & Y_{L_{qd}} \\ Y_{L_{dq}} & Y_{L_{qq}} \end{bmatrix} \\ &= \begin{bmatrix} L_{dd} & L_{qd} \\ L_{dq} & L_{qq} \end{bmatrix}\end{aligned} \tag{4.5}$$

The eigenvalues or characteristic gains of $\mathbf{L}_{dq}$ can be determined by finding the roots of the

following expression:

$$\det\left(\lambda\mathbf{I}-\mathbf{L}_{dq}\right)\triangleq\Delta\left(\lambda,s\right)=0 \tag{4.6}$$

where $\Delta(\lambda,s)$ is a polynomial as a function of λ and s. The reader is referred to [110] for the complete derivation of the resulting polynomial to obtain $\{\lambda_1,\lambda_2\}$. In summary, if we consider that the amplitude of L_{dq} and L_{qd} is very small, these eigenvalues can be approximated to:

$$\begin{aligned}\lambda_1 &= L_{dd}\\ \lambda_2 &= L_{qq}\end{aligned} \tag{4.7}$$

which facilitates the interpretation of results by looking at the diagonal terms of the equivalent impedances as will be shown later.

In order to obtain $\mathbf{L}_{dq}$, we need to extract the source ($\mathbf{Z}_{S_{dq}}$) and load impedances ($\mathbf{Z}_{L_{dq}}$) from the systems whose stability we want to analyse. In this context, we have assumed that in the case of the power converter, the ideal voltage source, its series impedance, Z_g, and the capacitor C_f of the *LC* filter are the source of the system and the rest is the load—i.e. the VSC with its control and the output series Z_f impedance (Figure 4.24). Regarding the SM, as the capacitor we have included in its output is very small (refer to Appendix A for more details), the source is composed by the ideal voltage source and its series impedance, and the load is the SM and its control strategy.

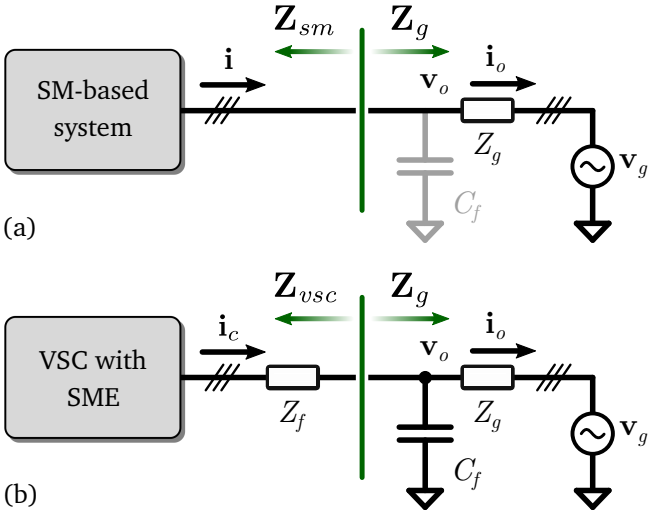

Figure 4.24: Point from which impedances are calculated and measured: (a) SM-based system and (b) VSC controlled by SME techniques.

The process followed to obtain the analytical impedances is the same for the SM-based generator and SME-controlled converter models. The usual approach in the literature is to obtain these impedances by rearranging the transfer functions of control as well as physical

parts of these systems, such as in [12, 109, 115, 116]. However, our approach is based on calculating these impedances directly from the developed small-signal state-space models.

This method has its own advantages and drawbacks compared to the one employed in the literature. At transfer function-based derivations we have information about which part of the system affects each of the terms in the $\mathbf{Z}_{dq}$ matrices. This information can be also obtained in the proposed method by doing all the process symbolically, but it can be challenging due to the large matrices that need to be inverted.

On the other hand, in the proposed method the calculation of the necessary impedances and admittances can be easily done by splitting state-space systems into two subsystems from the point we want to obtain them (Figure 4.25).

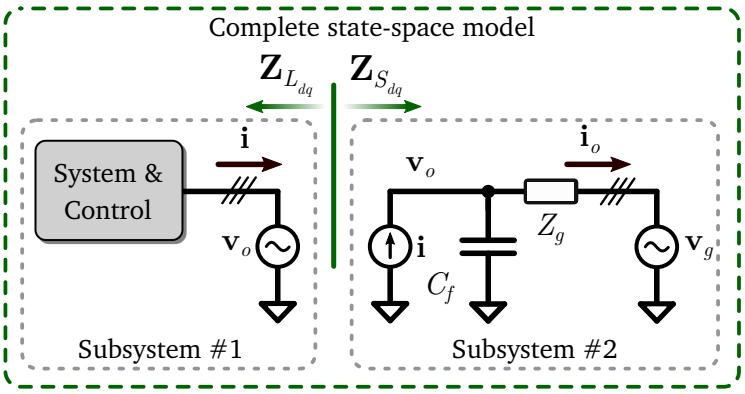

Figure 4.25: Block diagram of state-space models division to calculate analytical impedances.

Consider for instance the common parts of the complete state-space systems employed to model the previously studied systems:

$$\frac{d}{dt}\begin{bmatrix} \tilde{i}_d \\ \tilde{i}_q \\ \vdots \\ \tilde{v}_{o_d} \\ \tilde{v}_{o_q} \\ \vdots \end{bmatrix} = \mathbf{A}\begin{bmatrix} \tilde{i}_d \\ \tilde{i}_q \\ \vdots \\ \tilde{v}_{o_d} \\ \tilde{v}_{o_q} \\ \vdots \end{bmatrix} + \mathbf{B}\tilde{u} \tag{4.8}$$

Taking into account that Subsystem #2—i.e. the source in our case—is composed by an ideal voltage source, an *RL* series filter and a capacitor, it is straightforward to obtain its series impedance $\mathbf{Z}_{S_{dq}}$.

Therefore, our next step is to obtain from this small-signal state-space model the admittance matrix that corresponds to Subsystem #1—i.e. the load subsystem—which can be rep-

resented as:

$$\begin{aligned}\mathbf{Y}_{L_{dq}} &= \begin{bmatrix} Y_{L_{dd}} & Y_{L_{dq}} \\ Y_{L_{qd}} & Y_{L_{qq}} \end{bmatrix} \\ &= \begin{bmatrix} \tilde{i}_d/\tilde{v}_{o_d} & \tilde{i}_d/\tilde{v}_{o_q} \\ \tilde{i}_q/\tilde{v}_{o_d} & \tilde{i}_q/\tilde{v}_{o_q} \end{bmatrix}\end{aligned} \tag{4.9}$$

Splitting (4.8) in Subsystem #1 and #2 yields:

$$\frac{d}{dt}\begin{bmatrix} \tilde{i}_d \\ \tilde{i}_q \\ \vdots \\ \tilde{v}_{o_d} \\ \tilde{v}_{o_q} \\ \vdots \end{bmatrix} = \mathbf{A}\begin{bmatrix} \tilde{i}_d \\ \tilde{i}_q \\ \vdots \\ \tilde{v}_{o_d} \\ \tilde{v}_{o_q} \\ \vdots \end{bmatrix} + \mathbf{B}\tilde{u} \rightarrow \begin{cases} \dfrac{d}{dt}\begin{bmatrix} \tilde{i}_d \\ \tilde{i}_q \\ \vdots \end{bmatrix} = \mathbf{A}'\begin{bmatrix} \tilde{i}_d \\ \tilde{i}_q \\ \vdots \end{bmatrix} + \mathbf{B}'\begin{bmatrix} \tilde{u}' \\ \tilde{v}_{o_d} \\ \tilde{v}_{o_q} \end{bmatrix} \\ \dfrac{d}{dt}\begin{bmatrix} \tilde{v}_{o_d} \\ \tilde{v}_{o_q} \\ \vdots \end{bmatrix} = \mathbf{A}''\begin{bmatrix} \tilde{v}_{o_d} \\ \tilde{v}_{o_q} \\ \vdots \end{bmatrix} + \mathbf{B}''\begin{bmatrix} \tilde{u}'' \\ \tilde{i}_d \\ \tilde{i}_q \end{bmatrix} \end{cases} \tag{4.10}$$

By applying the following expression we can obtain the transfer functions of each subsystem, including the terms of (4.9):

$$\begin{aligned}\mathbf{G} &= \frac{\tilde{x}}{\tilde{u}} \\ &= (s\mathbf{I} - \mathbf{A})^{-1}\mathbf{B} \\ &= \begin{bmatrix} \tilde{x}_1/\tilde{u}_1 & \dots & \tilde{x}_1/\tilde{u}_n \\ \vdots & \ddots & \vdots \\ \tilde{x}_m/\tilde{u}_1 & \dots & \tilde{x}_m/\tilde{u}_n \end{bmatrix}\end{aligned} \tag{4.11}$$

Once we have derived the source impedance and load admittance we can solve the system in (4.6) to obtain the characteristic gains or eigenvalues $\{\lambda_1, \lambda_2\}$.

In the following sections we first show the impedances of the previously studied systems and then we plot the Nyquist plots of their eigenvalues to analyse their stability.

Output impedance comparative evaluation

In the following figures we illustrate the impedances of the grid side and the SM/converter side—by inverting the obtained admittances—for each case. Note that, as in Section 4.3.2, we have set the systems at a $p = 0.5$ p.u. point of operation, with the power flow going to the grid side.

In order to corroborate the correctness of the impedances prior to analysing their stability, we have derived them not only by following the above-mentioned procedure, but also by measuring them in the simulations with the original non-linear systems. For the latter, we have employed a single-tone injection of current at the point where we split the source and the load (Figure 4.26), following the procedure proposed by Rygg *et al.* in [116].

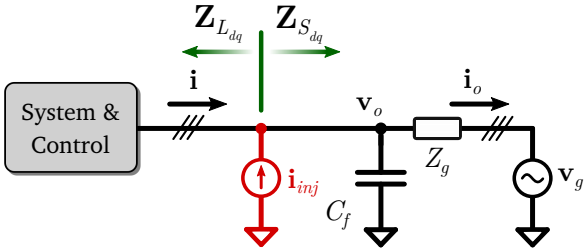

Figure 4.26: Current injection point to measure the source and load impedances.

Figure 4.27 shows the impedance of the SM-based generator with its control, and the impedance of the grid including the series impedance Z_g and the decoupling capacitor C_f mentioned in Appendix A.

We can observe that the shape of the *dd* and *qq* grid impedances resembles that of an *RL* circuit as expected, because the magnitude of the decoupling capacitor is very low compared to the rest of components in the grid. Moreover, its *dq* and *qd* impedances are completely flat, representing the behaviour of a resistor. It is worth noting however that the magnitude of these off-diagonal impedance terms is very small compared to the diagonal terms of the matrix $\mathbf{Z}_g$.

Regarding the impedance of the SM and its control, we can see that its diagonal terms $Z_{sm_{dd}}$ and $Z_{sm_{qq}}$ also have a very clear *RL* shape except in the very low frequency range ($< 7 \sim 8$ Hz), where it starts behaving as a capacitor.

This *RL* shape is due to the windings of the SM, as they predominate over most of the part of the frequency range. This is a very desired feature of systems connected to electric grids—which are very inductive—because they usually show a very stable behaviour. In this case, the *dd* impedance term of the machine is higher than the one from the grid side, and they do not cross in the analysed frequency range, meaning that most surely the eigenvalue associated with L_{dd} will not show any instabilities. Something similar occurs with the *qq* impedances, but in this case their magnitudes are very similar, which could weaken the stability margins of their associated eigenvalue.

Regarding the converters controlled by SME techniques, Figure 4.28 illustrates the frequency response of the impedances of the analysed four controller families, as well as the equivalent grid impedance in black—which is equal in the four cases.

These curves show very different characteristics of the impedances of each controller, which means they will also have very different characteristics in terms of stability. Moreover, we can

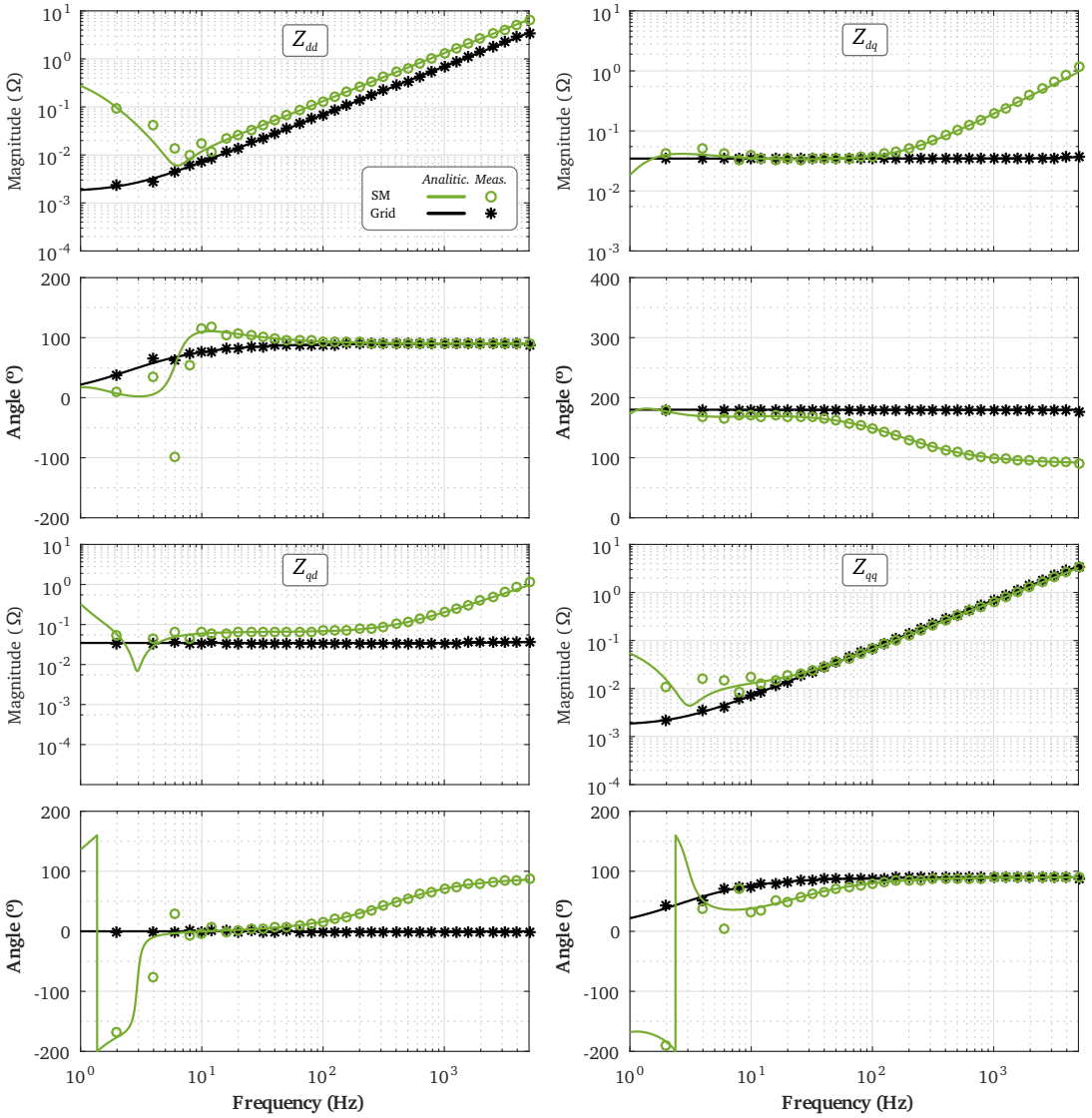

Figure 4.27: *dq* domain output impedances of SM-based generator and the grid.

observe that in this case the grid impedance has two resonance peaks at frequencies around 400 and 500 Hz. These peaks are caused by the interactions of the grid side inductance and the converter output filter capacitor, which has been included in the grid-side impedance. The reason for having two peaks instead of one is that the system is represented in the *dq* domain, which is rotating at the grid frequency of 50 Hz. Therefore the original resonance peak that would be around 450 Hz if it was represented in the *abc*-domain, is decomposed in two peaks of 450 ± 50 Hz.

Similar to the SM, the SV, CCVSM and VCVSM techniques show an *RL* shape in the *dd* and *qq* terms of their equivalent impedances.

Among these three approaches, the SV has the most clean shape in the entire frequency

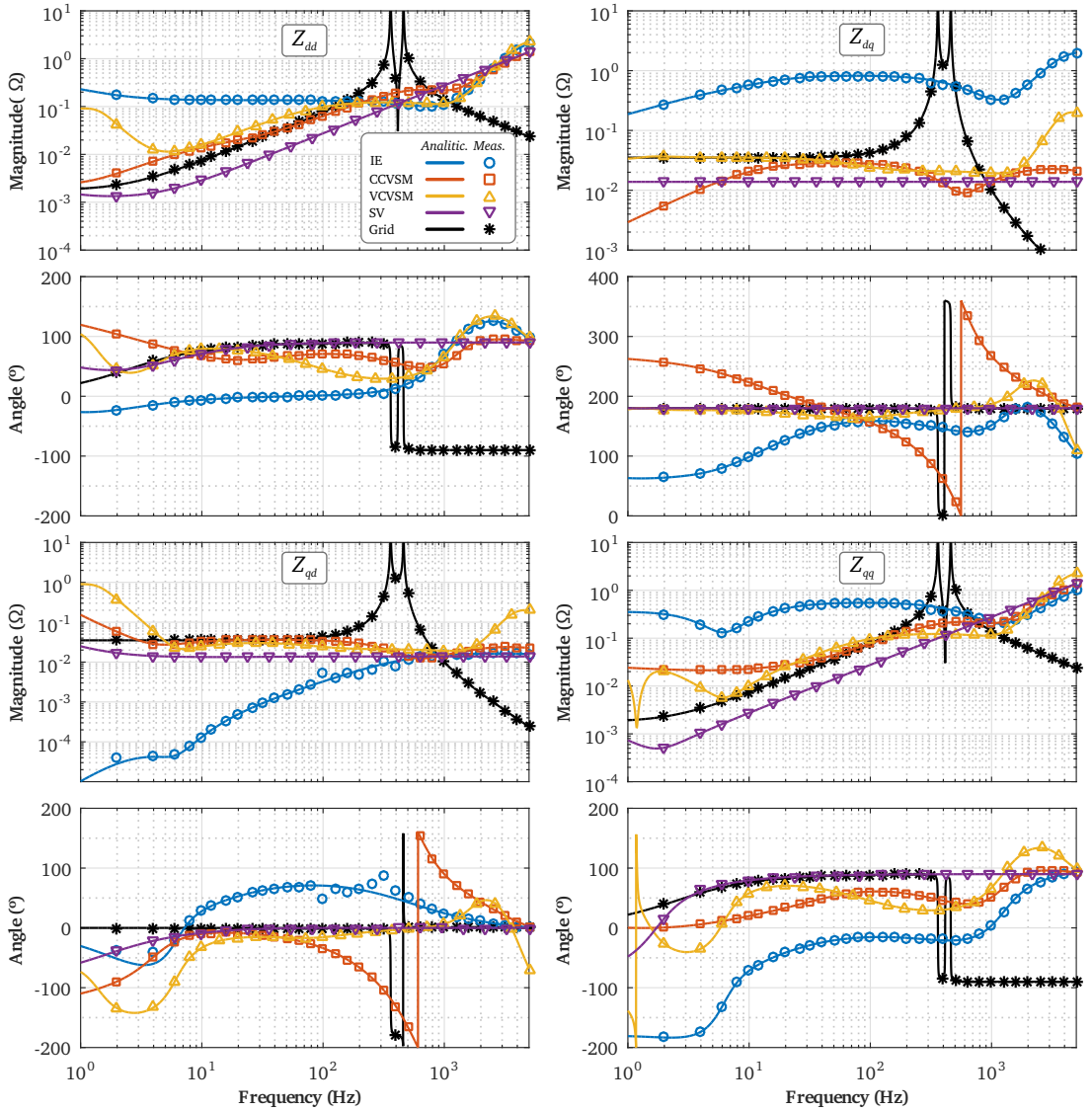

Figure 4.28: *dq* domain output impedances of SME-controlled VSC and the grid.

range, which is due to the simplicity of the controller itself. The low number of control loops compared to other techniques introduces less disturbances in the shape of these impedances, so the impedance of SVs is mainly dominated by the output *RL* filter of the converter. This is an interesting conclusion because it means that the stability characteristics of converters controlled with this technique will be determined significantly by their output filter and not so much by the parameters of the control technique.

The impedance of VSM techniques—i.e. the CCVSM and VCVSM—is more irregular than in the previous case, specially in the case of the VCVSM. As we mentioned before, the latter is the most complex technique among the analysed approaches, which has a direct impact on its impedance shape and stability. In any case, the impedances of the VSM techniques

show a relatively clean shape in the entire frequency range. Moreover, their magnitude is higher compared to the impedances of the SV in the most part of the plot, which as mentioned before is a desirable feature in terms of stability. One of the reasons for the higher magnitude impedances of VSM techniques is the virtual-impedances they integrate in the controllers. In the case of the CCVSM, for instance, these impedances could be adapted to emulate higher SM virtual windings in order to improve stability characteristics of the overall system; however, this would also modify the dynamic response of the converter under disturbances, so we have to reach a compromise to ensure a correct operation.

Among the studied configurations, the results of the IE-controlled converter are the most different ones in terms of the frequency response of their equivalent impedance. As we can see in Figure 4.28, the *dd* term of the impedance represents the behaviour of a resistance in most part of the analysed frequency range. Approximately at 500 Hz the phase of this term begins to increase and the magnitude resembles more the one seen at the rest of control techniques. Regarding the *qq* term, it shows a similar behaviour as the previous one but in this case with more irregularities primarily in the low frequency range. This irregular shape in the low-frequency range of the *qq* impedance term can be observed not only in the IE technique but also in the VCVSM one. This phenomena is mainly caused by the bandwidth of the PLL, which actuates on the *q*-axis voltage to find and lock to the grid frequency, and we can observe that this behaviour is not reproduced in the other two control techniques.

The main difference of the IE technique and the rest is observed in the off-diagonal terms of its equivalent impedance. The *qd* term, for instance, presents a negligible magnitude, whereas the *dq* term is clearly higher compared to the rest of techniques and even with the rest of impedances of the IE control. The main cause for this might be way the *swing equation* is implemented in the control, as in this case we are using the derivative of the frequency obtained with the PLL. Taking into account that this frequency is directly calculated from v_{o_q}, it could explain the high coupling between the *d*-axis current and *q*-axis voltage.

In general, it can be said that at frequencies higher than 500 Hz the output filter of the converter is the dominating impedance, and the control techniques have less impact. This can be clearly seen in the SV impedance, where the controller has shown a very low impact on the analysed frequency range.

Stability analysis based on the generalized Nyquist criterion

Based on the impedances obtained in the previous section, here we derive the return-ration matrix $\mathbf{L}_{dq}$ and the eigenvalues of each system in order to analyse their stability with the generalized Nyquist criterion as shown in Section 4.3.5.

As we consider the SM to be the benchmark system, we first illustrate its Nyquist plot in Figure 4.29. Note that the arrows indicate the direction of the plot for an increasing frequency.

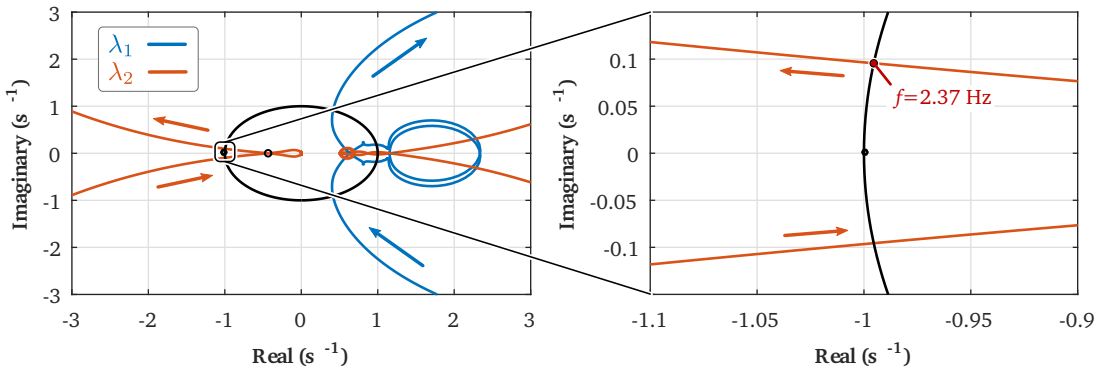

Figure 4.29: Nyquist plot of SM-based generator eigenvalues.

These curves show that the eigenvalues λ_1 and λ_2—associated to the L_{dd} and L_{qq} terms, respectively, when off-diagonal terms of $\mathbf{L}_{dq}$ are negligible—they cross the unit circle two times each, very close to the $(-1+j0)$ point in the imaginary plane. The closest point to $(-1+j0)$ where the eigenvalues cross the unity circle is when the frequency has a value of 2.37 Hz, which matches with the frequency of the oscillation we observed in the time-domain simulations of the SM (Section 4.3.2). This means that the Nyquist curve, as well as the dominant eigenvalues of the state-space model we showed in the previous section, is predicting properly the oscillatory phenomena of the machine.

In this case, the overall phase margin (PM) is 5.49° whereas the gain margin (GM) is 7.22 dB. Taking into account the variability of real systems and that the point of operation of the SM changes depending on the conditions of the grid, the PM is very low to ensure the stability of the system on the entire operating range. However, we must take into account that in this specific case we are considering the fundamental part of the SM-based generator and we have not included for instance any power system stabilizer, and the damper windings could be designed differently to improve this behaviour. Moreover, the grid-side inductance of the analysed system has a relatively high value (0.2 p.u.), which can reduce significantly the stability margins of this system and the following SME-controlled converters.

Figure 4.30 illustrates the Nyquist plots of the four analysed SME-controlled converters. In this case, we can notice that their curves are significantly different from each other, so we will analyse them separately.

The first case, which illustrates the eigenvalues of the SV control strategy (Figure 4.30(a)), shows that the two curves are very close to each other. Even though these eigenvalues do not encircle the $(-1+j0)$ point, it can be seen from the zoomed figure that they are very close from the horizontal axis. This means the PM is very low (0.21°) and, as in the case of the SM, the system could easily become unstable if some parameters vary.

From the curves we can observe that the frequency in which both eigenvalues cross the unity circle near the $(-1+j0)$ is around 720 Hz. If we have a look at the impedances shown

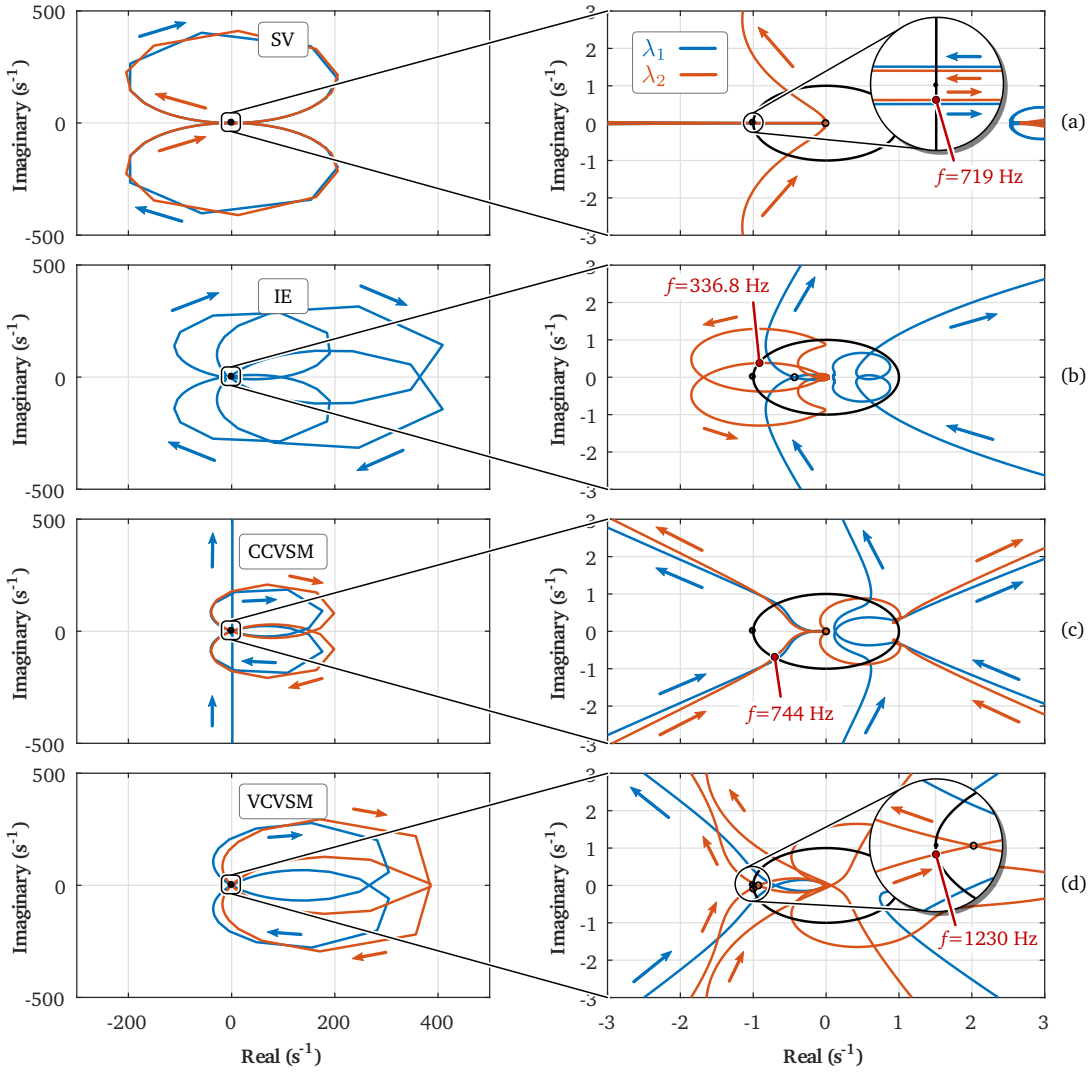

Figure 4.30: Nyquist plots of SME-controlled VSC eigenvalues: (a) Synchronverter, (b) Inertia-emulation, (c) Current-controlled VSM and (d) Voltage-controlled VSM.

in the previous section, we can see that this frequency coincides with the part in which the *dd* and *qq* terms of the converter and grid cross with each other. Considering the off-diagonal terms of the converter impedance are very small, we can say that the eigenvalues are directly related to the diagonal terms of the return-ration matrix. At these crossing points, the phase difference between the impedance of the converter and the grid is relatively high, which could be the cause of such a low stability margin. In this context, one of the possible solutions to improve the stability characteristics of a SV-controlled converter would be to include an active damper to avoid the resonances of the output *LC* filter or modify this filter to change the point of interaction.

The second case, related to the eigenvalues of the IE technique (Figure 4.30(b)), illus-

trates a very special and interesting case compared to the rest of analysed systems. Here, the eigenvalues encircle twice each the $(-1+j0)$ point, which at a first glance would mean that the system is unstable. However, the time-domain simulations and the stability analysis of the derived state-space system demonstrate that the system is stable, so we must interpret these encirclements in another way.

If we look at the Nyquist plots more in detail, we can notice that the direction of the encirclements is the opposite for both eigenvalues; λ_1 encircles two times the $(-1+j0)$ point in the clockwise direction, whereas λ_2 encircles it another two times in the counter-clockwise direction. If we consider the encirclements of the $(-1+j0)$ point to be the **total number of encirclements** done by the two eigenvalues—as if they were a single Nyquist curve—we notice that **the sum** in this case **equals zero**, which would mean the system is stable. After carrying out several tests and comparing the stability of the system based on the eigenvalues of the state-space model and based on the individual terms of the return-ratio matrix, we can conclude that our assumption is correct and the stability must be determined based on the net sum of encirclements.

An interesting conclusion of this analysis comes also from the impedance characteristics of this specific case. If we look in detail at Figure 4.28, we can see that a possible cause for these uncommon Nyquist curves could be the *dq* term of the impedance of the IE controlled converter. Usually, as it happens with the rest of analysed systems, off-diagonal terms are almost negligible compared to diagonal terms, so the stability is many times determined neglecting the off-diagonal terms in the analysis [117]. However, the results of the system we are analysing demonstrate that this assumption is not always valid, and there are cases where off-diagonal terms play a significant role in the stability of the overall system.

In any case, special care must be taken when defining the PM and GM of this specific case, because the classical rules of the Nyquist criterion do not apply directly. In this sense, we propose to calculate the PM by looking at the nearest crossing of the unity circle by any of the eigenvalues, and the GM by considering the absolute value of the gain margin obtained for the horizontal axis crossing that is most near to the $(-1+j0)$ point. Following these rules, the GM is 7.45 dB whereas the PM is approximately 22.54°. However, a more in depth analysis is required to redefine the theoretical background of the GNC to include systems with characteristics that are similar to the IE-controlled converter, and to select adequate criteria to determine the stability margins of such systems. As it is out of the scope of this thesis, we leave it as a possible future research line.

The results of the CCVSM technique (Figure 4.30(c)) show very good characteristics in terms of stability compared to the rest of SME strategies. The eigenvalues do not encircle the $(-1+j0)$ point and the system has a GM of ∞—as the eigenvalues do not cross the negative part of the real axis—and a PM of 45.24°, which demonstrates that the system is very robust under parameter variations.

In this case we can see that the frequency in which the eigenvalues cross the unity circle most near to the $(-1 + j0)$ point is near 744 Hz. Even though this frequency is very similar to the SV-controlled system, it is clear from the previously shown impedance figure that in this case the phase difference between the converter equivalent impedance and the impedance of the grid is much lower. This might be the reason for this significant difference in the SV and the CCVSM technique.

Finally, the curves of the VCVSM (Figure 4.30(d)) show that the system is very close to becoming unstable with a GM of 0.65 dB and a PM of 3.44°, determined by the second eigenvalue. Moreover, the frequency of the point in which the eigenvalues—in this case λ_2—cross the unity circle most near to the $(-1 + j0)$ point is nearly 1230 Hz, which means that the converter is interacting with the grid in this range of frequencies. Looking back at Figure 4.28, we can see that this frequency corresponds to the case where Z_{qq} crosses with the impedance of the grid, where they have a high phase difference. As in this case the off-diagonal terms of $\mathbf{Z}_{vsc_{dq}}$ are very low compared to the diagonal terms, we can say that Z_{qq} is closely related to λ_2, so it can be concluded that the qq term is the main responsible for such a low stability margin.

Even though in this case λ_1 shows better margins than λ_2, we can observe that both eigenvalues have a similar shape and are not so far from each other. A method for improving the stability margins of this specific case would be to integrate an active damping loop in the regulator of the converter to dampen the resonances of the output filter of the converter, as it is done in [92] or [23].

4.4 Summary and Discussion

Throughout the chapter we have seen that even though the analysed systems behave similarly under reference power and grid frequency perturbations, their impedance characteristics and hence stability when connected to the grid is very different.

Table 4.4 summarizes the most relevant characteristics of the analysed systems, compared to the SM.

Table 4.4: Properties of SM-based generators and SME-controlled converters.

System/ Technique	Complex.	PLL	Current Lim.	Flexib.	Stab.	GM (dB)	PM (°)	Crit. Freq. (Hz)
SM	n/a	✗	n/a	Low	Low	7.2	5.49	2.73
SV	Low	✗	✗	Low	Low	48.32	0.21	719
IE	Low	✓	✓	Medium	Medium	7.45	22.54	336.78
CCVSM	Medium	✗	✓	High	High	∞	45.24	744
VCVSM	High	✓	✓	High	Low	0.65	3.44	1230

Firstly, we have observed that the equivalent impedances of SMs have a very clear *RL* shape in the diagonal terms and off-diagonal terms behave as resistors with very low amplitudes. Although this is a desirable feature for systems connected to the grid, we can notice that the analysed system interacts with the grid at very low frequencies, causing severe oscillations and very low stability margins. The causes might be the design of the machine itself or its controller—e.g. its damping windings or the lack of a power system stabilizer—or the high grid impedance employed in the analysed systems.

Similarly, we have reached several conclusions by studying the different SME-controlled converters.

On the one hand, by looking at Table 4.4 we can say that CCVSM is the technique that provides the highest stability margins from the analysed non-augmented control techniques. Moreover, this technique shows a good compromise between complexity and flexibility in terms of the degrees of freedom to vary the dynamic behaviour of the converter under perturbations.

On the other hand, referring to the IE-controlled converter, we have identified a case that does not show standard characteristics in terms of impedance and stability. One of the off-diagonal terms of the impedance shows a higher amplitude compared to the other control techniques and compared to the diagonal terms. This is clearly reflected in the evolution of the eigenvalues in the imaginary plane, which encircle the critical $(-1 + j0)$ point twice in the clockwise direction and twice in the counter-clockwise direction. After carrying out several tests, we conclude that the stability is determined based on the net sum of encirclements of the critical point. However, special care must be taken when determining the stability margins by looking at these Nyquist curves, as classical methods are not applicable in this case.

In general, we have also seen that the stability of these converters is very dependant not only on the impedance of the grid, but also on the characteristics of the converter output filters. From the obtained results, we can see that in three of the four cases the frequency in which the converters interact with the grid are very close to the resonances of the implemented *LC* filter. Therefore, either these filters have to be designed considering the stability of the system or we have to include active damping loops in the control strategies to shape the equivalent impedance of the converter in this specific region.

Finally, several questions have arisen from the analysis carried out in the chapter: how must we analyse the stability of converters that emulate the behaviour of synchronous machines, i.e. in grid-forming mode? Who should be considered as the source and the load system for stability analyses? How should we analyse the stability of systems whose impedance off-diagonal terms cannot be neglected?

We leave these open questions for further research activities.

Chapter 5

DC Systems: Capacitance-Emulation Techniques

The synchronous machine emulation techniques analysed in the previous chapter are essential in order to provide inertial behaviour under different disturbances in converter-dominated grids.

However, the emulation of inertia has been entirely focused on ac systems, and there are no studies oriented to study the dynamic or "inertial behaviour" of dc grids, which are becoming a fundamental part in the distribution of energy. Unlike classical ac grids, these dc grids are mainly dominated by power electronic converters—because rotational devices with mechanical inertias cannot be directly connected—which makes them highly vulnerable under perturbations.

In this context, our objective in this chapter is to identify and analyse the aspects that ac and dc grids have in common, and propose novel low-level control techniques for power converters connected to dc grids that provide an analogous dynamic behaviour (Figure 5.1).

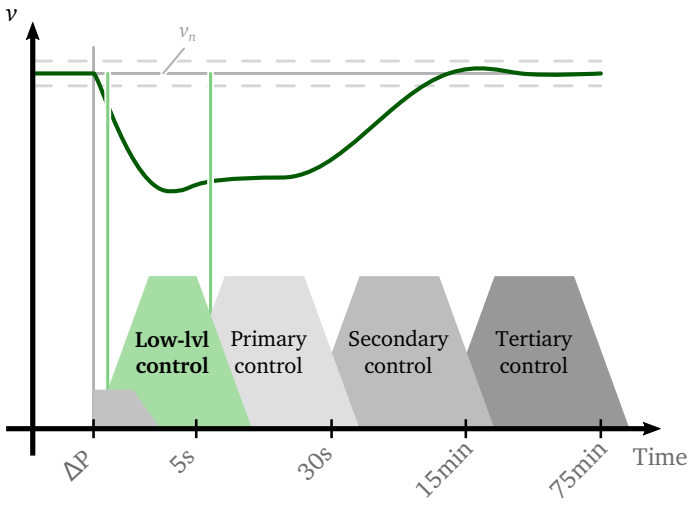

Figure 5.1: Operation range of the low-level control in the hierarchical regulation of a dc microgrid.

In Chapter 2 we showed that dc grids are arising as one of the most promising alternatives for the integration of distributed generation and energy storage systems into the ac infrastructure. Until recently most of the implemented dc parts have been point-to-point links to interconnect different ac grids, such as HVDC links. In most of these systems the voltage of the dc grid is determined by one of the terminal converters whereas the power flow is controlled with the other one. With the proliferation of MTDC grids and dc distribution grids in general, the control of the bus voltage becomes more challenging and the operation principles have to be redefined.

In this thesis, as mentioned before, our purpose is to operate dc grids in the same way ac grids are controlled nowadays, so the overall management of the network remains the same for the grid operator. The idea is to employ a hierarchically configured control structure to carry out the tertiary, secondary and also primary regulation of the voltage employing mode-adaptive droop controllers as explained in Chapter 3. This way, the control of the dc bus is not carried out by a single-unit but with several generation, storage systems and loads in parallel sharing all the perturbations.

Moreover, the purpose is to improve the dynamic or "inertial response" of dc grids through power electronic converters as it is done with SME-controlled systems at weak ac grids, shown in the previous chapter. In order to do so, we analyse the analogies between ac and dc grids to propose equivalent low-level techniques for the devices participating in the regulation of the bus voltage.

5.1 Equivalence to AC Systems

As we explained in Section 4.1, the magnitude of frequency deviations of an ac grid are proportional to the inertia connected to the grid, and can be represented with the *swing equation* as follows:

$$\boxed{2H\frac{d^2\delta}{dt^2} = \frac{p_m}{\omega} - \frac{p_e}{\omega} - K_D\Delta\omega} \tag{5.1}$$

Thanks to this inertia, rotating generators are capable of storing a kinetic energy that is released/absorbed when the frequency of the grid decreases/increases.

If we look at the quantity of kinetic energy that is stored in the grid, we can see that it is dependent not only on the inertia of the device but also on the frequency of the ac grid:

$$E_K = \frac{1}{2}J\omega^2 \tag{5.2}$$

As we can observe, (5.2) is very similar to the equation employed to measure the energy

of a capacitor:

$$E_C = \frac{1}{2} C v^2 \tag{5.3}$$

Equations (5.2) and (5.3) clearly show that ac and dc grids are equivalent in terms of how energy is stored. By comparing them we can see that the mechanical inertia is analogous to the capacitance, whereas the frequency in the ac system is equivalent to the voltage in dc. Therefore, we can say that in dc grid the elements that store energy and provide an inertial behaviour under perturbations are the capacitors directly connected to the bus.

This analogy can be also noticed by looking at how power is transferred in ac and dc systems. On the former, we can look at this by analysing the power exchange between two nodes interconnected by a reactance X_s as in Figure 5.2:

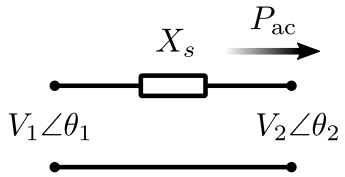

Figure 5.2: Power flow through a reactance in an ac grid.

In this system, we can express the exchanged power as follows:

$$P_{\text{ac}} = \frac{V_1 V_2}{X_s} \sin\underbrace{(\theta_1 - \theta_2)}_{\delta} \tag{5.4}$$

In this case, if we consider that the angle difference δ between V_1 and V_2 is very small, we can set $\sin(\delta) \approx \delta$, hence $\sin(\theta_1 - \theta_2) \approx \theta_1 - \theta_2$ and simplify (5.4) as follows:

$$\begin{aligned} P_{\text{ac}} &\approx \frac{V_1 V_2}{X_s} (\theta_1 - \theta_2) \\ &= \frac{V_1 V_2}{X_s} \int (\omega_1 - \omega_2)\, dt \end{aligned} \tag{5.5}$$

Here we can see that the transferred active power depends on the frequency difference between V_1 and V_2. If we consider for instance V_2 as the grid voltage—i.e. constant frequency—we can exchange power with the grid by adapting the output frequency of the system we are controlling. Basically, this is the principle of SME-controlled converters analysed in the previous chapter, in which active power is controlled by varying the frequency of the converter and reactive power with the voltage amplitude.

In dc, as there is no frequency we have no circulation of reactive power, and hence the exchange of active power is performed slightly different. Let us assume that we have the circuit shown in Figure 5.3 to analyse how power is exchanged at a dc circuit.

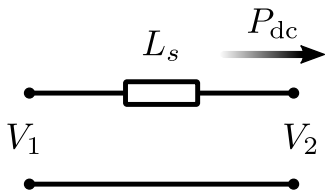

Figure 5.3: Power flow through an inductance in an dc grid.

Here, we can determine this power exchange as:

$$P_{\mathrm{dc}} = \frac{V_1}{L_s} \int (V_1 - V_2) dt \tag{5.6}$$

In this case, the power depends directly on the difference between V_1 and V_2. Therefore, if we consider V_2 to be the dc grid voltage, in order to control the power exchange with a dc grid, we need to control the output voltage of the system. This corroborates the previously mentioned analogy between the frequency of ac grids and voltage of dc grids.

This brief analysis shows that there are certain equivalences between ac and dc grids in terms of how energy stored and how power is transferred. Therefore, by taking advantage of the inertia/capacitance and frequency/voltage equivalences we can apply the same principles of operation in ac and dc grids.

In the previous chapter we showed that the inertial behaviour can be provided through power converters by employing SME techniques that emulate the response of classical synchronous generators. This is done by integrating the *swing equation* of these machines into the control strategies as shown in the left part of Figure 5.4. By employing such techniques, we reduce the RoCoF of the ac grid to avoid large frequency deviations and give more time for upper controllers to restore this frequency.

In the case of dc grids, we can follow the same procedure but emulating the behaviour of a capacitor instead of a mechanical inertia, and controlling the output voltage rather than the frequency. This means that in order to improve the dynamic or "inertial behaviour" of dc grids we have to reduce the rate of change of voltage (RoCoV) under a power perturbation by emulating a certain capacitance. We call this approach a virtual-capacitor (VC), because with such a control we would have a converter that responds as a capacitor directly connected to the bus, as shown in the right part of Figure 5.4.

Similar to how the normalized *swing equation* is obtained, we can also derive a per-unit version of the VC control technique [49]:

$$H_{dc} = \frac{1}{2} \frac{C V_b^2}{S_b} \tag{5.7}$$

As we will see in the following sections, the advantages of VCs are that we can adapt the

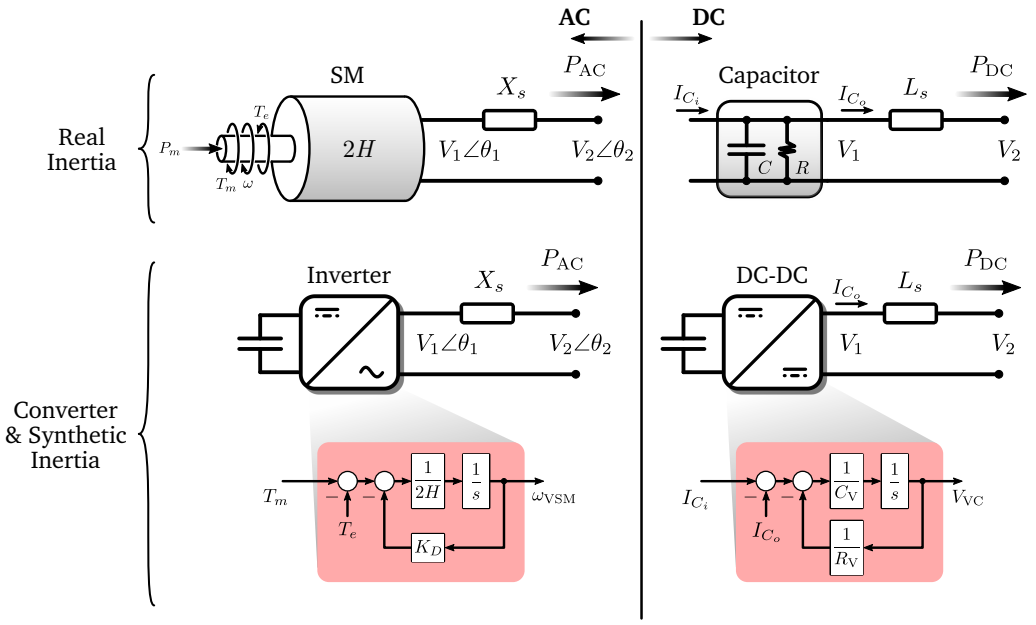

Figure 5.4: Analogy between SME techniques for ac and VC control for dc grids.

value of their virtual-capacitance in the controller to vary the dynamic characteristics of the converter and in consequence also the RoCoV of the grid.

5.2 Virtual-Capacitor Control

Inspired by the different SME control types identified in the literature, we propose two main approaches to integrate the VC technique in the controllers of power converters connected to dc grids:

- Voltage-controlled virtual-capacitor (VC2)
- Direct virtual-capacitor (DVC)

5.2.1 Voltage-Controlled Virtual Capacitor

Taking the classical droop control of dc-dc converters as the basis [13], and inspired by the concept of operation of VCVSMs techniques, we propose a technique that integrates the VC as illustrated in Figure 5.5.

As it can be observed, the lower-level part of the control is composed by classical cascaded current and voltage PI regulators. Here, considering that these regulators are fast, the dynamic behaviour of the converter with this technique under a power variation is mainly determined by the emulated capacitance, H_{dc}. In addition, the virtual-resistance R_V is analogous to the damping factor K_D of SMs. Usually, the damping torque of a SM is nearly 1% of the total torque

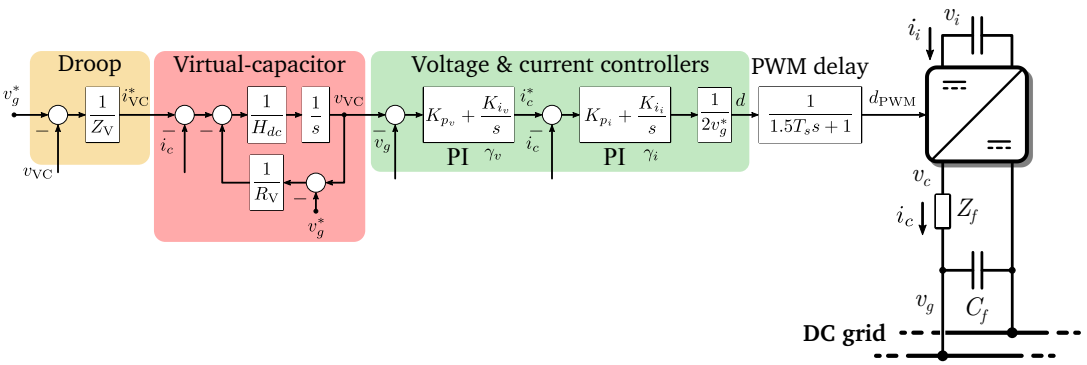

Figure 5.5: Voltage-controlled virtual-capacitor control technique inspired by VCVSM techniques.

of the machine, so the factor K_D is very small. In this case, as R_V is inversely proportional to K_D, its value must be high enough to reproduce a damping current.

In addition to the VC controller, an upper-level or primary control has been included in the form of a virtual-impedance (Z_V) which reacts based on the difference between the predetermined output voltage reference and the measured one. In this case Z_V is a real value, which means that it is merely a proportional gain. Therefore, it can be said that it is analogous to a classical P/V droop controller.

The main drawbacks of this technique are that the high number of control variables complicates the tuning of all parameters, and has a direct impact on the dynamic response of the converter due to the delays of the regulators.

However, having several control parameters also implies that there are more degrees of freedom to adapt the dynamic behaviour of the converter under perturbations, which improves the flexibility of the device. In addition, the integration of a current loop enables the direct limitation for instance under a fault condition.

5.2.2 Direct Virtual-Capacitor

This technique is inspired by the principle of operation of SVs, which means that unlike the proposed VC2 technique, it does not include any current or voltage regulator and feeds the voltage reference of the VC directly to the PWM (Figure 5.6).

As with the SV, this technique cannot directly limit the current of the converter, which can be problematic under fault conditions. Moreover, this technique does not offer many degrees of freedom to adjust the dynamic behaviour of the converter under perturbations, because of the low number of control parameters.

Nevertheless, the simplicity of this controller significantly facilitates its design and integration on a real platform. In addition, this technique has a very good behaviour because we can avoid oscillatory responses caused by current/voltage regulators.

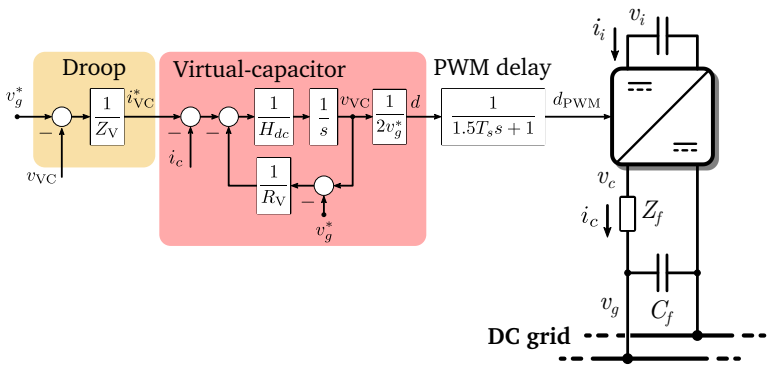

Figure 5.6: Direct virtual-capacitor control technique inspired by SV techniques.

5.3 Comparative Evaluation

The aim of this section is to analyse the dynamic performance and stability of the proposed VC techniques under grid perturbations for different controller parameters. On the one hand, we compare both approaches and demonstrate that we can reproduce the inertial behaviour of SME techniques in dc grids. On top of that, we carry out a parametric stability analysis to show the effect of different control as well as physical parameter variations in their dominant eigenvalues.

5.3.1 Dynamic Performance Under Perturbations

The structure of the proposed techniques are suitable for the integration of distributed systems as they enable the power sharing between parallel converters only with local measurements, which means there is no need for a communication network. This is an interesting feature for the control of systems connected not only to microgrids but also to weak or remote grids as mentioned in Section 2.2.

The main difference of the proposed controller over classical droop techniques is that the RoCoV of the dc microgrid under power variations can be adapted by modifying the virtual or synthetic capacitance.

Firstly, we have carried out various simplified simulations that do not consider any delays or dc-dc converter models in order to show the principles of operation of the proposed VC techniques.

The parameters employed for these simulations are shown in Table 5.1. In this case, based on the experimental platform we have developed, the base values are set for a very small-scale application, i.e. $S_b = 96$ W and $V_b = 48$ V.

The adaptation of the RoCoV by simply changing the virtual-capacitance value can be observed in Figure 5.7. Here, the dynamic response of a classical droop controller based on [13] is compared to the proposed DVC control with different virtual-capacitance values for a step-

Table 5.1: Parameter values for the simplified simulations.

Parameter	Value (p.u.)
L_f	0.0013
R_f	0.0042
C_f	0.23
v_g^*, v_i	1
i_g	0.5
Z_V	0.17, 0.125 and 0.083
R_V	42
H_{dc}	1.2, 12 and 60 s

shaped current perturbation.

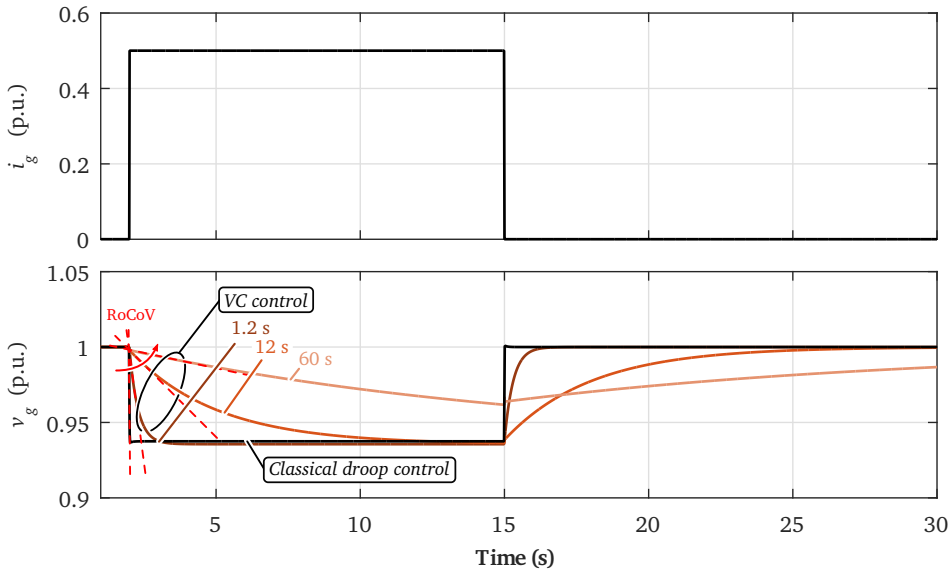

Figure 5.7: Response of a classical droop controller [13] and the proposed DVC controller under a power variation for different H_{dc} values.

The curves show that by varying H_{dc}, the transient behaviour of the bus voltage can be adapted—i.e. the RoCoV is decreased when the capacitor is increased—as it is done in VSM techniques by varying the emulated inertia (H). When several converters are combined with the same control strategy, the dynamics of the bus voltage under perturbations can be reduced so that supervisory or secondary controllers have more time to react and restore it to its rated value.

In addition, in Figure 5.8 we can also see that the steady-state operation point of the converter can be simply adapted by changing the virtual-impedance Z_V.

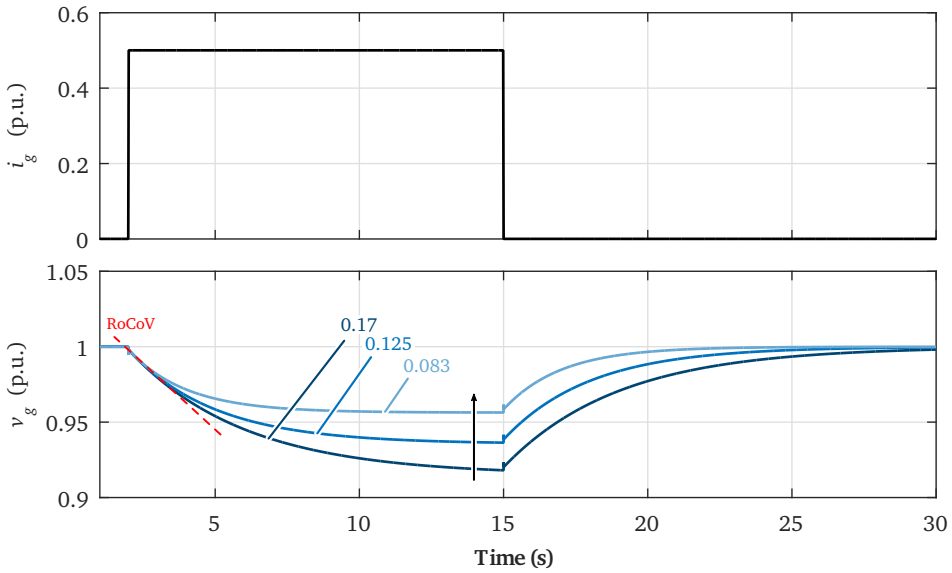

Figure 5.8: Response of the proposed DVC controller under a power variation for different Z_V values.

From this brief analysis we can conclude that the transient and steady-state behaviour of converters controlled by VC techniques can be adapted separately as it has been done with SME strategies for ac systems (Section 4.3.3). As we mentioned in the previous chapter, this is a very interesting feature for the integration of different dynamic systems into the grid, for example a battery-based or supercapacitor-based ESSs.

Let us employ a similar example as in the previous chapter composed by two converters connected in parallel—illustrated in Figure 5.9—the first one controlling an electrochemical battery module and the other a supercapacitor module.

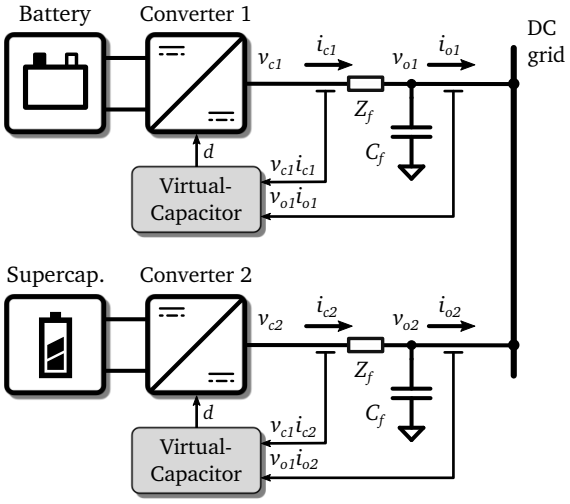

Figure 5.9: Different-dynamic VC-controlled converters connected in parallel.

We can configure the VC controllers so that the supercapacitors provide most of the power during transients and batteries operate mostly during the steady-state period. This way we could take advantage of the fast dynamics of supercapacitors in order to reduce the ageing of batteries by reducing their cycling.

Figure 5.10 shows a simplified simulation of this configuration for a sudden power variation in the grid. In this case, the controller of the battery is configured with a very low virtual-capacitance ($H_{dc} = 0.6$ s) and a small virtual-impedance ($Z_V = 0.8$) in comparison to the controller of the supercapacitor, which has a H_{dc} of 12 s and a Z_V of 100.

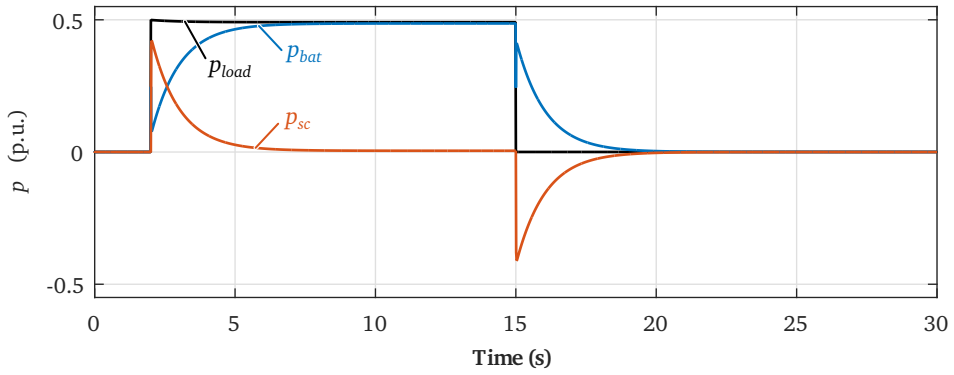

Figure 5.10: Different-dynamic VC-controlled converters connected in parallel.

The figure shows how the system with the highest inertial response—in this case the supercapacitor—provides most of the power during the transient period caused after the sudden load power variation. Then, in the steady-state part, this converter supplies no power and the battery converter becomes the responsible for supplying the load power. This corroborates that we can reproduce the principles of operation of SME techniques.

As we have already said, this is a very interesting and useful feature of the proposed VC strategies because we can integrate generation, storage systems or even loads of different dynamics in the grid by simply varying their control parameters. Combining SME techniques for inverters connected to ac grids and VC strategies for devices connected to dc grids the flexibility of the grid can be improved significantly—because they do not require any communication network to operate—while ensuring a robust operation thanks to the emulation of inertia.

Up to now we have shown the principles of operation of VC techniques by means of simplified simulation models. However, in order to study their stability characteristics we need detailed models that take into account different delays and the dynamics of the converters.

In this context, we have developed detailed small-signal state-space models of the proposed VC techniques following the steps ①–③ of the methodology employed in the previous chapter (Section 4.3.1). For the sake of simplicity, the analytical derivation of the equations of these small-signal models is included in Appendix C.

In order to evaluate performance of the controllers and the correctness and accuracy of

the analytical models shown in the appendix, we compare them to the non-linear models in time-domain simulations following the step ④ in the methodology. To do so, we first establish the point of operation of our systems to $i_g = 0.5$ p.u. and wait until they are in steady-state. Once at this point, we set a 0.1 p.u. current variation to observe how the power and voltage of the system respond.

The parameters of the converter and the filter are set as in Table 5.2. H_{dc} and Z_{V} are kept as in this table unless other thing is shown.

Table 5.2: Parameter values for the performance comparison.

Parameter	Value	Parameter	Value
L_c	0.0046	Z_{V}	0.125
r_{L_c}, r_{C_i}, r_{C_o}, r_n	0.00042	R_{V}	42
C_i, C_o	0.45	$T_{s_{\mathrm{PWM}}}$	10 μs
L_f	0.0013	K_{p_v}	0.6
R_f	0.0042	K_{i_v}	500
C_f	0.23	K_{p_i}	1.3
v_g^*, v_i	1	K_{i_i}	14
i_g	0.5	H_{dc}	12 s

Voltage-controlled virtual-capacitor

Figure 5.11 illustrates the curves of the non-linear and small-signal model of the dc-dc converter controlled by the proposed VC2 control strategy for a step-shaped current variation, for different virtual-capacitance values.

The curves show a very good accuracy between the non-linear and the linearized small-signal model, and demonstrate that even taking into account the delays of the PWM and the model of the dc-dc converter, the dynamic response can be varied by simply adapting H_{dc}. These results show however an oscillation at the beginning of the transient after the current step, which is mainly caused by the interactions of the converter passive elements and the output *LC* filter. In addition, after this oscillation the converter has a sudden drop due to the delays of the current and voltage PI regulators. As will be shown later, the tuning of these parameters to reach a compromise between a good dynamic response and stable operation is a challenging task.

Apart from that, in Figure 5.12 we show the time-domain simulations carried out for different Z_{V} values.

In this case we can also corroborate the conclusions obtained in the simplified simulations, as we can adapt the steady-state point of operation of the converter by changing the value of

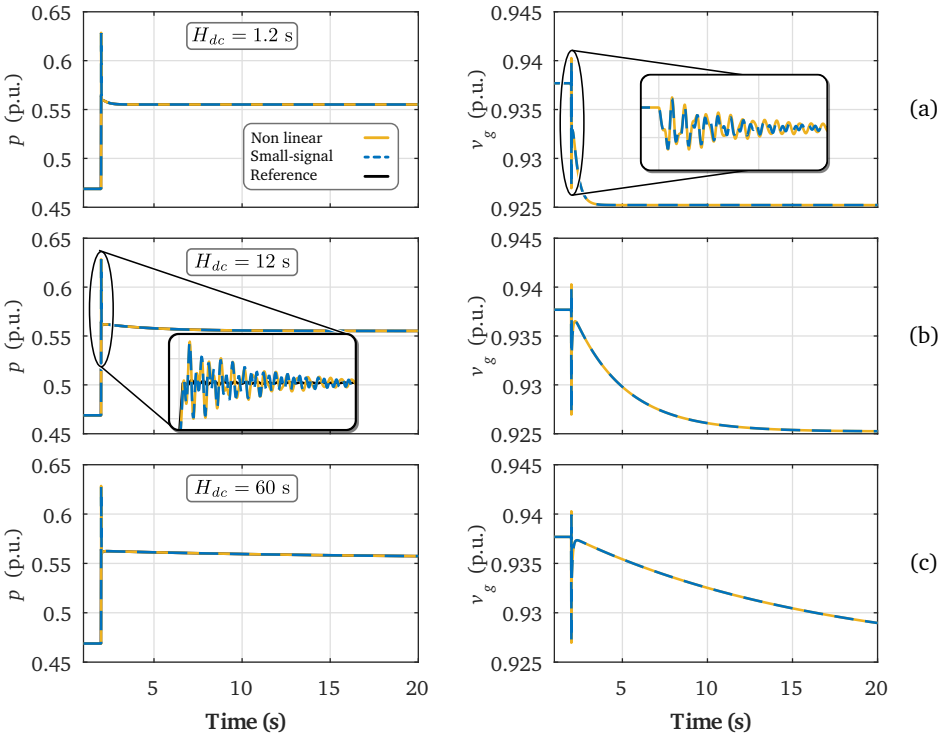

Figure 5.11: VC2 small-signal model validation for different H_{dc} values.

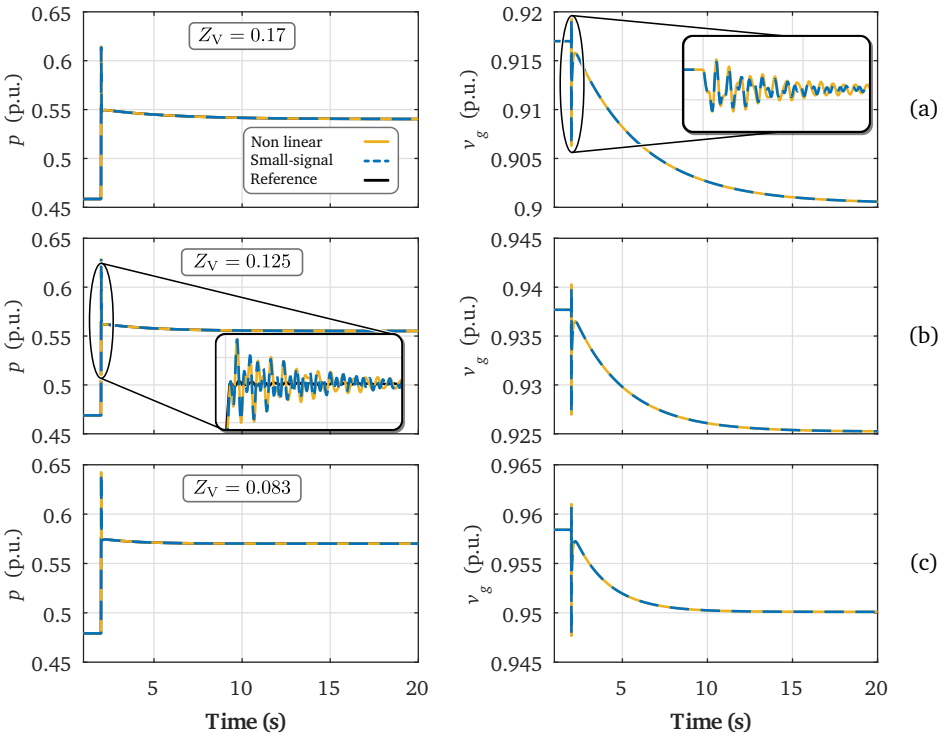

Figure 5.12: VC2 small-signal model validation for different Z_V values.

the virtual-impedance. Moreover, we can see that the curves of the non-linear and small-signal model match, meaning that the latter can be adequately employed later on to determine the stability of the system.

Direct virtual-capacitor

As in the previous section, we first show the curves of the DVC-controlled converter for different values of virtual-capacitance under a sudden load current variation (Figure 5.13).

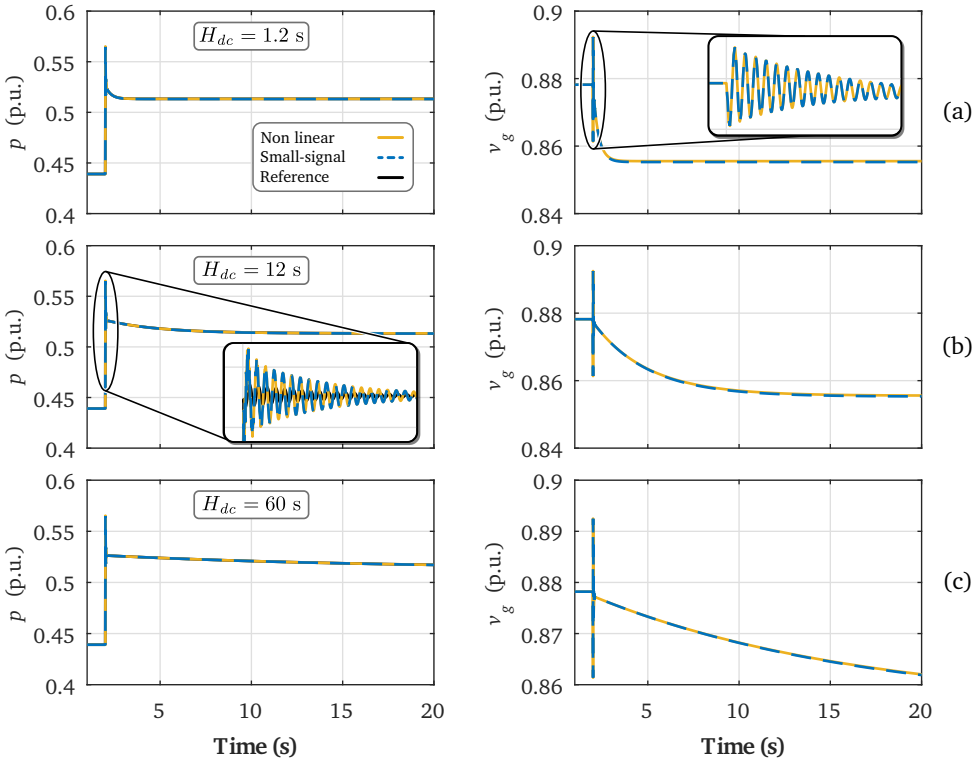

Figure 5.13: DVC small-signal model validation for different H_{dc} values.

These simulations show that the small-signal model in this case also reproduces very accurate the dynamics of the converter. In addition, we verify that with the proposed DVC technique the transient response of the converter can be modified as with the VC2. The main difference of these results and the ones shown in Figure 5.11 is the ripple at the beginning of the transient after the load variation. In this case, as there are no PI regulators, the response of the converter is immediate but it contains a ripple mainly caused by the interactions of the passive components of the converter and its output filter.

On top of that, we have also carried out various simulations varying the virtual-impedance Z_V to verify the operation of the proposed DVC technique in the steady-state interval (Figure 5.14).

The curves illustrate how the operation point is modified by changing the value of Z_V,

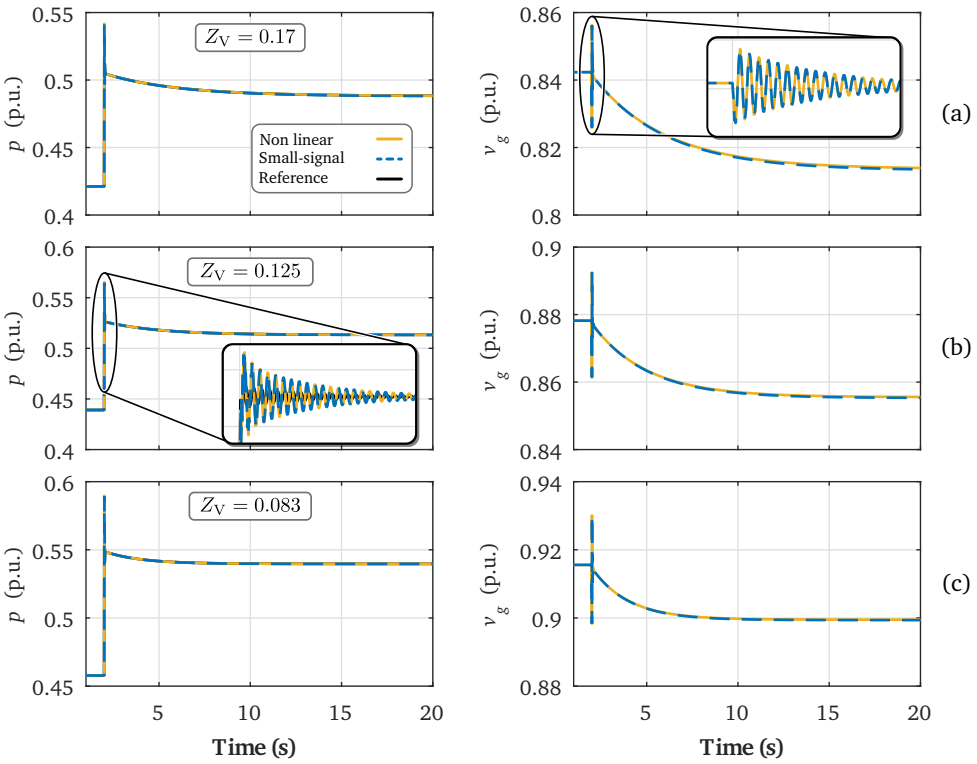

Figure 5.14: DVC small-signal model validation for different Z_V values.

and corroborate the good accuracy of the small-signal model, which validates our models for further analyses.

Therefore, we can say that in overall the results show a good accuracy of the linearized models even for a 20% variation over the linearization point, which validates them for the following stability analyses. However, we observe in both control cases that the converters have a small ripple when there is a sudden load variation caused by the resonances of the converter passive elements and the output filter. A possible solution to reduce this oscillation could be the addition of an active damping loop, but it is out of the scope of the thesis, so we propose it as a future research line.

5.3.2 Parametric Stability Analysis

As mentioned in the previous chapter, one of the main challenges for the design of control strategies is to define the parameters of regulators so that the system operates adequately at different operation points. Moreover, it is important to identify how variations in these parameters as well as other variables will affect the behaviour and response of the system. In this context, the stability analysis is a useful tool in order to define these values and design robust control strategies that ensure a stable operation for all the working range.

Similar to ac systems, several criteria can be found in the literature in order to evaluate the

stability of dc grids [118–120]. In this chapter, this aspect is verified by looking at the evolution of the dominant eigenvalues or poles of the developed small-signal state-space systems for different control as well as physical device values—e.g. passive components of the converter or filter.

Voltage-controlled virtual-capacitor

Figure 5.15 shows the location of the eigenvalues of the developed state-space model for different values of output current i_g. In total, the system has 9 eigenvalues, which correspond to the number of states in the state-space model. In this case, two pairs of complex-conjugated poles determine the small-signal stability and dynamic behaviour of the system—i.e. λ_4/λ_5 and λ_6/λ_7—as they are the nearest to the imaginary axis.

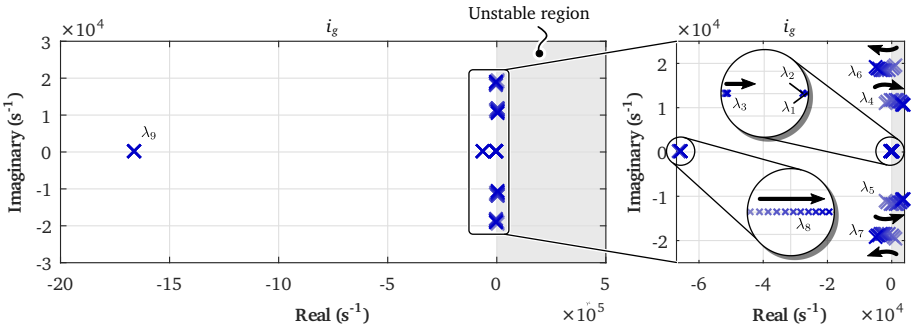

Figure 5.15: Root locus and zoom of the eigenvalues of the small-signal model for an output current (i_g) sweep from 0 to 2.5 p.u.

From Figure 5.15 it can be also observed that for the parameters shown in Table 5.2 the system becomes unstable when the load current is increased, as eigenvalues λ_4 and λ_5 enter into the unstable region.

Therefore, in order to determine controller parameters that ensure an stable operation for different load currents, a more in depth small-signal stability analysis has been carried out focusing on the movement of the poles near to the unstable region. In this context, Figure 5.16 illustrates the root loci of the analysed system for different control as well as physical parameter sweeps. Note that the arrows show the direction of these poles in the complex plane for an increment of the parameter swept. In addition, the title of subplots represents the parameter that has been swept in each case. The values of parameters that are not swept are kept as in Table 5.2. In this case, however, we have set $H_{dc} = 1.2$ s and $K_{p_v} = 0.875$, $K_{i_v} = 10$, $K_{p_i} = 6.5$ and $K_{i_i} = 1500$.

The (a)–(d) root loci demonstrate that the variation of physical parameters has a big impact on the stability of the system. This means that it is important not only to carefully choose and characterize the passive components used in the converter, but also to take into account the variations they might suffer because of ageing.

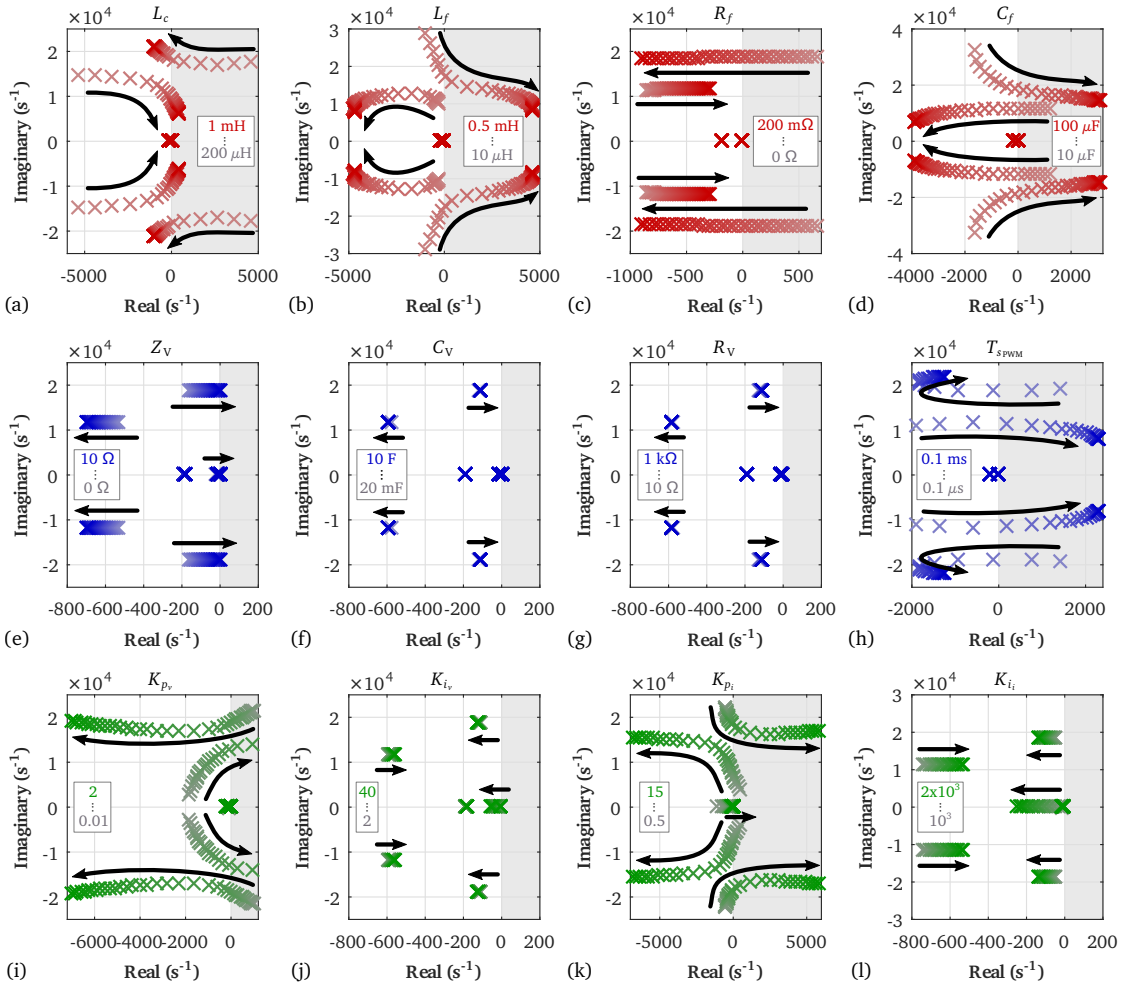

Figure 5.16: Root loci of the VC2-controlled system dominant poles for different physical parameter (upper plots, in red) and control parameter (middle and lower plots, in blue and green) sweeps.

In the case of the droop controller (root locus (e)) it can be said that that the virtual-impedance could negatively impact the stability of the system by moving λ_6 and λ_7 towards the unstable region. However, these eigenvalues would approach the unstable region for high values of Z_V. On a real application, the most usual approach would be to keep Z_V low so that there is not a large steady-state deviation in the bus voltage under power variations.

Regarding the VC controller, the virtual-capacitance as well as virtual-resistance do not have a significant impact on the stability of the system. This is an advantage because the value of C_V can be chosen freely to meet the required dynamic behaviour without compromising the overall stability. In the case of R_V, the regular approach would be to keep it high so as not to alter the steady-state output voltage.

It is also interesting to note how the delay of the PWM impacts the stability of the system. Although λ_4 and λ_5 move towards the stable region as T_s increases, the opposite occurs with

λ_6 and λ_7, which move fast to the unstable region for small increments of this delay.

Finally, it is worth mentioning that PI regulator (mainly proportional) terms cause a notorious movement of the eigenvalues of the system, which could cause the grid to become unstable in certain conditions. It is therefore crucial to determine the values of these gains to ensure a stable operation and also to meet the required dynamic characteristics of the system.

In this context, different simulations have been carried out with the previous parameters to observe the behaviour of the system illustrated in Figure 5.5 under a 20% load current variation for different voltage regulator parameter values. Figure 5.17 demonstrates that, as predicted, a low variation of K_{p_v} can determine the stability of the system for a small current variation.

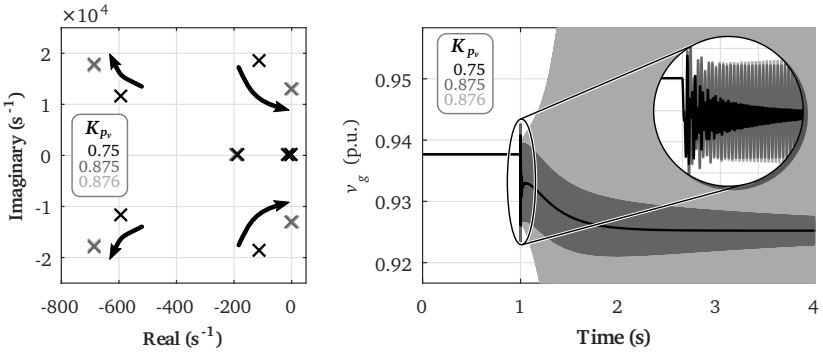

Figure 5.17: Dynamic response of the converter under a 20% load current variation for different K_{p_v} values.

Direct virtual-capacitor

In the case of the DVC-technique, we can see the complete root locus illustrated in Figure 5.19 for different load currents.

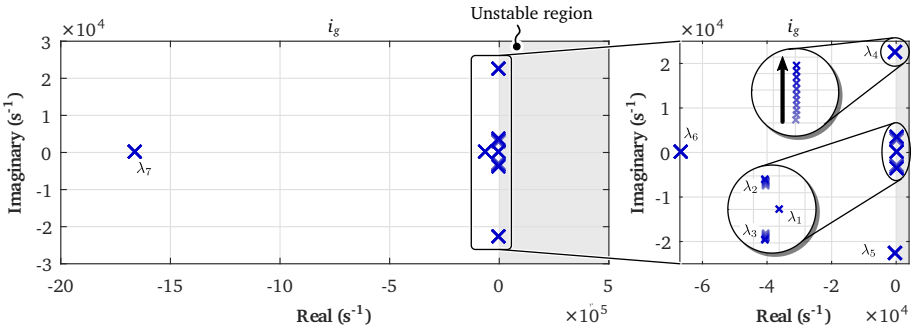

Figure 5.18: Root locus and zoom of the eigenvalues of the small-signal model for an output current (i_g) sweep from 0 to 2.5 p.u..

Here we can observe that the system has 7 eigenvalues, as this technique does not include current and voltage PI regulators. Unlike in the VC2 technique, in this case the dominant

eigenvalues of the system are not significantly affected by the increment in the load current, which means that the DVC-controlled converter is more robust under perturbations than the other approach.

In this case, the eigenvalues that determine the stability and dynamics of the system are the complex conjugate pair of poles λ_2–λ_3, and λ_4–λ_5.

Figure 5.19 shows a set of root loci focused on these dominant eigenvalues for different control as well as physical parameter value sweeps.

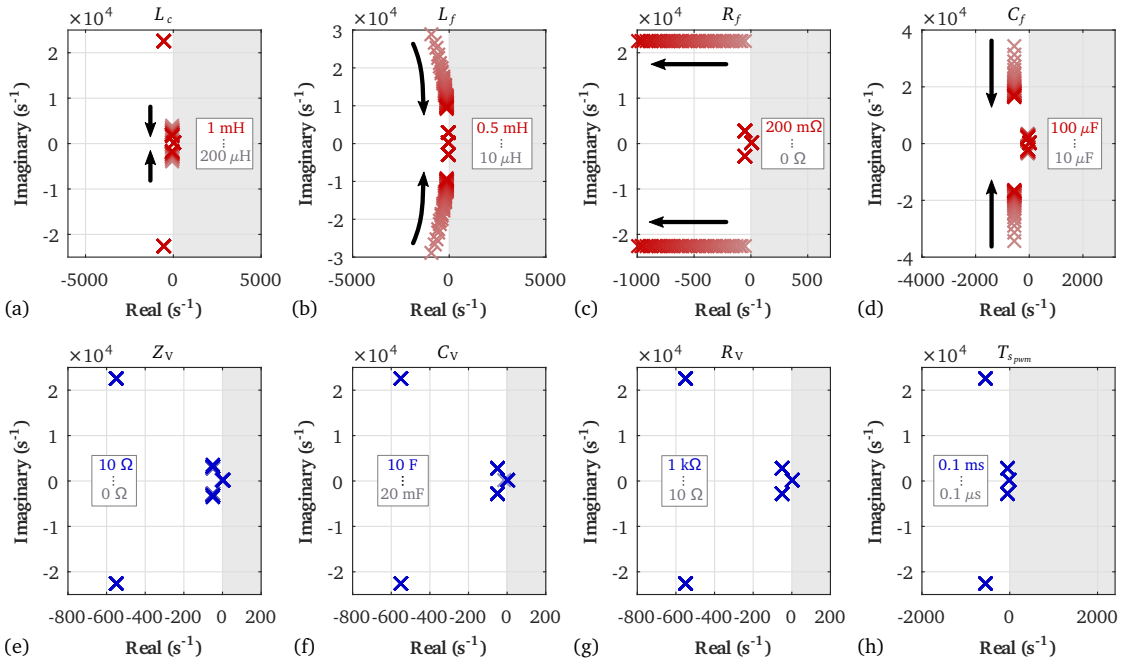

Figure 5.19: Root loci of the DVC-controlled system dominant poles for different physical parameter (upper plots, in red) and control parameter (lower plot, in blue) sweeps.

We can see that even though the variations in the physical elements move the dominant poles in the imaginary plane, they do not move the system towards the unstable region. Moreover, we can see that the control parameters and the delay of the PWM have a negligible effect in the movement of these eigenvalues, which means the DVC technique is very robust in terms of stability.

5.4 Experimental Results

Apart from the research purposes mentioned in the introduction of this dissertation, another objective set at the beginning of the thesis was to build an experimental microgrid to test all the developed control techniques. The aim is to build a hybrid ac/dc microgrid that allows us to evaluate control strategies for devices connected to the ac and dc subgrid and also for the interlinking converters between these subgrids.

Figure 5.20 shows a conceptual diagram of the hybrid microgrid we are building at the laboratories of Mondragon Unibertsitatea in the context of this thesis.

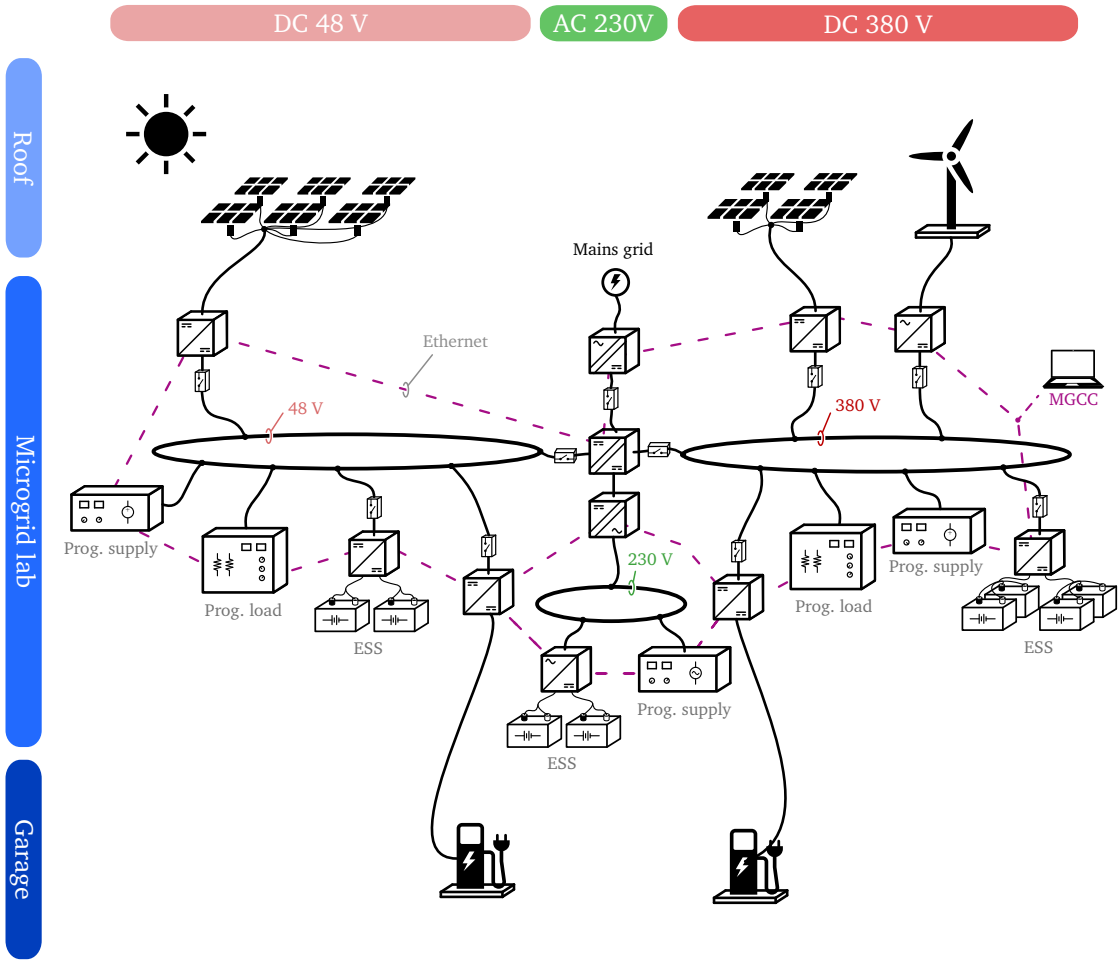

Figure 5.20: Conceptual diagram of the hybrid ac/dc microgrid being built in the laboratories of Mondragon Unibertsitatea.

In this figure we can see that there are various PV panels and a wind turbine located at the roof of the building. Moreover, we have various programmable power sources and loads, and some ESSs located through the different buses of the microgrid. We also have the possibility to connect light electric vehicles in the garage of the building.

Most of these systems are interfaced by a power converter, but one of the main challenges to validate low-level control techniques—mainly for dc-dc systems—is that manufacturers many times include their own current or voltage regulators in commercial devices and keep them as black box systems. This means that most of the times the modification of internal parameters is very limited and the user needs to develop its own hardware to evaluate this type of control strategies.

In this context, throughout the thesis we have developed various converters based on the

four-switch buck-boost topology—including the sizing, circuit design, control platform etc.—to interface the different systems connected to the 48 V bus of the hybrid microgrid. This topology and the parameter values are the same as the one whose analytical model has been derived in this chapter (refer to Appendix C for more details).

However, due to time constraints we have been able to complete just a portion of the entire microgrid. For instance, we have the PV panels physically connected by the developed dc-dc converters but have not integrated their control techniques yet. Moreover, these converters are designed to operate in 48 V and therefore we can only test them in the low-voltage dc bus.

In conclusion, at the moment we have at our disposal a couple of buck-boost converters connected to a 48 V battery pack from Kokam—which includes a BMS—that allows us to test the principles of operation of the VC techniques proposed in this chapter.

For the sake of simplicity, and taking into account that both VC techniques are very similar, in the following figures we only show the results of the DVC strategy for different control parameters and load current perturbations.

The configuration of the reduced experimental platform employed to validate these techniques can be seen in Figure 5.21.

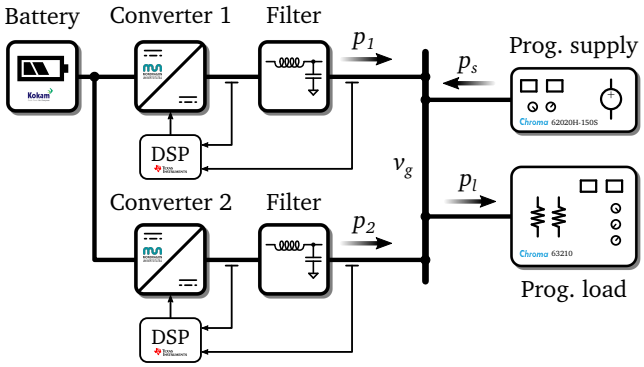

Figure 5.21: Diagram of the experimental platform.

At the moment, the two dc-dc converters of the setup are connected to the battery pack and operate all the time in the buck-boost mode.

The control technique of each dc-dc converter is integrated into a TMS320F28335 experimenter kit from Texas Instruments, which is programmed in the Matlab/Simulink® environment. More details about how the test bench is configured, how have we done the sizing of the converters, and how the different devices are intercommunicated can be found in the paper [C3].

Apart from the converters, we include a programmable source and load from Chroma to reproduce positive and negative current variations in this bus in order to test the dynamic behaviour of the proposed control techniques.

Figure 5.22 is a picture of the Microgrid lab of Mondragon Unibertsitatea where the hybrid

ac/dc microgrid is being built and the current experimental setup is located.

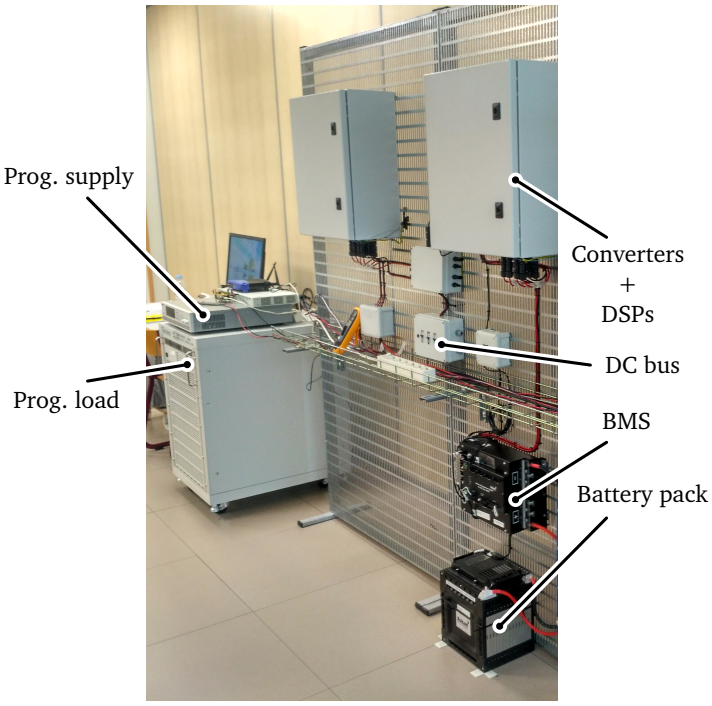

Figure 5.22: Picture of the experimental setup in the laboratories of Mondragon Unibertsitatea.

The experimental tests are divided in three main groups, explained in detail in the following sections.

5.4.1 Equal Control Parameters

We configure both converters with the same DVC control parameters. The aim of these tests is to verify the principles of operation of the proposed VC control in a more realistic environment.

In this context, we have chosen five different sets of parameters to observe how the dynamic and steady-state response of the converters vary for the same load current variation:

- $Z_{V1} = Z_{V2} = 0.125$ p.u. and $H_{dc1} = H_{dc2} = 1.2$ s
- $Z_{V1} = Z_{V2} = 0.125$ p.u. and $H_{dc1} = H_{dc2} = 60$ s
- $Z_{V1} = Z_{V2} = 0.125$ p.u. and $H_{dc1} = H_{dc2} = 12$ s
- $Z_{V1} = Z_{V2} = 0.17$ p.u. and $H_{dc1} = H_{dc2} = 12$ s
- $Z_{V1} = Z_{V2} = 0.083$ p.u. and $H_{dc1} = H_{dc2} = 12$ s

In the first three cases we keep the virtual-impedance Z_V constant and vary the virtual-capacitance H_{dc} to analyse if the dynamic behaviour of the converters changes. Similarly, in cases 3–5 we keep $H_{dc} = 12$ s and vary the virtual-impedance to study the steady-state operation of the converters.

Figure 5.23 depicts the results for the first three cases.

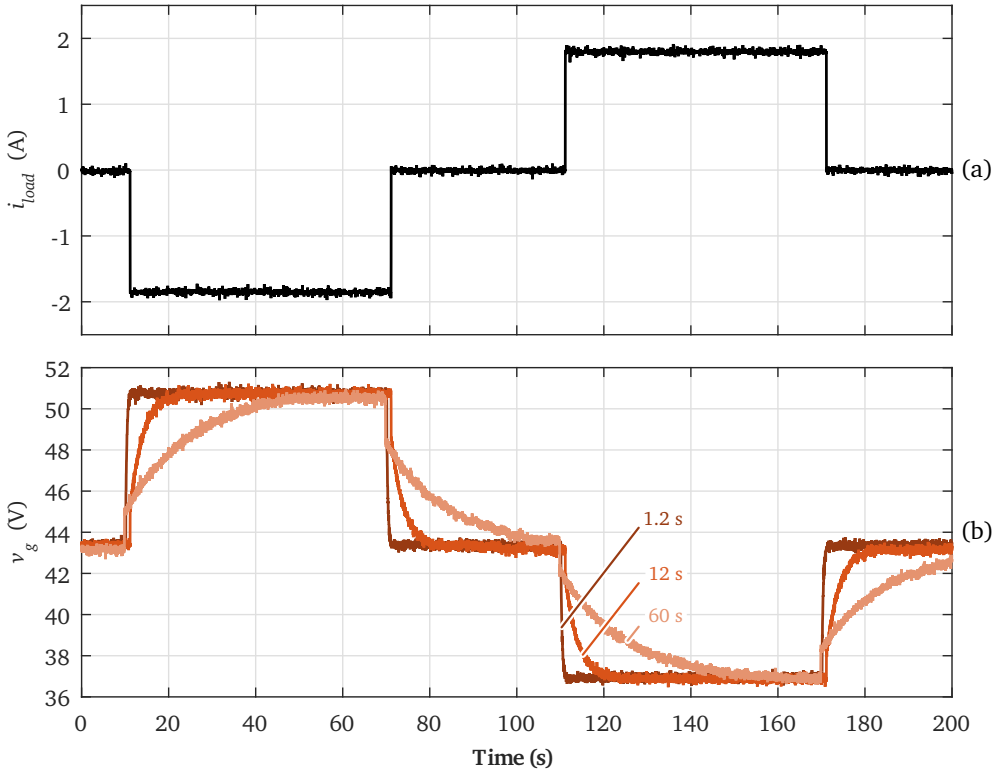

Figure 5.23: Experimental results of two parallel converters with the same DVC control parameters, varying the virtual-capacitance ($Z_V = 0.125$ p.u.).

Here we can observe that the RoCoV is reduced when we increase the emulated capacitance H_{dc}, which corroborates the results obtained in simulations.

Similarly, Figure 5.24 shows the response of converters for different Z_V values.

Therefore, we can conclude that, as predicted in the simulations, we can adapt the transient and steady-state behaviour of the converters independently.

5.4.2 Different Control Parameters

The purpose of the following tests is to verify that we can employ VC techniques not only to adapt the RoCoV of the grid under perturbations but also to modify the behaviour of each system depending on its dynamic characteristics.

As we have previously mentioned, we can adapt the H_{dc} and Z_V of each converter to take advantage of the system it is controlling, which is an interesting feature for instance for the

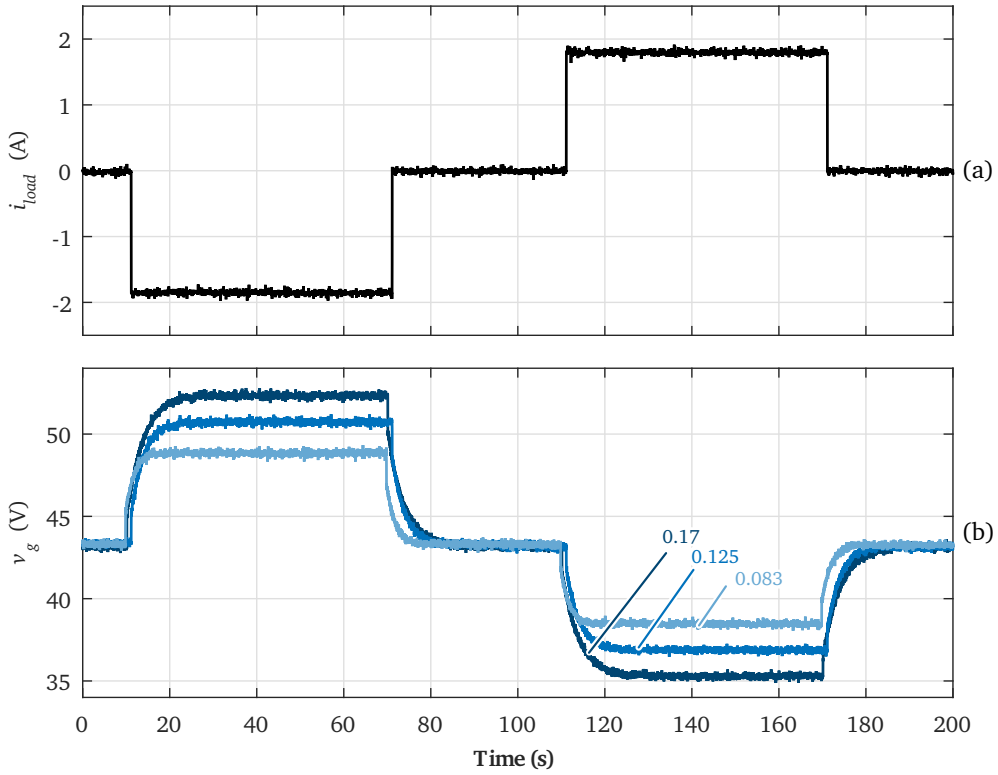

Figure 5.24: Experimental results of two parallel converters with the same DVC control parameters, varying the virtual-impedance ($H_{dc} = 12$ s).

integration of different types of ESSs.

In this case we connect both converters to the same battery pack, but we can validate this operation concept by simply changing the control parameters of each converter. In this context, we have configured the controllers as shown in Figure 5.10 so that the first converter provides most of the power in the steady-state interval whereas the second converter is responsible for handling the transient power variations. Specifically, the parameters are set as $Z_{\mathrm{V1}} = 0.033$ p.u. and $H_{dc1} = 0.6$ s for the first converter and $Z_{\mathrm{V2}} = 4.17$ p.u. and $H_{dc2} = 12$ s for the second one.

Figure 5.25 illustrates the power delivered by each converter for a sudden load variation. We can see that, as shown in the simulations, the second converter provides most of the power during the transient period because it integrates the highest virtual-capacitance whereas its power decreases towards zero in steady-state operation. On the contrary, the first converter supplies less power during the transient and it becomes the dominant device in the steady-state period, providing most of the demanded power.

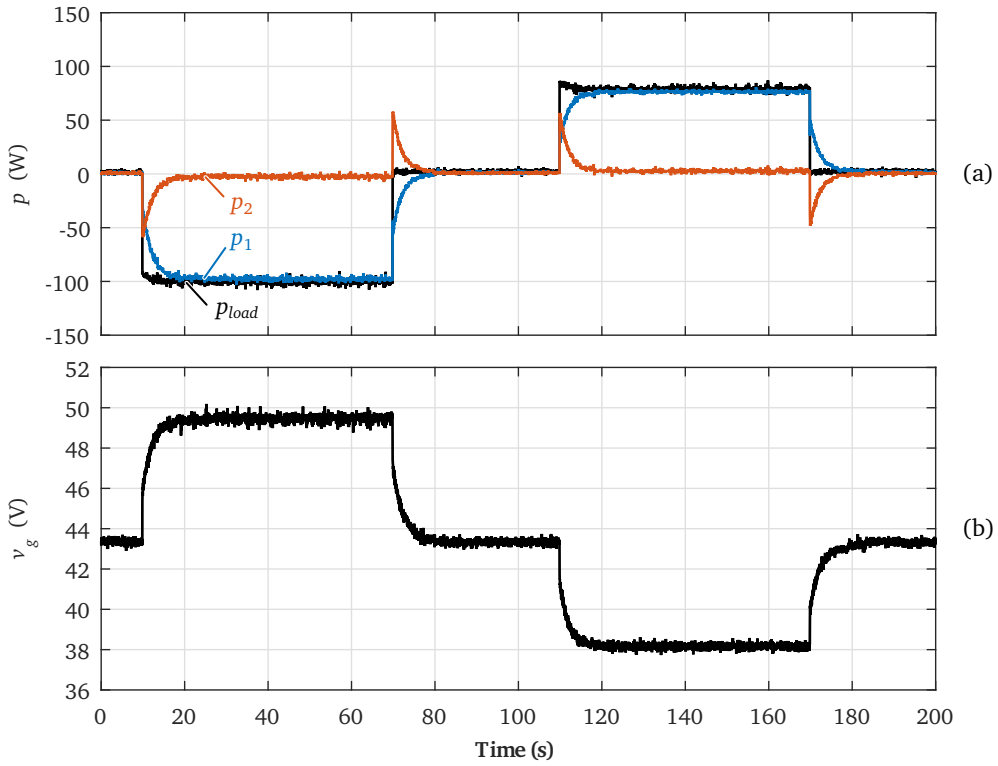

Figure 5.25: Experimental results of two parallel converters with different DVC control parameters for a step-shaped load current variation: (a) converter and load powers and (b) grid voltage.

5.4.3 Dynamic Load Profile

The last case consists of testing the DVC-controlled converters under a dynamic current profile reproducing a real grid perturbation.

The parameters in this case are set as in Section 5.4.2, and Figure 5.26 shows the power delivered by each converter for the dynamic load variation.

From the curves we can see that the converter with the highest inertia responds much faster under load perturbations, and the other provides power with a much lower dynamic.

Moreover, we notice from the figures that every time there is a load current variation the bus suffers a voltage drop, which is mainly caused by the characteristics of the output filters of the converters.

5.5 Summary and Discussion

The analysis carried out in this chapter shows that we can follow different approaches to improve the dynamic behaviour of dc grids. These grids are specially susceptible under power perturbations because they are mainly dominated by power converters, and the number of

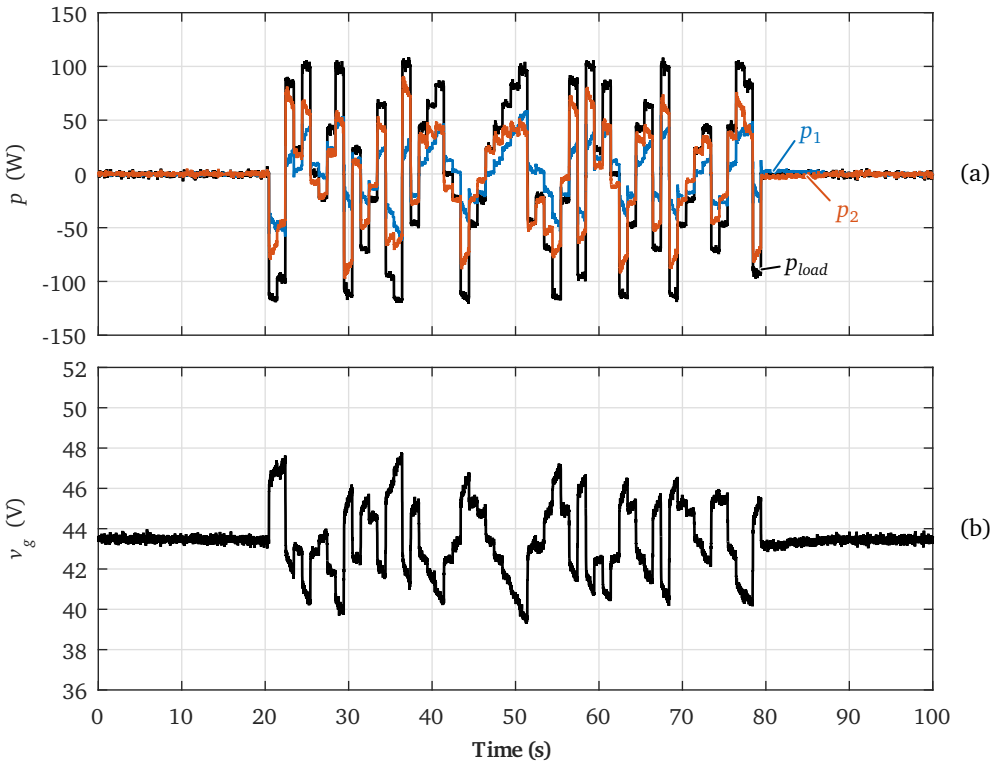

Figure 5.26: Experimental results of two parallel converters with different DVC control parameters for a dynamic load current profile: (a) converter and load powers and (b) grid voltage.

elements that provide this dynamic response—in this case capacitors directly connected to the bus—is very low.

Therefore, inspired by the principles of operation of classical grids and SME techniques for ac grids, we propose two control techniques that enable the emulation of the dynamic behaviour under power perturbations.

The VC2 provides direct current limitation because it includes voltage and current PI regulators. Moreover, these controllers can be adapted to modify the dynamic behaviour of the converter, improving the flexibility of the converter. However, the complexity of this technique makes the tuning of parameters a challenging task, and the delays of the regulators significantly influence the dynamic performance and stability characteristics of the converter.

On the other hand, the DVC technique has a very simple structure that reduces the delays in the control of the converter and significantly facilitates the configuration of the controller. Moreover, this techniques shows better characteristics in terms of stability compared to the previous approach, and is mainly affected by variations in physical parameters. Nevertheless, this approach does not include a direct way to limit the current, which could be problematic under fault conditions.

To sum up, Table 5.3 summarizes the main characteristics of the proposed techniques.

Table 5.3: Properties of VC-controlled converters.

VC Technique	Complexity	Current Limitation	Flexibility	Stability
VC2	High	✓	High	Low
DVC	Low	✗	Low	High

The experimental results corroborate the analyses and demonstrate that the VC control concept can be easily applied in reality. The tests show that by simply varying the virtual-impedance and capacitance, we can modify the behaviour of the converter to take advantage of the dynamics of the system they are controlling.

However, there are still several aspects of these novel techniques that due to time constraints have not been analysed during this thesis but need to be thoroughly addressed. For instance, which are the stability margins of VC techniques when connected to dc grids or constant power loads? What is the effect of output filter resonances in their dynamic behaviour? How is their response and how can we control these converters under fault conditions?

Chapter 6

Conclusions and Outlook

In this chapter we collect the most important remarks of the thesis and the research areas that we consider could be the continuation of our work.

6.1 Conclusions

Throughout the thesis we have highlighted some of the most important advantages that make microgrids interesting for the integration of distributed generation systems, such as the capacity to disconnect from the main grid or the flexibility provided by the autonomous management of the connected devices. The evolution of these type of systems is fundamental to cope with the high dependency on fossil fuels and the increment in the energy consumption.

However, microgrids are most of the times dominated by power converters that replace classical generators, so they have different operation principles. Therefore, there are still several challenges that need to be tackled before their large-scale implementation.

As we have shown in the second chapter of this dissertation—which is directly related to the first objective set at the beginning of the thesis—most of these challenges are related not only to the topological aspects of microgrids, but also to their management strategies. We believe that in the near future the electric grids will be a mixture of ac and dc subgrids interconnected by power electronic converters, forming hybrid ac/dc systems. Depending on how the interconnections between the subgrids are done, the system will have different characteristics for instance in terms of controllability, isolation or coupling. Moreover, we have carried out a thorough review of the literature analysing the different approaches to control these future grids regardless of the type of current they employ. Hierarchical management structures, which are employed classically in current electric systems, appear to be one of the most interesting solutions for this purpose. In this sense, distributed techniques that do not require any communication network—such as droop controllers—are envisioned as a suitable alternative for the integration of small-scale generation or energy storage systems. All these reflections have led to the publication of two journal reviews [J4], [J5], which are an extension of the content included in the Chapter 2 of this dissertation.

Based on this analysis of the state of the art, we have focused the rest of the thesis in the study and development of lower-level control methods in the hierarchical management structure.

In Chapter 3 we have shown that in converter-dominated grids, the primary regulation based on droop controllers does not have to be done only by generation systems as in classical grids. In fact, with the penetration of renewable-energy based generators, the optimal approach is to extract as much power as possible from these sources and carry out the primary regulation with other systems such as energy storage modules. Throughout this chapter we have proposed the use of mode-adaptive primary controls that vary their operation mode depending on some external condition such as the frequency or the voltage of the grid. In addition, we generalize this approach showing that all the converted-interfaced generation, energy storage systems, loads, the interconnections to the main grid or even the interlinking converters between subgrids can contribute to some extent in the primary regulation. These studies

have been also published in the form of a conference paper [C5] and a book chapter [B1].

Apart from the lack of primary regulation, converter-dominated grids suffer from a low number of inertial devices that oppose to variations in the grid frequency and voltage. Therefore, following the third objective set at the beginning of the thesis, in Chapter 4 and Chapter 5 we have identified, analysed and developed different control strategies that provide synthetic inertia for ac and dc grids, respectively.

In the case of converters connected to ac grids, we have focused the analysis of Chapter 4 on comparing existing synchronous machine emulation techniques to the characteristics of classical synchronous machines. We have shown that the non-augmented version of these techniques are capable of reducing the rate of change of frequency of ac grids under perturbations by simply varying the virtual inertia in the controller. This is a very interesting feature because we could significantly improve the dynamic behaviour of converter-dominated grids. Among the studied solutions, the current-controlled virtual synchronous machine appears as one of the most interesting techniques thanks to its simplicity, flexibility, dynamic performance and stability characteristics compared to other solutions. Among the contributions of this chapter, we can highlight the performance and impedance-based stability analyses employing the generalized Nyquist criterion, which have been submitted for publication as a conference proceeding [C1] and two journal papers [J1], [J2]. Moreover, we have also proposed the use of synchronous machine emulation techniques for the connection of systems with different characteristics to the grid, taking advantage of the dynamics of the system they are controlling, which to the best of our knowledge has not been discussed in the literature before.

In Chapter 5 we have identified some of the most relevant analogies between ac and dc systems in order to propose novel control techniques for converters connected to dc grids. In this context, we have demonstrated that capacitors connected to dc grids are equivalent to mechanical inertias connected to ac systems. Therefore, we can operate the converters connected to dc grids with the same principles of operation of synchronous machine emulation techniques for ac ones. Instead of emulating a mechanical inertia, we have introduced the concept of virtual-capacitance as a means to improve the dynamic behaviour of dc grids. We call this technique a virtual-capacitor, and we have verified that it can be implemented in different ways in the controllers. The performance and stability evaluation and the experimental results shown in this chapter demonstrate that we can reproduce the same operation principles at converters connected to dc grids, which means that we can reduce the rate of change of the voltage under grid perturbations. Moreover, we have also shown that we can design the transient and dynamic behaviour of converters separately, which is envisioned as an interesting approach to take advantage of the dynamic characteristics of the devices they are controlling. The findings of the studies carried out in this chapter have been published in the form of three conference proceedings [C2]–[C4] and a journal paper [J3].

6.2 Future Research Areas

One of the most important conclusions of this thesis is that there are still several fields that require further investigation, so in this section we mention some of the most interesting research paths that we have identified.

On the one hand, we have noticed that the filters of converters and line impedances play a key role in the transient behaviour of ac as well as dc grids. Although it was out of the scope of this thesis, we think it is fundamental to develop accurate models of these impedances to approximate to real systems and analyse their performance and stability more precisely.

Moreover, the analyses of stability carried out in this thesis have been focused on a single element connected either to the grid or to a constant current source. Even though we have started looking at interconnected systems with multiple devices, more detailed studies are required to identify unwanted interactions between converters and instability problems. Related to this, it would be interesting also to consider the use of non-linear, large-signal stability analysis methods such as Lyapunov, taking into account the non-linear nature of power electronic-systems.

Another research line, very close to the previous point, would be the use of non-linear techniques in the controllers of converters connected to ac and dc systems. For instance, a technique that has gained a lot of interest in the last years is the so-called virtual-oscillator, which we have mentioned in Chapter 2 of this thesis.

If we focus specifically on the work done in this thesis, we can mention various aspects that can be further analysed.

In the case of ac systems, some of these aspects could be the use of switched models for the impedance derivations, the use of dynamic dc buses instead of constant voltages (which have been identified as a possible source for instabilities in the literature), the effect of active damping techniques on the stability of the analysed control strategies or the experimental validation of all the analytical studies. Moreover, it would be interesting to recall the theoretical background of the generalized Nyquist criterion to analyse the case of the inertia-emulation control with more detail, and establish some guidelines to determine the stability margins of these type of systems.

Regarding dc systems, we could also study several aspects such as the stability of virtual-capacitor techniques with impedance-based methods to determine the stability margins, the use of active damping loops to reduce transient oscillations or corroborate the stability boundaries experimentally.

In general, we could also carry out the experimental validation of all the techniques employed in the thesis in a hybrid ac/dc scenario with multiple interconnected converters.

Appendix A

SM-Based System Modelling

Before jumping to the modelling of the grid-connected SM, it is important to clarify the most important conventions followed throughout the process.

On the one hand, the variables in the *dq*-domain are represented in the vector form as follows:

$$\mathbf{x} = x_d + jx_q \tag{A.1}$$

On top of that, the superscripts G, L and R denote that the current or voltage is referenced in the GRF, the LRF and the DRF (in this case aligned with the rotor) of the synchronous machine, respectively. The variables can be shifted from one reference frame to another by applying a rotation matrix $\mathbf{T}$ as shown in Figure 4.13. This matrix can be easily derived from the phasor diagram illustrated in Figure 4.14, employing the following equation:

$$\begin{aligned}\mathbf{x}^R &= \mathbf{x}^G e^{-j(\theta_{sm}-\theta_g)} \\ &= \mathbf{x}^G e^{-j\delta\theta_{sm}} \\ &= \mathbf{x}^G \left(\cos(\delta\theta_{sm}) - j\sin(\delta\theta_{sm})\right)\end{aligned} \tag{A.2}$$

which in matrix notation can be represented as:

$$\begin{bmatrix} x_d^R \\ x_q^R \end{bmatrix} = \underbrace{\begin{bmatrix} \cos(\delta\theta_{sm}) & \sin(\delta\theta_{sm}) \\ -\sin(\delta\theta_{sm}) & \cos(\delta\theta_{sm}) \end{bmatrix}}_{\mathbf{T}} \begin{bmatrix} x_d^G \\ x_q^G \end{bmatrix} \tag{A.3}$$

Finally, in order to facilitate the comparison among different controllers, all the equations are represented in per unit (p.u.) quantities following the approach in [70]. The variables that are represented in their natural units are the time and the angles employed in the controllers, such as the angular position of the rotor of the SM θ_{sm}.

Refer to the glossary for a more detailed description of each symbol used in the analytical

equations.

In the following sections we model the different parts that compose the system shown in Figure 4.4, including the control strategy, the synchronous machine itself and the electrical grid.

A.1 Control Strategy

As mentioned in Section 4.1, the control of SM-based generators is generally composed by two main parts, namely the active power and the reactive power controllers.

The former consists of an active power reference added to the output of a frequency droop regulator, which can be represented as follows:

$$p_{m_{\text{ref}}} = p_{\text{ref}} + K_\omega \left(\omega_{\text{ref}} - \omega_m\right) \tag{A.4}$$

where K_ω is the frequency droop slope, ω_{ref} the rated frequency and ω_m the real frequency of the SM.

The obtained power reference is then fed to the governor, which regulates the fuel flow going to the prime mover or turbine as illustrated in Figure 4.4. These two systems introduce some delays in the system, and can be approximated by a first order transfer function:

$$\begin{aligned} G_{gt} &= \frac{p_m}{p_{m_{\text{ref}}}} \\ &= \frac{1}{sT_{gt}+1} \end{aligned} \tag{A.5}$$

which can be represented in differential form as below:

$$\frac{dp_m}{dt} = \frac{1}{T_{gt}}\left(p_{m_{\text{ref}}} - p_m\right) \tag{A.6}$$

where T_{gt} is the combined time constant of the governor and the turbine.

The RPC, on the other hand, includes a predefined voltage amplitude reference added to the output of a voltage droop regulator:

$$\hat{\mathbf{v}}_{rpc} = \hat{\mathbf{v}}_{\text{ref}} + K_q\left(q_{\text{ref}} - q_f\right) \tag{A.7}$$

where K_q is the voltage droop slope. Here, q_f refers to the low-pass filtered reactive power,

which is obtained by applying the following transfer function:

$$\begin{aligned} G_{q_f} &= \frac{q_f}{q} \\ &= \frac{\omega_f}{s+\omega_f} \end{aligned} \tag{A.8}$$

where ω_f represents the filter cut-off frequency, and which can be rewritten in differential form as:

$$\frac{dq_f}{dt} = \omega_f \left(q - q_f\right) \tag{A.9}$$

In this case, the reactive power is calculated as follows:

$$q = -v^G_{sm_d} i^G_{sm_q} + v^G_{sm_q} i^G_{sm_d} \tag{A.10}$$

The derived reference voltage $\hat{\mathbf{v}}_q$ is fed to the active voltage regulator in order to calculate the dc voltage to be applied to the exciter (v^*_{fd}). This is done employing a conventional PI regulator:

$$\begin{aligned} G_{avr} &= \frac{v^*_{fd}}{\hat{\mathbf{v}}_{rpc} - \hat{\mathbf{v}}} \\ &= K_{p_{ex}} + \frac{K_{iex}}{s} \end{aligned} \tag{A.11}$$

which can be represented in the differential form as:

$$v^*_{fd} = K_{p_{ex}} \left(\hat{\mathbf{v}}_{rpc} - \hat{\mathbf{v}}\right) + K_{iex} \gamma_{ex} \tag{A.12}$$

In (A.12), γ_{ex} represents the state related to the integrator of the PI and can be calculated as follows:

$$\frac{d\gamma_{ex}}{dt} = \hat{\mathbf{v}}_{rpc} - \hat{\mathbf{v}} \tag{A.13}$$

Similar to the governor and the prime mover, the exciter also introduces some delay in the system and therefore the classical approach is to model it as a first order transfer function.

$$\begin{aligned} G_{ex} &= \frac{v_{fd}}{v^*_{fd}} \\ &= \frac{1}{sT_{ex}+1} \end{aligned} \tag{A.14}$$

which in the differential form is expressed as:

$$\frac{dv_{fd}}{dt} = \frac{1}{T_{ex}}\left(v_{fd}^{*} - v_{fd}\right) \tag{A.15}$$

A.2 Synchronous Machine

The model of the synchronous machine can be differentiated in two main parts, namely the electrical circuits of the stator and rotor, and the mechanical part already explained in Section 4.1.

This type of machine has been widely studied in the literature, and hence we can find a wide variety of models to represent its electrical circuitry. Depending on the order of the model we employ, different features of the machine such as the dampers or the amortisseur windings are omitted. In this case we have decided to use the 5^{th} order model derived by Kundur in [70]. This model provides an adequate balance between accuracy and complexity, as it takes into account the damping windings of the machine with a relatively low order model. By including the dampers of the machine, our purpose is to approximate to a real SM so that we can compare it to SME-controlled converters in a more realistic manner.

Figure A.1 illustrates the rotor and stator circuits of the synchronous machine modelled in this thesis in the *abc*-domain.

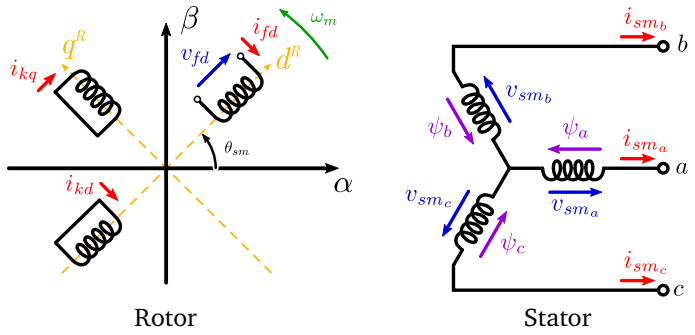

Figure A.1: SM rotor and stator circuits in the *abc*-domain, adapted from [70].

In this case the model is composed by a single damper winding (denoted with subscript *fd*) and an amortisseur circuit whose flux is assumed to flow in line with the one of the field in the *d* axis and in the *q* axis (denoted with subscripts *kd* and *kq*) [70].

These circuits can be converted into the *dq*-domain by means of applying the amplitude invariant Park transformation. Figure A.2 shows the equivalent circuits for the *d* and *q* axis, where all the variables are referred to the rotor rotating reference frame—i.e. the DRF.

Based on the electric circuits illustrated in Figure A.2, the terminal voltages of the SM can

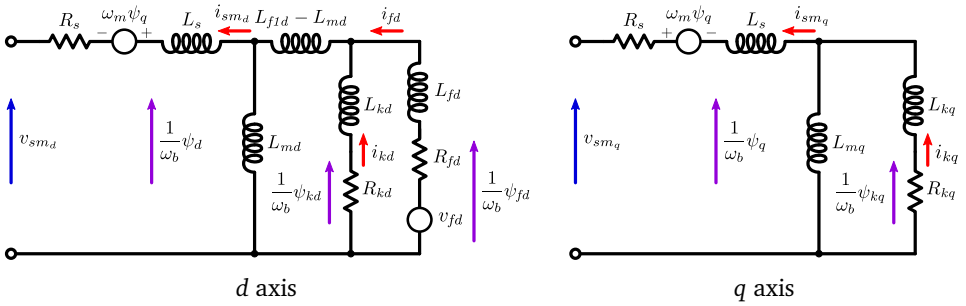

Figure A.2: SM rotor and stator circuits in the *dq*-domain, adapted from [70].

be modelled as follows:

$$\mathbf{v}_{sm}^R = \frac{1}{\omega_b}\frac{d\boldsymbol{\psi}}{dt} + j\omega_m\boldsymbol{\psi} - R_s\mathbf{i}_{sm}^R \tag{A.16}$$

where stator flux linkages are represented as:

$$\begin{aligned}\psi_d &= -(L_s + L_{md})\, i_{sm_d}^R + L_{md}\left(i_{fd}^R + i_{kd}^R\right)\\ \psi_q &= -\left(L_s + L_{mq}\right) i_{sm_q}^R + L_{mq}\left(i_{kq}^R\right)\end{aligned} \tag{A.17}$$

Here, R_s and L_s are the SM winding resistance and inductance, respectively, and L_m denotes the mutual inductance.

If we introduce the expressions in (A.17) in (A.16), we obtain two equations that are a function of $\frac{di_{sm_d}^R}{dt}$, $\frac{di_{sm_q}^R}{dt}$, $\frac{di_{fd}^R}{dt}$, $\frac{di_{kd}^R}{dt}$ and $\frac{di_{kq}^R}{dt}$.

In addition, we can represent the circuits of the field and amortisseur windings through the following system of equations:

$$\begin{aligned}v_{fd}^R &= \frac{1}{\omega_b}\left[\left(L_{f1d} + L_{fd}\right)\frac{di_{fd}^R}{dt} + L_{f1d}\frac{di_{kd}^R}{dt} - L_{md}\frac{di_{sm_d}^R}{dt}\right] + R_{fd}i_{fd}^R\\ 0 &= \frac{1}{\omega_b}\left[L_{f1d}\frac{di_{fd}^R}{dt} + \left(L_{f1d} + L_{kd}\right)\frac{di_{kd}^R}{dt} - L_{md}\frac{di_{sm_d}^R}{dt}\right] + R_{kd}i_{kd}^R\\ 0 &= \frac{1}{\omega_b}\left[\left(L_{kq} + L_{mq}\right)\frac{di_{kq}^R}{dt} - L_{mq}\frac{di_{sm_q}^R}{dt}\right] + R_{kq}i_{kq}^R\end{aligned} \tag{A.18}$$

where

$$L_{f1d} = L_{ffd} - L_{fd} \tag{A.19}$$

In order to build the state-space model we need to represent all the system as a set of independent differential equations. Therefore, as we need to isolate the differential terms

in the previous equations, we have to solve this system of five equations and five unknowns symbolically in order to obtain the expressions for $\frac{di^R_{sm_d}}{dt}$, $\frac{di^R_{sm_q}}{dt}$, $\frac{di^R_{fd}}{dt}$, $\frac{di^R_{kd}}{dt}$ and $\frac{di^R_{kq}}{dt}$. Due to the large length of the resulting expressions, they are not shown in this document.

Regarding the mechanical part of the SM, starting from Equation 4.3 we can obtain the expressions for ω_m and $\delta\theta_{sm}$ as follows:

$$\begin{aligned} \frac{d\omega_m}{dt} &= \frac{1}{2H}\left[\tau_m - \tau_m - K_D\Delta\omega_m\right] \\ \frac{d\delta\theta_{sm}}{dt} &= \omega_b\left(\omega_m - \omega_g\right) \end{aligned} \tag{A.20}$$

A.3 Decoupling Output Filter

Although SM-based generators do not include any output filter to be connected to the grid, in this case we have included a very small capacitor at the terminals of the machine (10 μ p.u.). This helps us to decouple the states of the currents of the SM and the currents of the grid impedance, enabling us to calculate the equivalent impedance of the machine and the grid separately. The differential equation of the voltage of this capacitor—which in this case coincides with the SM terminal voltage—can be written as follows:

$$\frac{d\mathbf{v}^G_{sm}}{dt} = \omega_b\left[\frac{1}{C_f}\left(\mathbf{i}^G_{sm} - \mathbf{i}^G_o\right) - j\omega_g\mathbf{v}^G_{sm}\right] \tag{A.21}$$

A.4 Electric Grid

In this case we have simplified the electric grid to an ideal voltage source in series with an impedance that represents the line and transformer impedances of a classical grid.

$$\frac{d\mathbf{i}^G_o}{dt} = \omega_b\left[\frac{1}{L_o}\left(\mathbf{v}^G_{sm} - R_o\mathbf{i}^G_o - \mathbf{v}^G_g\right) - j\omega_g\mathbf{i}^G_o\right] \tag{A.22}$$

As the decoupling capacitor has a very small value, in practice this current will be almost the same as $\mathbf{i}^G_{sm}$.

A.5 Non-Linear System

Considering the states of the SM, its controllers, the output capacitor and the electric grid impedance, we have defined a set of 15 differential equations that will be used to get the

small-signal state-space model. In this context, the state vector x has been defined as:

$$x = \begin{bmatrix} v^G_{sm_d} & v^G_{sm_q} & i^G_{sm_d} & i^G_{sm_q} & i^R_{fd} & i^R_{kd} & i^R_{kq} & i^G_{o_d} & i^G_{o_q} & \omega_m & \delta\theta_{sm} & p_m & q_m & \gamma_{ex} & v_{fd} \end{bmatrix} \tag{A.23}$$

Similarly, the input vector u has been set as:

$$u = \begin{bmatrix} p_{\text{ref}} & q_{\text{ref}} & v^G_{g_d} & v^G_{g_q} & \omega_g & \hat{\mathbf{v}}_{\text{ref}} & \omega_{\text{ref}} \end{bmatrix} \tag{A.24}$$

A.6 Small-Signal State-Space Model

This system consists of a set of non-linear equations that must be linearized over a point of operation $\bar{x}$ to obtain the equivalent impedances and carry out the stability analysis. As shown in Section 4.3.1, we first solve the set of non-linear equations by setting all the derivatives to zero. This way we eliminate the dynamic components of the system and calculate the steady-state values of x, that is, $\bar{x}$, for a certain input u:

$$f(x,u,t) = 0 \tag{A.25}$$

We then linearize our system of non-linear equations using Taylor series expansion over $\bar{x}$ and neglecting second- and higher-order terms in the process.

The final set of equations can be represented in a small-signal state-space form as:

$$\frac{d\tilde{x}}{dt} = \mathbf{A}\tilde{x} + \mathbf{B}\tilde{u} \tag{A.26}$$

For the sake of simplicity and due to the large size of matrices, we do not show them in the document.

Appendix B

SME-Controlled System Modelling

In this section we develop the analytical models of the SME-controlled power converters, following the same modelling conventions as in Appendix A. The difference resides in that in this case the angle employed to carry out the reference frame rotations is not θ_{sm} but rather the angle of the controller θ_c. In the case of the IE control technique this angle corresponds to the angle of the PLL (θ_{pll}), whereas in the case of the CCVSM and VCVSM strategies this angle represents the VSM angle, θ_{vsm}. Finally, in the case of the SV control this angle refers to θ_{sv}, which is generated by the *swing equation* integrated in this technique.

The equations shown in the following sections correspond on the one hand to the common parts of the four controllers—i.e. the PWM, the converter itself, its output passive filter and the electric grid—and on the other hand to specific parts of each control configuration, such as voltage loops, virtual-impedances, the PLL, etc.

B.1 Common Parts of SME Control Strategies

B.1.1 Pulse-Width Modulator

In this case we have modelled the PWM as a second order transfer function following the Padé approximation proposed in [121], which takes into account the computation delay, the sampler and the zero order hold:

$$G_{pwm} = \frac{1 - 0.5T_s s}{(1 + 0.5T_s s)^2} \tag{B.1}$$

This second order transfer function can be represented in the differential form as follows:

$$\begin{aligned} \frac{d\boldsymbol{\rho}_1}{dt} &= -\frac{4}{T_s}\boldsymbol{\rho}_1 - \frac{4}{T_s^2}\boldsymbol{\rho}_2 + \mathbf{m}^C \\ \frac{d\boldsymbol{\rho}_2}{dt} &= \boldsymbol{\rho}_1 \end{aligned} \tag{B.2}$$

where $\boldsymbol{\rho}_1$ and $\boldsymbol{\rho}_2$ are the two states of the second order PWM transfer function, and $\mathbf{m}^C$ represents the modulation index in the *dq*-domain.

B.1.2 Converter, Output Filter and Electric Grid

We have decided to employ a two-level VSC to evaluate the behaviour of SME techniques as it is one of the most employed topologies in low-voltage applications. In order to avoid the electrical noise produced by the switching of the semiconductors, in this case we use an average model of the converter:

$$\mathbf{v}_c^G = \mathbf{m}_{pwm}^G V_{dc} \tag{B.3}$$

As it can be noticed from (B.3), we have considered a constant dc voltage, V_{dc}, in the dc side of the converter. In this case, we assume that there is another converter regulating this voltage and therefore it does not vary over time, which simplifies significantly the stability analyses.

Every power converter connected to the electric grid includes some kind of passive circuit to filter the noise produced by the switching of the semiconductors. Even though we employ an average model for the VSC, these filters have a significant influence in the transient response of the converter, so we must take them into account in the models. In this context, we have included an LC filter at the output of each converter (Figure 4.8), and the corresponding inductance current and capacitor voltage differential equations can be modelled as follows:

$$\begin{aligned}
\frac{d\mathbf{i}_c^G}{dt} &= \frac{\omega_b}{L_f}\mathbf{m}_{pwm}^G V_{dc} - \omega_b\left(\frac{R_f}{L_f} + j\omega_g\right)\mathbf{i}_c^G - \frac{\omega_b}{L_f}\mathbf{v}_o^G \\
\frac{d\mathbf{v}_o^G}{dt} &= \omega_b\left[\frac{1}{C_f}\left(\mathbf{i}_c^G - \mathbf{i}_o^G\right) - j\omega_g\mathbf{v}_o^G\right]
\end{aligned} \tag{B.4}$$

The modulation index included in this equation—which takes into account the PWM delay—can be calculated as:

$$\mathbf{m}_{pwm}^C = -\frac{2}{T_s}\boldsymbol{\rho}_1 + \frac{4}{T_s^2}\boldsymbol{\rho}_2 \tag{B.5}$$

Regarding the electric grid, we can notice from Figure 4.8 that it is configured as in the SM system. Its dynamic equation is hence defined as in Appendix A.4.

B.2 Specific Parts of SME Control Strategies

B.2.1 Synchronverter

This control strategy is the most simple among the studied ones and is only composed by two parts, namely the frequency regulation part and the reactive power controller.

Frequency regulation

As in the APC of SMs, the active power reference of the converter is calculated by adding a power reference to the output of a frequency droop regulator. This can be expressed as:

$$p_{m_{\text{ref}}} = p_{\text{ref}} + K_\omega \left(\omega_{\text{ref}} - \omega_{sv}\right) \tag{B.6}$$

In this case, θ_{sv} and the angle difference $\delta\theta_{sv}$ necessary to convert signals in the dq-domain to the abc-domain are obtained from the inertia emulation part, which can be written in the differential form as follows:

$$\begin{aligned} \frac{d\omega_{sv}}{dt} &= \frac{1}{2H}\left[\frac{p_{m_{\text{ref}}}}{\omega_{sv}} - \frac{p}{\omega_{sv}} - K_D\left(\omega_{sv} - \omega_{\text{ref}}\right)\right] \\ \frac{d\delta\theta_{sv}}{dt} &= \omega_b\left(\omega_{sv} - \omega_g\right) \end{aligned} \tag{B.7}$$

The active power is obtained from the measured currents and voltages as:

$$p = v^G_{o_d} i^G_{o_d} + v^G_{o_q} i^G_{o_q} \tag{B.8}$$

Reactive power controller

The RPC of synchronverters is very similar to the one employed at SMs, adding a reactive power reference with the value coming from a voltage droop regulator, and finally integrating this value divided by the constant K:

$$\frac{dM_f i_f}{dt} = \frac{1}{K}\left[q_{\text{ref}} + K_q\left(\hat{\mathbf{v}}_{\text{ref}} - \hat{\mathbf{v}}_o\right) - q\right] \tag{B.9}$$

Here the reactive power is obtained from the measured currents and voltages as:

$$q = -v^G_{o_d} i^G_{o_q} + v^G_{o_q} i^G_{o_d} \tag{B.10}$$

State and input vectors

If we take into account the common parts of the modelled SME-controlled converters and the specific parts of the SV technique, we can define a set of 13 differential equations whose

state vector x is:

$$x = \begin{bmatrix} v_{o_d}^G & v_{o_q}^G & i_{c_d}^G & i_{c_q}^G & i_{o_d}^G & i_{o_q}^G & \rho_{1_d} & \rho_{1_q} & \rho_{2_d} & \rho_{2_q} & \omega_{sv} & \delta\theta_{sv} \end{bmatrix} \tag{B.11}$$

Similarly, the input vector u can be defined as:

$$u = \begin{bmatrix} p_{\text{ref}} & q_{\text{ref}} & v_{g_d}^G & v_{g_q}^G & V_{dc} & \omega_g & \hat{\mathbf{v}}_{\text{ref}} & \omega_{\text{ref}} \end{bmatrix} \tag{B.12}$$

B.2.2 Inertia-Emulation

The IE technique integrates different control parts compared to the previous approach, such as the PLL, the current regulators or the current reference calculation blocks (Figure 4.10).

Synchronization Unit

The synchronization algorithm or PLL employed for the IE and VCVSM control techniques is illustrated in Figure B.1. As it can be noticed, it consists of a classical PI regulator controlling the value of v_{o_q} towards zero.

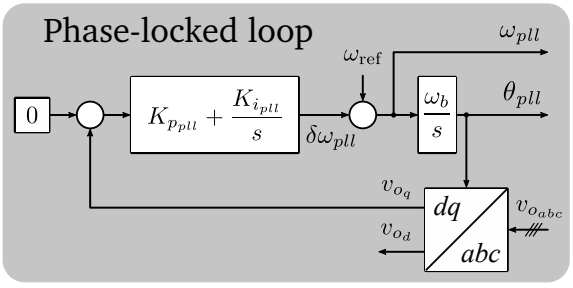

Figure B.1: PLL configuration used for the IE and VCVSM control.

The differential equations that represent this PLL can be formulated as follows:

$$\begin{aligned} \frac{d\delta\theta_{pll}}{dt} &= \omega_b K_{p_{pll}} v_{o_q}^C + \omega_b K_{i_{pll}} \gamma_{pll} \\ \frac{d\gamma_{pll}}{dt} &= v_{o_q}^C \end{aligned} \tag{B.13}$$

where γ_{pll} is the operator that represents the integrator of the PI.

Here, ω_{pll} can be expressed as:

$$\omega_{pll} = \left(K_{p_{pll}} v_{o_q}^C + K_{i_{pll}} \gamma_{pll} + \omega_{\text{ref}} \right) \tag{B.14}$$

Current-controller

The current-control employed in this technique and in the VSM techniques of the following sections is a classical *dq* control based on PI regulators. In this case we have included the decoupling terms and we also divide the output of this controller by V_{dc}. Although in the simulations carried out in this thesis V_{dc} is kept constant, we have included this term for future analyses where dynamic dc buses are considered.

The equation to calculate the modulation index $\mathbf{m}^C$ coming from the current-control can be expressed as follows:

$$\mathbf{m}^C = \frac{1}{V_{dc}} \left[\left(\mathbf{i}_c^* - \mathbf{i}_c^C \right) K_{p_i} + K_{i_i} \gamma_i + j \omega_{pll} L_f \mathbf{i}_c^C \right] \tag{B.15}$$

In this equation γ_i refers to the states of PI regulators, and can be expressed in differential form as:

$$\frac{d\gamma_i}{dt} = \mathbf{i}_c^* - \mathbf{i}_c^C \tag{B.16}$$

Current-reference calculation

The current reference is obtained from the active and reactive power reference and the measured output voltages as:

$$\mathbf{i}_c^* = \frac{\mathbf{v}_o^C p_{m_{\text{ref}}} + j \mathbf{v}_o^C q_{\text{ref}}}{v_{o_d}^{C2} + v_{o_q}^{C2}} \tag{B.17}$$

Power control

The active power reference that is necessary for the current-reference calculation is obtained using the inverted *swing equation*, an external power reference and the output power of a frequency droop as in previous approaches:

$$p_{m_{\text{ref}}} = p_{\text{ref}} + K_D \left(\omega_{\text{ref}} - \omega_{pll} \right) + 2H \frac{d\omega_{pll}}{dt} \tag{B.18}$$

In the case of the reactive power reference, we have set $q_{\text{ref}} = 0$ in order to facilitate the comparison among controllers.

State and input vectors

If we take into account the common parts of the modelled SME-controlled converters and the specific parts of the IE technique, we can define a set of 14 differential equations whose

state vector x is:

$$x = \begin{bmatrix} v_{o_d}^G & v_{o_q}^G & i_{c_d}^G & i_{c_q}^G & i_{o_d}^G & i_{o_q}^G & \rho_{1_d} & \rho_{1_q} & \rho_{2_d} & \rho_{2_q} & \delta\theta_{pll} & \gamma_{pll} & \gamma_{i_d} & \gamma_{i_q} \end{bmatrix} \quad \text{(B.19)}$$

Similarly, the input vector u can be defined as:

$$u = \begin{bmatrix} p_{\text{ref}} & q_{\text{ref}} & v_{g_d}^G & v_{g_q}^G & V_{dc} & \omega_g & \omega_{\text{ref}} \end{bmatrix} \quad \text{(B.20)}$$

B.2.3 Current-Controlled Virtual Synchronous Machines

The approach followed to model the CCVSM control technique is inspired by [86].

Current-controller

The current-control employed in this approach is the same as the one modelled in Section B.2.2.

SM electrical dynamic model

This part of the controller emulates the stator windings of a real SM, and according to [86], its equation can be represented as a dynamic or quasi-stationary model. In this case, we have chosen the former approach because it resembles the more the windings of a real SM:

$$\frac{d\mathbf{i}_s}{dt} = \frac{\omega_b}{L_s}\left[\hat{\mathbf{v}}_{rpc} - \hat{\mathbf{v}}_o^C - (R_s + jL_s\omega_{vsm})\,\mathbf{i}_s\right] \quad \text{(B.21)}$$

Reactive power controller

In (B.21) the term $\hat{\mathbf{v}}_{rpc}$ is obtained from the RPC as follows:

$$\hat{\mathbf{v}}_{rpc} = K_{p_q}\left[\hat{\mathbf{v}}_{\text{ref}} - \hat{\mathbf{v}}_o^C + K_q\left(q_{\text{ref}} - q_f\right)\right] + K_{iq}\gamma_q \quad \text{(B.22)}$$

Here, γ_q corresponds to the state of the PI included in the RPC to calculate the value of $\hat{\mathbf{v}}_{rpc}$, and its differential equation can be represented as:

$$\frac{d\gamma_q}{dt} = \hat{\mathbf{v}}_{\text{ref}} - \hat{\mathbf{v}}_o^C + K_q\left(q_{\text{ref}} - q_f\right) \quad \text{(B.23)}$$

In the RPC employed in [86] the authors include a low-pass filter to remove the noise of the measured output reactive power. This approach is the same as in the SM controller, and it can be modelled employing the equation (A.9).

Active power controller

This part of the CCVSM is very similar to other approaches; the main difference resides in that, in this case, the controller does not require the frequency of the grid from a PLL and it is instead calculated by filtering the frequency generated through the inertia-emulation. The equation of this part can be expressed as follows:

$$\frac{d\omega_{vsm}}{dt} = \frac{1}{2H}\left[p_{\text{ref}} - p + K_\omega\left(\omega_{\text{ref}} - \omega_{vsm}\right) - K_D\left(\omega_{vsm} - \omega_{vsmf}\right)\right] \tag{B.24}$$

where ω_{vsmf} represents the filtered VSM frequency ω_{vsm}.

The differential equation of this filter can be written as:

$$\frac{d\omega_{vsmf}}{dt} = \omega_d\left(\omega_{vsm} - \omega_{vsmf}\right) \tag{B.25}$$

State and input vectors

If we take into account the common parts of the modelled SME-controlled converters and the specific parts of the CCVSM technique, we can define a set of 18 differential equations whose state vector x is:

$$x = \left[\begin{array}{cccccccccccc} v_{o_d}^G & v_{o_q}^G & i_{c_d}^G & i_{c_q}^G & i_{o_d}^G & i_{o_q}^G & i_{s_d} & i_{s_q} & \rho_{1_d} & \rho_{1_q} & \rho_{2_d} & \rho_{2_q} \\ & & & & & & \omega_{vsm} & \delta\theta_{vsm} & \omega_{vsmf} & \gamma_{i_d} & \gamma_{i_q} & \gamma_q \end{array}\right] \tag{B.26}$$

Similarly, the input vector u can be defined as:

$$u = \left[\begin{array}{cccccccc} p_{\text{ref}} & q_{\text{ref}} & v_{g_d}^G & v_{g_q}^G & V_{dc} & \omega_g & \hat{\mathbf{v}}_{\text{ref}} & \omega_{\text{ref}} \end{array}\right] \tag{B.27}$$

B.2.4 Voltage-Controlled Virtual Synchronous Machines

The model employed in the analysis is taken from the studies carried out by D'Arco *et al.* for instance in [92, 122]. The difference resides in that in our case we do not include any active damping technique in order to keep the dynamic characteristics of the controller in their original form.

Synchronization Unit

The model for the PLL employed in this control strategy is the same as the one developed in Section B.2.2.

Current-controller

The current-control used in this case is the same as the one for the IE and the CCVSM technique, modelled in Section B.2.2.

Voltage-controller

This part of the controller is cascaded with the current-control and has its same structure, including the PI regulators and decoupling terms (Figure 4.12).

The current references for the current-controller are calculated using the following equation:

$$\mathbf{i}_c^{*C} = \left(\mathbf{v}_o^* - \mathbf{v}_o^C\right) K_{p_v} + K_{i_v} \boldsymbol{\gamma}_v + j\omega_{vsm} L_f \mathbf{v}_o^C \tag{B.28}$$

where $\boldsymbol{\gamma}_i$ corresponds to the states of the PIs included in the voltage-controller.

The differential equation of this parameter can be expressed as:

$$\frac{d\boldsymbol{\gamma}_v}{dt} = \mathbf{v}_o^* - \mathbf{v}_o^C \tag{B.29}$$

Virtual-impedance

This impedance serves to emulate an *RL* impedance in the output of the converter, which enables modifying the dynamic behaviour of the converter. With this impedance, we calculate the voltage reference for the above-mentioned voltage-controller:

$$\mathbf{v}_o^* = \hat{\mathbf{v}}_{rpc} - (R_v + j\omega_{vsm} L_v)\, \mathbf{i}_o \tag{B.30}$$

Reactive power controller

The voltage amplitude $\hat{\mathbf{v}}_{rpc}$ is calculated from the RPC as follows:

$$\hat{\mathbf{v}}_{rpc} = \hat{\mathbf{v}}_{\text{ref}} + K_q \left(q_{\text{ref}} - q_f\right) \tag{B.31}$$

As in the control of SM and in the CCVSM, the measured reactive power is filtered to obtain the reactive power q_f using a low-pass filter, which can be modelled with (A.9).

Active power controller

This controller is the same as the one used in the CCVSM control, with the difference that in this case the grid frequency is obtained from a PLL instead of using the filtered version of the internally generated frequency. The remaining equation that models this part of the control is

as follows:

$$\frac{d\omega_{vsm}}{dt} = \frac{1}{2H}\left[p_{\text{ref}} - p + K_\omega\left(\omega_{\text{ref}} - \omega_{vsm}\right) - K_D\left(\omega_{vsm} - \omega_{pll}\right)\right] \tag{B.32}$$

State and input vectors

If we take into account the common parts of the modelled SME-controlled converters and the specific parts of the VCVSM technique, we can define a set of 18 differential equations whose state vector x is:

$$\begin{aligned} x = \Big[\; & v_{o_d}^G \quad v_{o_q}^G \quad i_{c_d}^G \quad i_{c_q}^G \quad i_{o_d}^G \quad i_{o_q}^G \quad \rho_{1_d} \quad \rho_{1_q} \quad \rho_{2_d} \quad \rho_{2_q} \\ & \delta\theta_{pll} \quad \gamma_{pll} \quad \omega_{vsm} \quad \delta\theta_{vsm} \quad \gamma_{i_d} \quad \gamma_{i_q} \quad \gamma_{v_d} \quad \gamma_{v_q} \; \Big] \end{aligned} \tag{B.33}$$

Similarly, the input vector u can be defined as:

$$u = \left[\; p_{\text{ref}} \quad q_{\text{ref}} \quad v_{g_d}^G \quad v_{g_q}^G \quad V_{dc} \quad \omega_g \quad \hat{\mathbf{v}}_{\text{ref}} \quad \omega_{\text{ref}} \; \right] \tag{B.34}$$

Appendix C

Virtual-Capacitor-Controlled System Modelling

The following sections cover the analytical development of the small-signal state-space model of the proposed VC techniques for converters connected to dc systems.

The equations shown in the following sections correspond on the one hand to the common parts of the two VC controllers—i.e. the PWM, the converter itself, its output passive filter, the electric grid, the droop controller and the virtual capacitor—and on the other hand to specific parts of the VC2 technique—i.e. the voltage and current loops.

C.1 Common Parts of VC Control Strategies

C.1.1 Buck-Boost DC-DC Converter

In this thesis, a four switch buck-boost converter has been chosen for interfacing a 48 V lithium-ion battery pack to a 48 V dc microgrid (Figure C.1). This dc-dc converter can be operated as a buck, boost or buck-boost depending on the configuration of the four switches. However, as the voltages of the ESS and the microgrid are very similar, the converter is configured to operate exclusively in the buck-boost mode. Therefore, S_1 and S_3 are activated at the same time and S_2 and S_4 are complementary, which, as can be observed in Figure C.1, leads to two switching states in the converter.

In the switching state ① the input voltage is applied to the inductor and therefore it is charged during this interval. Then, in the switching state ②, the output voltage is inversely applied to the inductor and therefore its energy is transferred to the output. From these two switching states, and taking into account the parasitics of passive elements and switches, the

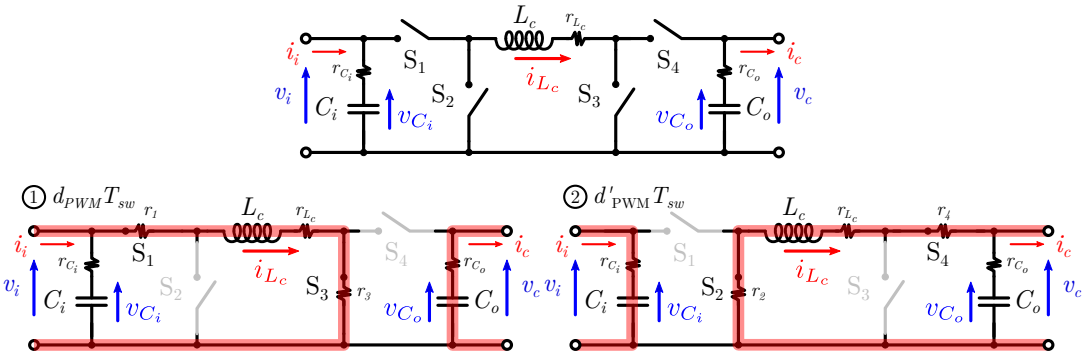

Figure C.1: Four switch buck-boost converter schematic and operating states in buck-boost mode.

average non-linear equations of the buck-boost can be defined as follows:

$$\frac{di_{L_c}}{dt} = \left(\frac{r_1 + r_3 + r_L}{L_c} i_{L_c} + \frac{1}{L_c} v_i\right) d_{\mathrm{PWM}} + \left(\frac{r_{C_o}}{L_c} i_c - \frac{r_2 + r_4 + r_L + r_{C_o}}{L_c} i_{L_c} - \frac{1}{L_c} v_{C_o}\right) d'_{\mathrm{PWM}} \tag{C.1}$$

where i_{L_c}, v_{C_i} and v_{C_o} are the buck-boost inductor current, input capacitor voltage and output capacitor voltage, respectively. The name of passive components is represented in Figure C.1, and v_i represents the converters input voltage. Moreover, d_{PWM} denotes the duty cycle taking into account the PWM delay and d'_{PWM} refers to $1 - d_{\mathrm{PWM}}$.

C.1.2 Pulse-Width Modulator

In this case, the PWM delay is expressed as a first-order transfer function that depends on the sampling time T_s (included in the diagrams of Figure 5.5 and Figure 5.6), and can be represented in differential form by:

$$\frac{dd_{\mathrm{PWM}}}{dt} = \frac{1}{1.5T_s}\left(-d_{\mathrm{PWM}} + \frac{1}{2v_g^*}\left(K_{p_i}\left(i_c^* - i_c\right) + K_{i_i}\gamma_i\right)\right) \tag{C.2}$$

where

$$i_c^* = K_{p_v}\left(v_{\mathrm{VC}} - v_g\right) + K_{i_v}\gamma_v$$

C.1.3 Converter Output Filter

As shown in Figure 5.5 and Figure 5.6, the output filter employed in this case is an *LC* filter, whose dynamics can be expressed by the dbferential equations of the filter inductor current

(i_c) and capacitor voltage (v_g) as follows:

$$\frac{di_c}{dt} = \frac{1}{L_f}\left(v_c - R_f i_c - v_g\right) \qquad \text{where} \qquad v_c = v_{C_o} + r_{C_o}\left(i_{L_c} - i_c\right) \tag{C.3}$$

$$\frac{dv_g}{dt} = \frac{dv_{C_f}}{dt} = \frac{1}{C_f}\left(i_c - i_g\right) \tag{C.4}$$

C.1.4 Virtual-Capacitor Control

The virtual-capacitor control is equivalent to a first order transfer function, which means its dynamics can be represented with a single differential equation:

$$\frac{dv_{\text{VC}}}{dt} = -\frac{1}{R_{\text{V}}C_{\text{V}}}v_{\text{VC}} + \frac{1}{C_{\text{V}}}\left(i^*_{\text{VC}} - i_c\right) + \frac{1}{R_{\text{V}}C_{\text{V}}}v^*_g \qquad \text{where} \qquad i^*_{\text{VC}} = \frac{1}{Z_{\text{V}}}\left(v^*_g - v_g\right) \tag{C.5}$$

C.2 Specific Parts of the VC2 Control Strategy

Cascaded Voltage and Current Controllers

The voltage and current controllers are composed by two cascaded PI regulators that reduce the voltage and current error, respectively. The dynamics of their integrators can be expressed by two differential equations by:

$$\frac{d\gamma_v}{dt} = v_{\text{VC}} - v_g \tag{C.6}$$

$$\frac{d\gamma_i}{dt} = i^*_c - i_c \tag{C.7}$$

C.3 Small-Signal State-Space Models

C.3.1 Voltage-Controlled Virtual-Capacitor

From Equation C.1 and Equation C.2 the state vector x and input vector u of the proposed VC2 technique can be defined as:

$$x = \begin{bmatrix} i_c & v_g & i_{L_c} & v_{C_i} & v_{C_o} & d_{\text{PWM}} & v_{\text{VC}} & \gamma_v & \gamma_i \end{bmatrix} \tag{C.8}$$

$$u = \begin{bmatrix} v^*_g & v_i & i_g \end{bmatrix} \tag{C.9}$$

This system consists of a set of 9 non-linear equations that must be linearized over a point of operation $\bar{x}$ to carry out the analysis of its dominant eigenvalues. The final set of equations

can be represented in a small-signal state-space form as:

$$\frac{d\tilde{x}}{dt} = \mathbf{A}\tilde{x} + \mathbf{B}\tilde{u} \tag{C.10}$$

Below the linearized state-space model **A** and **B** matrices are shown, where $r_{eq_1} = r_1 + r_3 + r_L$, $r_{eq_2} = r_2 + r_4 + r_L + r_{C_o}$ and $r_{eq_3} = r_{eq_2} - r_{eq_1}$:

$$\mathbf{A} = \begin{bmatrix}
-\frac{R_f + r_{C_o}}{L_f} & -\frac{1}{L_f} & \frac{r_{C_o}\bar{d}'_{\text{PWM}}}{L_f} & 0 & \frac{1}{L_f} & -\frac{r_{C_o}\bar{i}_{L_c}}{L_f} & 0 & 0 & 0 \\
\frac{1}{C_f} & 0 & 0 & 0 & 0 & 0 & 0 & 0 & 0 \\
\frac{r_{C_o}\bar{d}'_{\text{PWM}}}{L_c} & 0 & -\frac{r_{eq_1}\bar{d}_{\text{PWM}} + r_{eq_2}\bar{d}'_{\text{PWM}}}{L_c} & 0 & -\frac{\bar{d}'_{\text{PWM}}}{L_c} & \frac{\bar{v}_{C_o} + \bar{v}_i + r_{eq_3}\bar{i}_{L_c} - r_{C_o}\bar{i}_c}{L_c} & 0 & 0 & 0 \\
0 & 0 & 0 & -\frac{1}{r_{C_i}C_i} & 0 & 0 & 0 & 0 & 0 \\
-\frac{1}{C_o} & 0 & \frac{\bar{d}'_{\text{PWM}}}{C_o} & 0 & 0 & -\frac{\bar{i}_{L_c}}{C_o} & 0 & 0 & 0 \\
-\frac{K_{p_i}}{3T_s\bar{v}_g^*} & -\frac{K_{p_i}K_{p_v}}{3T_s\bar{v}_g^*} & 0 & 0 & 0 & -\frac{1}{1.5T_s} & \frac{K_{p_i}K_{p_v}}{3T_s\bar{v}_g^*} & \frac{K_{p_i}K_{i_v}}{3T_s\bar{v}_g^*} & \frac{K_{i_i}}{3T_s\bar{v}_g^*} \\
-\frac{1}{C_V} & -\frac{1}{Z_V C_V} & 0 & 0 & 0 & 0 & -\frac{1}{R_V C_V} & 0 & 0 \\
0 & -1 & 0 & 0 & 0 & 0 & 1 & 0 & 0 \\
-1 & -K_{p_v} & 0 & 0 & 0 & 0 & K_{p_v} & K_{i_v} & 0
\end{bmatrix}$$

$$\mathbf{B} = \begin{bmatrix}
0 & 0 & 0 \\
0 & 0 & -\frac{1}{C_f} \\
0 & \frac{1}{L_c}\bar{d}_{\text{PWM}} & 0 \\
0 & \frac{1}{r_{C_i}C_i} & 0 \\
0 & 0 & 0 \\
-\frac{K_{p_i}\left(K_{p_v}\left(\bar{v}_{\text{VC}} - \bar{v}_g\right) - \bar{i}_c + K_{i_v}\bar{\gamma}_v\right) + K_{i_i}\bar{\gamma}_i}{3T_s\bar{v}_g^{*2}} & 0 & 0 \\
\frac{R_V + Z_V}{Z_V R_V C_V} & 0 & 0 \\
0 & 0 & 0 \\
0 & 0 & 0
\end{bmatrix}$$

C.3.2 Direct Virtual-Capacitor

The input vector x and output vector u of the proposed DVC technique are very similar to the previous case. The difference is that here there are no states related to the voltage and current regulators, and the output of the virtual-capacitor loop is sent directly to the PWM. This yields in the following x and u vectors:

$$x = \begin{bmatrix} i_c & v_g & i_{L_c} & v_{C_i} & v_{C_o} & d_{\text{PWM}} & v_{\text{VC}} \end{bmatrix} \tag{C.11}$$

$$u = \begin{bmatrix} v_g^* & v_i & i_g \end{bmatrix} \tag{C.12}$$

This system consists of a set of 7 non-linear equations, and the final linearized state-space model **A** and **B** matrices are represented below:

$$\mathbf{A} = \begin{bmatrix} -\frac{R_f + r_{C_o}}{L_f} & -\frac{1}{L_f} & \frac{r_{C_o}\bar{d}'_{\text{PWM}}}{L_f} & 0 & \frac{1}{L_f} & -\frac{r_{C_o}\bar{i}_{L_c}}{L_f} & 0 \\ \frac{1}{C_f} & 0 & 0 & 0 & 0 & 0 & 0 \\ \frac{r_{C_o}\bar{d}'_{\text{PWM}}}{L_c} & 0 & -\frac{r_{eq_1}\bar{d}_{\text{PWM}} + r_{eq_2}\bar{d}'_{\text{PWM}}}{L_c} & 0 & -\frac{\bar{d}'_{\text{PWM}}}{L_c} & \frac{\bar{v}_{C_o} + \bar{v}_i + r_{eq_3}\bar{i}_{L_c} - r_{C_o}\bar{i}_c}{L_c} & 0 \\ 0 & 0 & 0 & -\frac{1}{r_{C_i}C_i} & 0 & 0 & 0 \\ -\frac{1}{C_o} & 0 & \frac{\bar{d}'_{\text{PWM}}}{C_o} & 0 & 0 & -\frac{\bar{i}_{L_c}}{C_o} & 0 \\ 0 & 0 & 0 & 0 & 0 & -\frac{1}{1.5T_s} & \frac{1}{3T_s\bar{v}_g^*} \\ -\frac{1}{C_{\text{V}}} & 0 & 0 & 0 & 0 & 0 & -\frac{R_{\text{V}} + Z_{\text{V}}}{Z_{\text{V}}R_{\text{V}}C_{\text{V}}} \end{bmatrix}$$

$$\mathbf{B} = \begin{bmatrix} 0 & 0 & 0 \\ 0 & 0 & -\frac{1}{C_f} \\ 0 & \frac{1}{L_c}\bar{d}_{\text{PWM}} & 0 \\ 0 & \frac{1}{r_{C_i}C_i} & 0 \\ 0 & 0 & 0 \\ -\frac{\bar{v}_{\text{VC}}}{3T_s\bar{v}_g^{*2}} & 0 & 0 \\ \frac{R_{\text{V}} + Z_{\text{V}}}{Z_{\text{V}}R_{\text{V}}C_{\text{V}}} & 0 & 0 \end{bmatrix}$$

List of Figures

List of Tables

List of References

[1] B. Kroposki, B. Johnson, Y. Zhang, V. Gevorgian, P. Denholm, B.-M. Hodge, and B. Hannegan, "Achieving a 100% Renewable Grid: Operating Electric Power Systems with Extremely High Levels of Variable Renewable Energy," *IEEE Power Energy Mag.*, vol. 15, no. 2, pp. 61–73, mar 2017. DOI: 10.1109/MPE.2016.2637122.

[2] B. Nordman, K. Christensen, and A. Meier, "Think Globally, Distribute Power Locally: The Promise of Nanogrids," *Computer (Long. Beach. Calif).*, vol. 45, no. 9, pp. 89–91, sep 2012. DOI: 10.1109/MC.2012.32.

[3] H. Farhangi, "The path of the smart grid," *IEEE Power Energy Mag.*, vol. 8, no. 1, pp. 18–28, jan 2010. DOI: 10.1109/MPE.2009.934876.

[4] P. Asmus and M. Lawrence, "Market Data: Microgrids," Navigant Research, Tech. Rep., 2016.

[5] J. Brisebois and N. Aubut, "Wind farm inertia emulation to fulfill Hydro-Québec's specific need," in *2011 IEEE Power Energy Soc. Gen. Meet.*, vol. 7. IEEE, jul 2011, pp. 1–7. DOI: 10.1109/PES.2011.6039121.

[6] Australian Energy Market Operator (AEMO), "Update Report – Black System Event in South Australia on 28 September 2016," Tech. Rep. October, 2016.

[7] ENTSO-E, "Need for synthetic inertia (SI) for frequency regulation," Brussels, Tech. Rep., 2017.

[8] ——, "High Penetration of Power Electronic Interfaced Power Sources (HPoPEIPS)," Brussels, Tech. Rep., 2017.

[9] P. Kundur, J. Paserba, V. Ajjarapu, G. Andersson, A. Bose, C. Canizares, N. Hatziargyriou, D. Hill, A. Stankovic, C. Taylor, T. Van Cutsem, and V. Vittal, "Definition and Classification of Power System Stability IEEE/CIGRE Joint Task Force on Stability Terms and Definitions," *IEEE Trans. Power Syst.*, vol. 19, no. 3, pp. 1387–1401, aug 2004. DOI: 10.1109/TPWRS.2004.825981.

[10] E. Hossain, E. Kabalci, R. Bayindir, and R. Perez, "Microgrid testbeds around the world: State of art," *Energy Convers. Manag.*, vol. 86, pp. 132–153, oct 2014. DOI: 10.1016/j.enconman.2014.05.012.

[11] B. Wen, D. Dong, D. Boroyevich, R. Burgos, P. Mattavelli, and Z. Shen, "Impedance-based analysis of grid-synchronization stability for three-phase paralleled converters," *IEEE Trans. Power Electron.*, vol. 31, no. 1, pp. 26–38, 2016. DOI: 10.1109/TPEL.2015.2419712.

[12] M. Amin, A. Ardal, and M. Molinas, "Self-synchronisation of Wind Farm in MMC-based HVDC System: A Stability Investigation," *IEEE Trans. Energy Convers.*, vol. 8969, no. c, pp. 1–1, 2017. DOI: 10.1109/TEC.2017.2661540.

[13] J. M. Guerrero, J. C. Vasquez, J. Matas, L. G. de Vicuna, and M. Castilla, "Hierarchical Control of Droop-Controlled AC and DC Microgrids—A General Approach Toward Standardization," *IEEE Trans. Ind. Electron.*, vol. 58, no. 1, pp. 158–172, jan 2011. DOI: 10.1109/TIE.2010.2066534.

[14] A. Bidram and A. Davoudi, "Hierarchical Structure of Microgrids Control System," *IEEE Trans. Smart Grid*, vol. 3, no. 4, pp. 1963–1976, dec 2012. DOI: 10.1109/TSG.2012.2197425.

[15] F. Blaabjerg, R. Teodorescu, M. Liserre, and A. V. Timbus, "Overview of Control and Grid Synchronization for Distributed Power Generation Systems," *IEEE Trans. Ind. Electron.*, vol. 53, no. 5, pp. 1398–1409, oct 2006. DOI: 10.1109/TIE.2006.881997.

[16] O. Palizban and K. Kauhaniemi, "Hierarchical control structure in microgrids with distributed generation: Island and grid-connected mode," *Renew. Sustain. Energy Rev.*, vol. 44, pp. 797–813, 2015. DOI: 10.1016/j.rser.2015.01.008.

[17] V. Natarajan and G. Weiss, "Synchronverters with better stability due to virtual inductors, virtual capacitors and anti-windup," *IEEE Trans. Ind. Electron.*, vol. 0046, no. c, pp. 1–1, 2017. DOI: 10.1109/TIE.2017.2674611.

[18] Q.-C. Zhong, "Power Electronics-enabled Autonomous Power Systems: Architecture and Technical Routes," *IEEE Trans. Ind. Electron.*, vol. 0046, no. c, pp. 1–1, 2017. DOI: 10.1109/TIE.2017.2677339.

[19] D. Chen, Y. Xu, and A. Q. Huang, "Integration of DC Microgrids as Virtual Synchronous Machines into the AC Grid," *IEEE Trans. Ind. Electron.*, vol. 0046, no. c, pp. 1–1, 2017. DOI: 10.1109/TIE.2017.2674621.

[20] D. Wu, F. Tang, T. Dragicevic, J. M. Guerrero, and J. C. Vasquez, "Coordinated Control Based on Bus-Signaling and Virtual Inertia for DC Islanded Microgrids," *IEEE Trans. Smart Grid*, vol. 6, no. 6, pp. 1–12, 2015. DOI: 10.1109/TSG.2014.2387357.

[21] J. A. Suul, S. DArco, and G. Guidi, "Virtual Synchronous Machine-Based Control of a Single-Phase Bi-Directional Battery Charger for Providing Vehicle-to-Grid Services," *IEEE Trans. Ind. Appl.*, vol. 52, no. 4, pp. 3234–3244, jul 2016. DOI: 10.1109/TIA.2016.2550588.

[22] Q.-C. Zhong, "Virtual Synchronous Machines: A unified interface for grid integration," *IEEE Power Electron. Mag.*, vol. 3, no. 4, pp. 18–27, dec 2016. DOI: 10.1109/MPEL.2016.2614906.

[23] S. D'Arco, J. A. Suul, and O. B. Fosso, "Small-signal modeling and parametric sensitivity of a virtual synchronous machine in islanded operation," *Int. J. Electr. Power Energy Syst.*, vol. 72, pp. 3–15, nov 2015. DOI: 10.1016/j.ijepes.2015.02.005.

[24] M. Sinha, F. Dörfler, B. B. Johnson, and S. V. Dhople, "Uncovering droop control laws embedded within the nonlinear dynamics of van der Pol oscillators," *IEEE Trans. Control Netw. Syst.*, vol. PP, no. 99, 2015. DOI: 10.1109/TCNS.2015.2503558.

[25] B. B. Johnson, S. V. Dhople, A. O. Hamadeh, and P. T. Krein, "Synchronization of parallel single-phase inverters with virtual oscillator control," *IEEE Trans. Power Electron.*, vol. 29, no. 11, pp. 6124–6138, 2014. DOI: 10.1109/TPEL.2013.2296292.

[26] A. M. Bouzid, J. M. Guerrero, A. Cheriti, M. Bouhamida, P. Sicard, and M. Benghanem, "A survey on control of electric power distributed generation systems for microgrid applications," *Renew. Sustain. Energy Rev.*, vol. 44, pp. 751–766, 2015. DOI: 10.1016/j.rser.2015.01.016.

[27] J. Rocabert, A. Luna, F. Blaabjerg, and P. Rodríguez, "Control of Power Converters in AC Microgrids," *IEEE Trans. Power Electron.*, vol. 27, no. 11, pp. 4734–4749, nov 2012. DOI: 10.1109/TPEL.2012.2199334.

[28] T. L. Vandoorn, J. C. Vasquez, J. De Kooning, J. M. Guerrero, and L. Vandevelde, "Microgrids: Hierarchical control and an overview of the control and reserve management strategies," *IEEE Ind. Electron. Mag.*, vol. 7, no. 4, pp. 42–55, 2013. DOI: 10.1109/MIE.2013.2279306.

[29] O. Palizban, K. Kauhaniemi, and J. M. Guerrero, "Microgrids in active network management - Part I: Hierarchical control, energy storage, virtual power plants, and market participation," *Renew. Sustain. Energy Rev.*, vol. 36, pp. 428–439, aug 2014. DOI: 10.1016/j.rser.2014.01.016.

[30] T. L. Vandoorn, J. De Kooning, B. Meersman, and L. Vandevelde, "Review of primary control strategies for islanded microgrids with power-electronic interfaces," *Renew. Sustain. Energy Rev.*, vol. 19, pp. 613–628, mar 2013. DOI: 10.1016/j.rser.2012.11.062.

[31] T. Dragicevic, J. M. Guerrero, and J. C. Vasquez, "A Distributed Control Strategy for Coordination of an Autonomous LVDC Microgrid Based on Power-Line Signaling," *IEEE Trans. Ind. Electron.*, vol. 61, no. 7, pp. 3313–3326, jul 2014. DOI: 10.1109/TIE.2013.2282597.

[32] Y. Gu, X. Xiang, W. Li, and X. He, "Mode-Adaptive Decentralized Control for Renewable DC Microgrid With Enhanced Reliability and Flexibility," *IEEE Trans. Power Electron.*, vol. 29, no. 9, pp. 5072–5080, 2014. DOI: 10.1109/TPEL.2013.2294204.

[33] M. Baharizadeh, H. R. Karshenas, and J. M. Guerrero, "Control strategy of interlinking converters as the key segment of hybrid AC–DC microgrids," *IET Gener. Transm. Distrib.*, vol. 10, no. 7, pp. 1671–1681, may 2016. DOI: 10.1049/iet-gtd.2015.1014.

[34] F. Gao, S. Bozhko, A. Costabeber, C. Patel, P. Wheeler, C. I. Hill, and G. Asher, "Comparative Stability Analysis of Droop Control Approaches in Voltage-Source-Converter-Based DC Microgrids," *IEEE Trans. Power Electron.*, vol. 32, no. 3, pp. 2395–2415, mar 2017. DOI: 10.1109/TPEL.2016.2567780.

[35] Z. Jin, L. Meng, and J. M. Guerrero, "Comparative Admittance-based Analysis for Different Droop Control Approaches in DC Microgrids," in *Second IEEE Int. Conf. DC Microgrids*, 2017.

[36] U. B. Tayab, M. A. B. Roslan, L. J. Hwai, and M. Kashif, "A review of droop control techniques for microgrid," *Renew. Sustain. Energy Rev.*, vol. 76, no. November 2016, pp. 717–727, 2017. DOI: 10.1016/j.rser.2017.03.028.

[37] P. C. Loh, D. Li, Y. K. Chai, and F. Blaabjerg, "Autonomous operation of hybrid microgrid with ac and dc subgrids," *IEEE Trans. Power Electron.*, vol. 28, no. 5, pp. 2214–2223, may 2013. DOI: 10.1109/TPEL.2012.2214792.

[38] X. Wang, Y. W. Li, F. Blaabjerg, and P. C. Loh, "Virtual-Impedance-Based Control for Voltage-Source and Current-Source Converters," *IEEE Trans. Power Electron.*, vol. 30, no. 12, pp. 7019–7037, 2015. DOI: 10.1109/TPEL.2014.2382565.

[39] H. Shi, F. Zhuo, H. Yi, F. Wang, D. Zhang, and Z. Geng, "A novel real-time voltage and frequency compensation strategy for photovoltaic-based microgrid," *IEEE Trans. Ind. Electron.*, vol. 0046, no. 6, pp. 3545–3556, 2014. DOI: 10.1109/TIE.2014.2371434.

[40] Y. W. Li and C.-n. N. Kao, "An accurate power control strategy for power-electronics-interfaced distributed generation units operating in a low-voltage multibus microgrid," *IEEE Trans. Power Electron.*, vol. 24, no. 12, pp. 2977–2988, dec 2009. DOI: 10.1109/TPEL.2009.2022828.

[41] J. Kim, J. M. Guerrero, P. Rodriguez, R. Teodorescu, and K. Nam, "Mode Adaptive Droop Control With Virtual Output Impedances for an Inverter-Based Flexible AC Microgrid," *IEEE Trans. Power Electron.*, vol. 26, no. 3, pp. 689–701, mar 2011. DOI: 10.1109/TPEL.2010.2091685.

[42] M. Zhang, Z. Du, X. Lin, and J. Chen, "Control Strategy Design and Parameter Selection for Suppressing Circulating Current Among SSTs in Parallel," *IEEE Trans. Smart Grid*, vol. 6, no. 4, pp. 1602–1609, jul 2015. DOI: 10.1109/TSG.2015.2402835.

[43] T. Dragicevic, J. M. Guerrero, J. C. Vasquez, and D. Skrlec, "Supervisory control of an adaptive-droop regulated DC microgrid with battery management capability," *IEEE Trans. Power Electron.*, vol. 29, no. 2, pp. 695–706, feb 2014. DOI: 10.1109/TPEL.2013.2257857.

[44] X. Yu, A. M. Khambadkone, H. Wang, and S. T. S. Terence, "Control of parallel-connected power converters for low-voltage microgrid - Part I: A hybrid control architecture," *IEEE Trans. Power Electron.*, vol. 25, no. 12, pp. 2962–2970, 2010. DOI: 10.1109/TPEL.2010.2087393.

[45] Q. Shafiee, T. Dragicevic, J. C. Vasquez, and J. M. Guerrero, "Hierarchical Control for Multiple DC-Microgrids Clusters," in *IEEE Trans. Energy Convers.*, vol. 29, no. 4. IEEE, feb 2014, pp. 1–6. DOI: 10.1109/TEC.2014.2362191.

[46] C. Yuen, A. Oudalov, and A. Timbus, "The provision of frequency control reserves from multiple microgrids," *IEEE Trans. Ind. Electron.*, vol. 58, no. 1, pp. 173–183, 2011. DOI: 10.1109/TIE.2010.2041139.

[47] E. Planas, A. Gil-de Muro, J. Andreu, I. Kortabarria, and I. Martínez de Alegría, "General aspects, hierarchical controls and droop methods in microgrids: A review," *Renew. Sustain. Energy Rev.*, vol. 17, pp. 147–159, jan 2013. DOI: 10.1016/j.rser.2012.09.032.

[48] L. Meng, Q. Shafiee, G. Ferrari Trecate, H. Karimi, D. Fulwani, X. Lu, and J. M. Guerrero, "Review on Control of DC Microgrids," *IEEE J. Emerg. Sel. Top. Power Electron.*, no. March, pp. 1–1, 2017. DOI: 10.1109/JESTPE.2017.2690219.

[49] K. Rouzbehi, A. Miranian, A. Luna, and P. Rodriguez, "DC Voltage Control and Power Sharing in Multiterminal DC Grids Based on Optimal DC Power Flow and Voltage-Droop

Strategy," *IEEE J. Emerg. Sel. Top. Power Electron.*, vol. 2, no. 4, pp. 1171–1180, 2014. DOI: 10.1109/JESTPE.2014.2338738.

[50] A. A. A. Radwan and Y. A.-R. I. Mohamed, "Networked Control and Power Management of AC/DC Hybrid Microgrids," *IEEE Syst. J.*, pp. 1–12, 2014. DOI: 10.1109/JSYST.2014.2337353.

[51] Q. Shafiee, J. M. Guerrero, and J. C. Vasquez, "Distributed secondary control for islanded microgrids-a novel approach," *IEEE Trans. Power Electron.*, vol. 29, no. 2, pp. 1018–1031, 2014. DOI: 10.1109/TPEL.2013.2259506.

[52] M. Yazdanian and A. Mehrizi-Sani, "Distributed Control Techniques in Microgrids," *IEEE Trans. Smart Grid*, vol. 5, no. 6, pp. 2901–2909, nov 2014. DOI: 10.1109/TSG.2014.2337838.

[53] A. Bidram, A. Davoudi, F. L. Lewis, and J. M. Guerrero, "Distributed cooperative secondary control of microgrids using feedback linearization," *IEEE Trans. Power Syst.*, vol. 28, no. 3, pp. 3462–3470, 2013. DOI: 10.1109/TPWRS.2013.2247071.

[54] H. Liang, B. J. Choi, W. Zhuang, X. Shen, a. S. A. Awad, and A. Abdr, "Multiagent coordination in microgrids via wireless networks," *IEEE Wirel. Commun.*, vol. 19, no. 3, pp. 14–22, 2012. DOI: 10.1109/MWC.2012.6231155.

[55] Q. Shafiee, T. Dragicevic, F. Andrade, J. C. Vasquez, and J. M. Guerrero, "Distributed Consensus-Based Control of Multiple DC-Microgrids Clusters," in *40th Annu. Conf. IEEE Ind. Electron. Soc.*, 2014, pp. 2056–2062. DOI: 10.1109/IECON.2014.7048785.

[56] Q. Shafiee, C. Stefanovic, T. Dragicevic, P. Popovski, J. C. Vasquez, and J. M. Guerrero, "Robust networked control scheme for distributed secondary control of islanded microgrids," *IEEE Trans. Ind. Electron.*, vol. 61, no. 10, pp. 5363–5374, 2014. DOI: 10.1109/TIE.2013.2293711.

[57] Q. Shafiee, V. Nasirian, J. M. Guerrero, F. L. Lewis, and A. Davoudi, "Team-oriented adaptive droop control for autonomous AC microgrids," in *IECON Proc. (Industrial Electron. Conf.*, 2014, p. 7. DOI: 10.1109/IECON.2014.7048755.

[58] F. Guo, C. Wen, J. Mao, and Y.-D. Song, "Distributed Secondary Voltage and Frequency Restoration Control of Droop-Controlled Inverter-Based Microgrids," *IEEE Trans. Ind. Electron.*, vol. 0046, no. c, p. 1, 2014. DOI: 10.1109/TIE.2014.2379211.

[59] N. L. Diaz, T. Dragicevic, J. C. Vasquez, and J. M. Guerrero, "Intelligent Distributed Generation and Storage Units for DC Microgrids—A New Concept on Cooperative Control Without Communications Beyond Droop Control," *IEEE Trans. Smart Grid*, vol. 5, no. 5, pp. 2476–2485, sep 2014. DOI: 10.1109/TSG.2014.2341740.

[60] P. Wang, C. Jin, D. Zhu, Y. Tang, P. C. Loh, and F. H. Choo, "Distributed control for autonomous operation of a three-port ac/dc/ds hybrid microgrid," *IEEE Trans. Ind. Electron.*, vol. 62, no. 2, pp. 1279–1290, 2015. DOI: 10.1109/TIE.2014.2347913.

[61] P. T. Baboli, M. Shahparasti, M. P. Moghaddam, and M. R. H. M. Mohamadian, "Energy management and operation modelling of hybrid AC–DC microgrid," *IET Gener. Transm. Distrib.*, vol. 8, no. 10, pp. 1700–1711, oct 2014. DOI: 10.1049/iet-gtd.2013.0793.

[62] W. Shi, X. Xie, C.-c. C. Chu, and R. Gadh, "Distributed Optimal Energy Management in Microgrids," *IEEE Trans. Smart Grid*, vol. 6, no. 3, pp. 1137–1146, 2015. DOI: 10.1109/TSG.2014.2373150.

[63] K. De Brabandere, K. Vanthournout, J. Driesen, G. Deconinck, and R. Belmans, "Control of microgrids," in *2007 IEEE Power Eng. Soc. Gen. Meet. PES*, 2007, pp. 1–7. DOI: 10.1109/PES.2007.386042.

[64] L. Meng, T. Dragicevic, J. Guerrero, J. Vasquez, M. Savaghebi, and F. Tang, "Agent-based distributed unbalance compensation for optimal power quality in islanded microgrids," in *2014 IEEE 23rd Int. Symp. Ind. Electron.* IEEE, jun 2014, pp. 2535–2540. DOI: 10.1109/ISIE.2014.6865019.

[65] Y. Gu, W. Li, and X. He, "Frequency-coordinating virtual impedance for autonomous power management of DC microgrid," *IEEE Trans. Power Electron.*, vol. 30, no. 4, pp. 2328–2337, 2015. DOI: 10.1109/TPEL.2014.2325856.

[66] Y. Liu, X. Hou, X. Wang, C. Lin, and J. Guerrero, "A Coordinated Control for Photovoltaic Generators and Energy Storages in Low-Voltage AC/DC Hybrid Microgrids under Islanded Mode," *Energies*, vol. 9, no. 8, p. 651, 2016. DOI: 10.3390/en9080651.

[67] S. Peyghami-Akhuleh, H. Mokhtari, P. Davari, P. C. Loh, and F. Blaabjerg, "Smart power management of DC microgrids in future milligrids," in *2016 18th Eur. Conf. Power Electron. Appl. (EPE'16 ECCE Eur.*, no. November. IEEE, sep 2016, pp. 1–10. DOI: 10.1109/EPE.2016.7695459.

[68] P. C. Loh, D. Li, Y. K. Chai, and F. Blaabjerg, "Hybrid AC-DC microgrids with energy storages and progressive energy flow tuning," in *IEEE Trans. Power Electron.*, vol. 28, no. 4. IEEE, feb 2013, pp. 1533–1543. DOI: 10.1109/TPEL.2012.2210445.

[69] P. Palensky and D. Dietrich, "Demand side management: Demand response, intelligent energy systems, and smart loads," *IEEE Trans. Ind. Informatics*, vol. 7, no. 3, pp. 381–388, 2011. DOI: 10.1109/TII.2011.2158841.

[70] P. Kundur, *Power System Stability And Control*, ser. EPRI power system engineering series. New York: McGraw-Hill Education (India) Pvt Limited, 1994.

[71] S. D'Arco and J. A. Suul, "Virtual synchronous machines—Classification of implementations and analysis of equivalence to droop controllers for microgrids," in *2013 IEEE Grenoble Conf.* IEEE, jun 2013, pp. 1–7. DOI: 10.1109/PTC.2013.6652456.

[72] H. Bevrani, T. Ise, and Y. Miura, "Virtual synchronous generators: A survey and new perspectives," *Int. J. Electr. Power Energy Syst.*, vol. 54, pp. 244–254, jan 2014. DOI: 10.1016/j.ijepes.2013.07.009.

[73] Z. Shuai, Y. Hu, Y. Peng, C. Tu, and Z. J. Shen, "Dynamic Stability Analysis of Synchronverter-dominated Microgrid Based on Bifurcation Theory," *IEEE Trans. Ind. Electron.*, vol. 0046, no. c, pp. 1–1, 2017. DOI: 10.1109/TIE.2017.2652387.

[74] D. Pullaguram, S. Achary Buragappu, S. Mishra, and D. Ramasubramanian, "Single-phase synchronverter for a grid-connected roof top photovoltaic system," *IET Renew. Power Gener.*, vol. 10, no. 8, pp. 1187–1194, sep 2016. DOI: 10.1049/iet-rpg.2015.0224.

[75] S. Peyghami, P. Davari, H. Mokhtari, P. C. Loh, and F. Blaabjerg, "Synchronverter-based Power Sharing Approach for LVDC Microgrids," *IEEE Trans. Power Electron.*, vol. 8993, no. c, pp. 1–1, 2016. DOI: 10.1109/TPEL.2016.2632441.

[76] Q.-C. Zhong, Z. Ma, W.-L. Ming, and G. C. Konstantopoulos, "Grid-friendly wind power systems based on the synchronverter technology," *Energy Convers. Manag.*, vol. 89, pp. 719–726, jan 2015. DOI: 10.1016/j.enconman.2014.10.027.

[77] Q.-C. Zhong and G. Weiss, "Synchronverters: Inverters That Mimic Synchronous Generators," *IEEE Trans. Ind. Electron.*, vol. 58, no. 4, pp. 1259–1267, apr 2011. DOI: 10.1109/TIE.2010.2048839.

[78] V. Karapanos, S. W. H. De Haan, and K. H. Zwetsloot, "Testing a Virtual Synchronous Generator in a Real Time Simulated Power System," *Int. Conf. Power Syst. Transients*, vol. 31, no. 0, 2011.

[79] M. Torres and L. A. C. Lopes, "Frequency control improvement in an autonomous power system: An application of virtual synchronous machines," in *8th Int. Conf. Power Electron. - ECCE Asia*. IEEE, may 2011, pp. 2188–2195. DOI: 10.1109/ICPE.2011.5944413.

[80] M. P. N. van Wesenbeeck, S. W. H. de Haan, P. Varela, and K. Visscher, "Grid tied converter with virtual kinetic storage," in *2009 IEEE Bucharest PowerTech Innov. Ideas Towar. Electr. Grid Futur.*, no. 1. IEEE, jun 2009, pp. 1–7. DOI: 10.1109/PTC.2009.5282048.

[81] M. Torres and L. A. C. Lopes, "Virtual synchronous generator control in autonomous wind-diesel power systems," in *2009 IEEE Electr. Power Energy Conf.*, no. 1. IEEE, oct 2009, pp. 1–6. DOI: 10.1109/EPEC.2009.5420953.

[82] J. Zhu, C. D. Booth, G. P. Adam, A. J. Roscoe, and C. G. Bright, "Inertia emulation control strategy for VSC-HVDC transmission systems," *IEEE Trans. Power Syst.*, vol. 28, no. 2, pp. 1277–1287, 2013. DOI: 10.1109/TPWRS.2012.2213101.

[83] M. Dreidy, H. Mokhlis, and S. Mekhilef, "Inertia response and frequency control techniques for renewable energy sources: A review," *Renew. Sustain. Energy Rev.*, vol. 69, no. July 2016, pp. 144–155, mar 2017. DOI: 10.1016/j.rser.2016.11.170.

[84] D. Duckwitz and B. Fischer, "Modeling and Design of df/dt-based Inertia Control for Power Converters," *IEEE J. Emerg. Sel. Top. Power Electron.*, vol. PP, no. 99, pp. 1–1, 2017. DOI: 10.1109/JESTPE.2017.2703814.

[85] E. Rakhshani and P. Rodriguez, "Inertia Emulation in AC/DC Interconnected Power Systems Using Derivative Technique Considering Frequency Measurement Effects," *IEEE Trans. Power Syst.*, vol. 8950, no. c, pp. 1–1, 2016. DOI: 10.1109/TPWRS.2016.2644698.

[86] O. Mo, S. D'Arco, and J. A. Suul, "Evaluation of Virtual Synchronous Machines with Dynamic or Quasi-stationary Machine Models," *IEEE Trans. Ind. Electron.*, vol. 0046, no. c, pp. 1–1, 2016. DOI: 10.1109/TIE.2016.2638810.

[87] Y. Hirase, K. Abe, K. Sugimoto, and Y. Shindo, "A grid-connected inverter with virtual synchronous generator model of algebraic type," *Electr. Eng. Japan*, vol. 184, no. 4, pp. 10–21, sep 2013. DOI: 10.1002/eej.22428.

[88] Y. Chen, R. Hesse, D. Turschner, and H.-P. Beck, "Comparison of methods for implementing virtual synchronous machine on inverters," in *Int. Conf. Renew. Energies Power Qual.*, 2012, pp. 1–6.

[89] R. Hesse, D. Turschner, and H.-P. Beck, "Micro grid stabilization using the Virtual Synchronous Machine (VISMA)," *2009 Int. Conf. Renew. Energies Power Qual.*, 2009.

[90] H.-P. Beck and R. Hesse, "Virtual synchronous machine," in *2007 9th Int. Conf. Electr. Power Qual. Util.* IEEE, oct 2007, pp. 1–6. DOI: 10.1109/EPQU.2007.4424220.

[91] D. J. Hogan, F. Gonzalez-Espin, J. G. Hayes, G. Lightbody, L. Albiol-Tendillo, and R. Foley, "Virtual synchronous-machine control of voltage-source converters in a low-voltage microgrid," in *2016 18th Eur. Conf. Power Electron. Appl. (EPE'16 ECCE Eur.* IEEE, sep 2016, pp. 1–10. DOI: 10.1109/EPE.2016.7695503.

[92] S. D'Arco, J. A. Suul, and O. B. Fosso, "A Virtual Synchronous Machine implementation for distributed control of power converters in SmartGrids," *Electr. Power Syst. Res.*, vol. 122, pp. 180–197, 2015. DOI: 10.1016/j.epsr.2015.01.001.

[93] S. D'Arco and J. A. Suul, "Equivalence of virtual synchronous machines and frequency-droops for converter-based Microgrids," *IEEE Trans. Smart Grid*, vol. 5, no. 1, pp. 394–395, 2014. DOI: 10.1109/TSG.2013.2288000.

[94] S. D'Arco, J. A. Suul, and O. B. Fosso, "Control system tuning and stability analysis of Virtual Synchronous Machines," in *2013 IEEE Energy Convers. Congr. Expo.*, no. September 2013. IEEE, sep 2013, pp. 2664–2671. DOI: 10.1109/ECCE.2013.6647045.

[95] E. Waffenschmidt and R. S. Hui, "Virtual inertia with PV inverters using DC-link capacitors," in *2016 18th Eur. Conf. Power Electron. Appl. (EPE'16 ECCE Eur.*, vol. 5. IEEE, sep 2016, pp. 1–10. DOI: 10.1109/EPE.2016.7695607.

[96] P. Rodriguez, I. Candela, and A. Luna, "Control of PV generation systems using the synchronous power controller," in *2013 IEEE Energy Convers. Congr. Expo*. IEEE, sep 2013, pp. 993–998. DOI: 10.1109/ECCE.2013.6646811.

[97] H. Alatrash, A. Mensah, E. Mark, G. Haddad, and J. Enslin, "Generator emulation controls for photovoltaic inverters," *IEEE Trans. Smart Grid*, vol. 3, no. 2, pp. 996–1011, 2012. DOI: 10.1109/TSG.2012.2188916.

[98] K. Koyanagi, Y. Hida, Y. Ito, K. Yoshimi, R. Yokoyama, M. Inokuchi, T. Mouri, and J. Eguchi, "A Smart Photovoltaic Generation System Integrated with Lithium-ion Capacitor Storage," *46th Int. Univ. Power Eng. Conf.*, no. September, pp. 1–6, 2011.

[99] H. Dharmawardena, K. Uhlen, and S. S. Gjerde, "Modelling wind farm with synthetic inertia for power system dynamic studies," in *2016 IEEE Int. Energy Conf.*, no. 2. IEEE, apr 2016, pp. 1–6. DOI: 10.1109/ENERGYCON.2016.7514098.

[100] P. F. Frack, P. E. Mercado, M. G. Molina, E. H. Watanabe, R. W. De Doncker, and H. Stagge, "Control Strategy for Frequency Control in Autonomous Microgrids," *IEEE J. Emerg. Sel. Top. Power Electron.*, vol. 3, no. 4, pp. 1046–1055, dec 2015. DOI: 10.1109/JESTPE.2015.2439053.

[101] C. D. Booth, W. Hung, J. M. Guerrero, J. Zhu, and G. P. Adam, "Generic inertia emulation controller for multi-terminal voltage-source-converter high voltage direct current systems," *IET Renew. Power Gener.*, vol. 8, no. 7, pp. 740–748, sep 2014. DOI: 10.1049/iet-rpg.2014.0109.

[102] E. Rakhshani, D. Remon, A. M. Cantarellas, and P. Rodriguez, "Analysis of derivative control based virtual inertia in multi-area high-voltage direct current interconnected power systems," *IET Gener. Transm. Distrib.*, vol. 10, no. 6, pp. 1458–1469, apr 2016. DOI: 10.1049/iet-gtd.2015.1110.

[103] Q.-C. Zhong and G. Weiss, "Static synchronous generators for distributed generation and renewable energy," in *2009 IEEE/PES Power Syst. Conf. Expo. PSCE 2009*. IEEE, mar 2009, pp. 1–6. DOI: 10.1109/PSCE.2009.4840013.

[104] Q.-C. Zhong, P.-L. Nguyen, Z. Ma, and W. Sheng, "Self-Synchronized Synchronverters: Inverters Without a Dedicated Synchronization Unit," *IEEE Trans. Power Electron.*, vol. 29, no. 2, pp. 617–630, feb 2014. DOI: 10.1109/TPEL.2013.2258684.

[105] Energy research Centre of the Netherlands (ECN). VSYNC Project. [Online]. Available: http://www.vsync.eu/. [Accessed: 2017-03-02].

[106] R. D. Middlebrook, "Input filter considerations in design and application of switching regulators," in *1976 IEEE Ind. Appl. Soc. Annu. Meet.*, 1976, pp. 366–382.

[107] J. Sun, "Impedance-based stability criterion for grid-connected inverters," *IEEE Trans. Power Electron.*, vol. 26, no. 11, pp. 3075–3078, 2011. DOI: 10.1109/TPEL.2011.2136439.

[108] B. Wen, D. Boroyevich, R. Burgos, P. Mattavelli, and Z. Shen, "Inverse Nyquist Stability Criterion for Grid-Tied Inverters," *IEEE Trans. Power Electron.*, vol. 32, no. 2, pp. 1548–1556, 2017. DOI: 10.1109/TPEL.2016.2545871.

[109] M. Amin, M. Molinas, J. Lyu, and X. Cai, "Impact of Power Flow Direction on the Stability of VSC-HVDC Seen From the Impedance Nyquist Plot," *IEEE Trans. Power Electron.*, vol. 32, no. 10, pp. 8204–8217, oct 2017. DOI: 10.1109/TPEL.2016.2608278.

[110] R. Burgos, D. Boroyevich, F. Wang, K. Karimi, and G. Francis, "On the Ac stability of high power factor three-phase rectifiers," in *2010 IEEE Energy Convers. Congr. Expo.* IEEE, sep 2010, pp. 2047–2054. DOI: 10.1109/ECCE.2010.5618091.

[111] O. Saborío, "Small-signal modelling and stability analysis of a traditional generation unit and a virtual synchronous machine in grid-connected operation," Master's thesis, Norwegian University of Science and Technology, 2015.

[112] M. Belkhayat, "Stability Criteria for AC Power Systems with Regulated Loads," Ph.D. dissertation, 1997.

[113] A. G. MacFarlane and I. Postlethwaite, "The generalized Nyquist stability criterion and multivariable root loci," *Int. J. Control*, vol. 25, no. 1, pp. 81–127, jan 1977. DOI: 10.1080/00207177708922217.

[114] A. G. MacFarlane, *Frequency-Response Methods in Control Systems*. IEEE Press, 1979, vol. 3, no. 1.

[115] S. Shah and L. Parsa, "Impedance Modeling of Three-Phase Voltage Source Converters in DQ, Sequence, and Phasor Domains," *IEEE Trans. Energy Convers.*, vol. 8969, no. c, pp. 1–1, 2017. DOI: 10.1109/TEC.2017.2698202.

[116] A. Rygg, M. Molinas, Chen Zhang, and Xu Cai, "Frequency-dependent source and load impedances in power systems based on power electronic converters," in *2016 Power Syst. Comput. Conf.* IEEE, jun 2016, pp. 1–8. DOI: 10.1109/PSCC.2016.7540891.

[117] R. Burgos, D. Boroyevich, F. Wang, K. Karimi, and G. Francis, "On the Ac stability of high power factor three-phase rectifiers," *2010 IEEE Energy Convers. Congr. Expo. ECCE 2010 - Proc.*, pp. 2047–2054, 2010. DOI: 10.1109/ECCE.2010.5618091.

[118] A. Riccobono and E. Santi, "Comprehensive review of stability criteria for DC power distribution systems," *IEEE Trans. Ind. Appl.*, vol. 50, no. 5, pp. 3525–3535, 2014. DOI: 10.1109/TIA.2014.2309800.

[119] T. Dragicevic, X. Lu, J. Vasquez, and J. Guerrero, "DC Microgrids–Part I: A Review of Control Strategies and Stabilization Techniques," *IEEE Trans. Power Electron.*, vol. 8993, no. c, pp. 1–1, 2015. DOI: 10.1109/TPEL.2015.2478859.

[120] A. Alacano, J. J. Valera, and G. Abad, "A multivariable modeling approach for the design of Power Electronics Based DC Distribution Systems in diesel-electric vessels," in *2016 IEEE 17th Work. Control Model. Power Electron.* IEEE, jun 2016, pp. 1–8. DOI: 10.1109/COMPEL.2016.7556680.

[121] J. L. Agorreta, M. Borrega, J. López, and L. Marroyo, "Modeling and Control of N-Paralleled Grid-Connected Inverters With LCL Filter Coupled Due to Grid Impedance in PV Plants," *IEEE Trans. Power Electron.*, vol. 26, no. 3, pp. 770–785, mar 2011. DOI: 10.1109/TPEL.2010.2095429.

[122] S. D'Arco and J. A. Suul, "Small-Signal analysis of an isolated power system controlled by a virtual synchronous machine," in *2016 IEEE Int. Power Electron. Motion Control Conf.* IEEE, sep 2016, pp. 462–469. DOI: 10.1109/EPEPEMC.2016.7752041.